DEVELOPMENT AND TEST OF AN ON-LINE COUPLING OF THERMODESORPTION WITH FAST GAS CHROMATOGRAPHY FOR STUDIES OF N-ALKANES IN ATMOSPHERIC PARTICULATE MATTER

by

Xueping Gong

Presented to the Faculty of Graduate Studies in fulfillment of the dissertation requirement for the degree of

Doctor of Philosophy

Graduate Programme in Chemistry
York University
Toronto, Ontario

February 2009

ABSTRACT

There are various methods to analyze carbon in atmospheric particles. Thermal desorption methods typically are used to determine "bulk" properties such as total carbon, organic carbon, elemental carbon (or black carbon), but generally do not allow compound specific analysis of the components of particulate organic matter (POM). Today gas chromatography is widely used to conduct compound specific measurements, either in combination with extraction procedures or pyrolysis of particulate organic matter. The intention of this work is to combine thermodesorption method with the separation power of gas chromatography equipped with high sensitive flame ionization detector (FID) to identify, quantify individual compounds without solvent extraction, investigate thermal behavior of different samples and measure some physical chemistry parameters, such as equilibrium vapor pressure, binary diffusion coefficient and activity coefficient. n-alkanes were chosen to be model substances in this work.

A thermal desorption instrument (TDI) based on the method of evolved gas analysis was developed and tested using different materials. Two different methods for detection were used. One detection method was based on conventional principles of detecting all carbonaceous gases evolved. For this purpose the evolved carbonaceous substances were oxidized to CO_2 and/or CO, and CO_2/CO was reduced to CH_4 which is measured by a flame ionization detector (FID). This was used to analyze atmospheric PM samples for total carbon (TC), organic carbon (OC) and elemental (or black) carbon (EC). A variety of tests demonstrated that this method is suitable to analyze carbonaceous

components in PM in the concentration range of 1 μg m^{-3} to 30 μg m^{-3} with a reproducibility of better than 10%. An exception is the analysis of EC. In this case variable extent of charring of OC resulted in a larger variability of the EC measurements. Due to the typically low EC content of atmospheric PM, this resulted in a relative variability of the EC measurements which significantly exceeded the good reproducibility achieved for TC and OC. Moreover, similar to effectively all existing methods for EC measurement in atmospheric PM, the results obtained for EC significantly depend on details of the measurement procedure.

The organic carbon thermograms of different particulate matter samples show often significant differences in their shapes. However, due to the numerous different organic compounds contributing to organic carbon in atmospheric particulate matter and the complex processes responsible for releasing carbon from the filter it is not possible to identify individual compounds from the thermograms alone. A medium fast (analysis duration in the range of 100s to 200 s) on-line GC-FID was added as "second dimension" to the thermal desorption procedure. This allows compound specific analysis of the evolved organic material. The TDI was interfaced to the GC using a cryogenic trap which collects the evolved organic compounds from the carrier gas passing through the TDI for periods between 100s and 200s and then rapidly releases the trapped substances for analysis on a short capillary column. The system operates automatically and allows programmed changes of the GC temperature independent of the TDI temperature program.

The on-line TDI/GC coupling was developed and tested using n-alkanes in the range of C_{18}-C_{34}. Different pure n-alkanes as well as mixtures spiked on different surfaces and n-alkanes in particulate matter sample were investigated. The n-alkane concentrations in a small set of particulate matter samples were determined.

Small modifications of the TDI/GC instrument allowed measurements of equilibrium vapor pressures and binary diffusion coefficients. A simple theoretical equation was derived to describe the dependence between measured vapor pressure and equilibrium vapor pressure and mass transfer resistance. This equation was used to interpret the dependence of the measured vapor pressures of n-alkanes on experimental parameters such as carrier gas flow, saturator dimension, surface area and diffusion coefficient. Based on the results of these studies the different conditions which allow unbiased measurements of equilibrium vapor pressures or binary diffusion coefficients were identified.

The principle of these measurements of equilibrium vapor pressures are those of established gas saturation methods. However, the variant developed here has several advantages over previously described methods. The use of GC-FID, a very sensitive and selective analytical method, allows fast measurements of very low vapor pressures and the selectivity of GC-FID measurements avoids interference from high volatility impurities of the studied materials. The low detection limits of GC-FID allow vapor pressure measurements down to $\sim 10^{-5}$ Pa. The use of a GC separation also provides the possibility to study equilibrium vapor pressures of mixtures. The wide dynamic range of the FID and the flexibility of GC allows to measure vapor pressures over a range of more than 7 orders of magnitude.

The vapor pressures of four n-alkanes were measured over wide temperature ranges and the temperature dependence of the equilibrium vapors pressures was used to determine evaporation enthalpies. The measured vapor pressures as well as the derived standard evaporation enthalpies are consistent with data from literature.

The partial vapor pressures of the n-alkanes in n-alkane mixtures were determined and their activity coefficients derived from comparison with predictions for ideal solutions. As expected, for mixtures of n-alkanes, within the uncertainty of the measurements, the activity coefficients were unity.

Several experiments were conducted measuring vapor pressures while changing the saturator temperature running a temperature program. It was found that for low heating rates in the range of 0.1 K/min the vapor pressures measured during the temperature program are effectively identical to isothermally determined equilibrium vapor pressures.

The binary diffusion coefficient for n-alkane C_{20} and C_{28} in helium were determined for a range of temperatures. Diffusion coefficient data for heavy n-alkanes in literature are scarce and experimentally determined diffusion coefficients for n-alkanes heavier than C_{18} are not available. The measured diffusion coefficients show good agreement with extrapolation of published diffusion coefficients for n-alkanes to higher carbon numbers.

The method used here is in principle a variant of the established evaporation tube method. The advantage of the newly developed variant is that it provides a relatively simple, reliable procedure to measure binary diffusion coefficients for heavy organic compounds with low vapor pressures, which is a significant experimental challenge for many of the established techniques to measure binary diffusion coefficients.

ACKNOWLEDGEMENTS

LIST OF TABLES

LIST OF FIGURES

COMMONLY USED ABBREVIATIONS AND NOTATIONS

Commonly known abbreviations and notations are not described in the following list.

TDI	Thermal Desorption Instrument
TC	Total carbon
OC	Organic carbon
EC	Elemental carbon
α	Extent of conversion
k (T)	Temperature dependent rate constant
$f(\alpha)$	Mathematical function named reaction model
A	Pre-exponential factor
E^a	Activation energy
ΔE^{des}	Desorption enthalpy
ΔE^{vap}	Vaporization enthalpy
$(\Delta m/\Delta t)_E$	Net evaporation rate
$(\Delta m/\Delta t)_D$	Diffusive mass flow rate
$(\Delta m/\Delta t)_R$	Mass flow rate removed by carrier gas
F	total carrier gas flow rate under room temperature and pressure
F*	total carrier gas flow rate under saturator temperature and pressure
φ	Evaporation coefficient
P_m	Measured partial vapor pressure in carrier gas
P_s	Equilibrium vapor pressure
P_v	Vapor pressure directly above sample surface
S	Surface area of the sample
k	Desorption rate constant
θ	Surface coverage
n	Reaction order
ν	Pre-exponential frequency factor for adsorption
D	Diffusion coefficient
C_m	Vapor concentration in carrier gas under steady-state
C_v	Vapor concentration at sample surface at steady-state
X	Diffusion distance from sample surface to carrier gas stream
γ_B	Activity coefficient
x_B	Mole fraction of B in the mixture
A_e	Effective area of PM_{10} high volume sampler filter
A_p	Area of punched sample
PA	Peak area counts
RF	Response factor
B	Carbon amount of field blank filter with an area of A_p
V	Sampling volume

1. Introduction

Atmospheric particulate matter (PM) is one of the major air pollutants in urban areas (Jacobson et al., 2000; Turpin et al., 2000). Particulate carbonaceous substances, which constitute a significant fraction of fine aerosol, are classified as total carbon (TC), organic carbon (OC), elemental carbon (EC) or black carbon (BC) (Kleefeld et al., 2002; Chow et al., 2002). The definitions of OC, EC are operational and depend on the technique used to isolate EC. Carbonaceous aerosol has been linked with adverse health effects (Allen et al., 1998; Reisen et al., 2005). It can affect visibility, surface temperature, cloud formation, and precipitation (Parungo et al., 1992; Eatough et al., 1996; Penner, et al., 1996). The concentrations of atmospheric trace gases can be influenced through heterogeneous chemical/catalytic reactions on the particles (Chang et al., 1975, 1982; Novakov et al., 1974, 1984; Gundel et al., 1989). Black carbon, the strongest light absorber commonly encountered in the atmosphere, is a primary pollutant emitted during incomplete combustion (Adams et al., 1990a, 1990b; Hansen et al., 1993). EC has a long lifetime in the atmosphere because of its inertness; the only way to remove EC from the atmosphere is through dry or wet deposition (Kadowaki 1990; Kim et al., 1999).

Primary OC is mainly formed during combustion while secondary OC originates from gas to particle conversion of volatile organic compounds to low vapor pressure compounds and condensation. The concentration of particulate OC, EC, as an important bulk property can only offer partial information on the atmospheric effects and life cycle of carbonaceous aerosol. For better understanding their environmental behavior, it is necessary to characterize specific organic species. However, for most of the organic speciation techniques, it is a challenge to obtain bulk properties. The fate, abundance and transport of organic compounds are governed by physico-chemical and thermodynamic parameters, such as chemical properties, concentrations, volatilities, diffusion and activity coefficients. Therefore, it is essential to measure the above parameters for quantitatively understanding of the many environmental processes determining concentration and composition of atmospheric particulate organic matter (POM). One motivation for this research is to determine these parameters, specifically vapor pressure and diffusion coefficients.

Thermal desorption is the most often used method among many kinds of techniques for measuring particulate OC and EC (Gustafsson et al., 1997; Hitzenberger et al., 2006; Minoura et al., 2006). TD measures EC based on its chemical/thermal inertness and there are great varieties of thermal methods available today differing in the EC isolation method: 1 Carbonaceous component is analyzed in an oxidative atmosphere throughout the entire analysis process under two-step temperature program, and the different temperature are used to differentiate between OC and EC (Rupprecht et al., 1995; Holler et al., 2002); 2. OC is removed by a pre-combustion step under specific conditions, and the remaining carbon is defined as EC (Gelinas 2001; Hitzenberger at al. 2006); 3. OC can be measured under temperature programmed heating in He or O_2/He atmosphere, the residue carbon is defined as EC (Countess 1990; Minoura et al 2006); 4.

OC and EC are separated by selectively oxidation using a MnO_2 catalyst at different temperatures (Fung 1990); 5). In an oxygen free atmosphere, the charring of some organic compounds causes bias, The charring is often corrected by an optical technique - thermal/optical reflectance (Cao et al., 2004; Chow et al., 1993, 2001, 2004.) and/or thermal/optical transmittance (Widmann et al., 2005; Arhami et al., 2006). It is worthy to note that because of the complex thermal and chemical natures of PM samples, the precise determination of OC, EC is still one of the most difficult challenges.

Thermal desorption is widely used to extract volatile, semi-volatile organic compounds from various absorbing matrices such as urban dust and particulate matter on filters etc (Kos et al., 2006; Williams et al., 2006; Banar et al., 2007; Tolgyessy et al., 2007). It has advantages over conventional organic solvent extraction method, such as simplicity, speed, high extraction efficiency, small sample size, and reduced risk of contaminations. Due to numerous organic compounds contributing to OC in atmospheric PM and the complex processes responsible for releasing organic compounds from the samples collected on filter, however, it is not possible to identify the individual compounds from a thermogram alone. When thermal desorption couples to mass spectrometry (MS) (Kamruddin et al., 2003; Meszaros et al., 2007) or Fourier transform infrared spectrometry (FTIR) (Li et al., 2001; Materazzi et al., 2006), the time and/or temperature dependence of evolved gas profiles can be obtained. Gas Chromatography is the most widely used technique to conduct compound specific measurements, either in combination with solvent extraction or thermal desorption extraction procedures. Since thermal desorption is a relatively slow process and high resolution GC requires the sample to be injected as a sharp symmetrical band, the evolved gases have to be collected and/or focused by an online or offline trap (Jansen et al., 1988; Campostrini et al., 1996; Waterman et al., 2000; Schnelle-Kreis et al., 2003; Williams et al., 2006; Guo et al., 2007). Thermal desorption -GC techniques are able to identify the evolved compounds and the time and/or temperature dependence of gas evolution profiles can be provided with various time resolutions. Coupling thermal desorption to GC or GC/MS via an online trap allows separation of, organic compounds extracted from PM on filters as well as their identifications, and quantitative analysis. Thus it is possible to obtain organic speciation and to obtain bulk properties at the same time.

The measurement of vapor pressure over a range of as much as 12 orders of magnitude (10^7 to 10^{-5} Pa), has been underway for over a century. Numerous techniques exist for measuring vapor pressures, but no single technique is capable of measuring the entire range. Summaries of vapor pressure measuring techniques are given by Weissberger (1959) and Hala et al. (1967). The techniques that have been widely applied include: static (manometric) (Chirico et al., 1989; Morgan et al., 1994); ebulliometric (boiling or dynamic) (Gregorowicz et al., 1985; Chirico et al., 1989); Knudsen/Torsion effusion (Knudsen 1909; Piacente et al., 1991, 1993); correlation gas chromatography (CGC) (Jensen et al., 1966; Bidleman 1984; Chickos et al., 2003, 2004) and gas saturation (transport, transpiration or flow). The gas saturation (GS) method is generally considered the most accurate experimental method for low vapor pressures. Although the gas saturation method was proposed more than a century ago (Regnault 1845; Verevkin 2004; Vasiltsova et al., 2005), only its more recent coupling with highly sensitive analytical techniques (such as GC, FID etc) allowed its wide use to measure low vapor pressures. It is well-known that carrier gas flow rate, saturator dimensions and sample surface area are critical factors for measuring equilibrium vapor pressures, but there is no theory available today to interpret the relationships among these factors. The accurate measurement of very low vapor pressures is challenging and time-consuming, especially for refractory organic compound at low temperature. If highly volatile impurities exist in the test material, the result will be significantly affected because none of above methods except CGC has the ability to distinguish the contributions to vapor pressure from the impurities or test material. When a GC in combination with a trapping procedure is used, the separation power of GC and high sensitivity of GC-detectors such as the FID, many disadvantages of the above methods can be overcome, and it is possible to measure extremely low equilibrium vapor pressures of pure substances or components of a complex mixture.

Many methods exist for measuring binary gas diffusion coefficient. The most used methods are closed tube (Baranski et al., 2003; Beatty 1969), two-bulb apparatus (Malinauskas 1965,1966), point source (Strehlow, 1953; Walker et al., 1960), GC (Rouholahnejad et al., 2006; Zeng et al., 2006; Zhao et al., 2006) and evaporation tube (Stefan 1873; Kwon et al., 2003, 2004; Erbil et al., 2002). Among the aforementioned methods, no method has the potential to be applied to very heavy organic compounds.

For the evaporation tube method, the sample loss or concentration in a carrier gas is measured by trapping and weighing; the change of liquid height in the vertical tube, an ionization sensor etc. When combining the evaporation tube with GC and trapping the measurement of diffusion coefficients for pure heavy compounds or a component in a mixture becomes possible.

In this work, heavy n-alkanes are used as model substances because of their thermal stability, non-toxicicity and commercial availability. A thermal desorption instrument (TDI) was developed. TC, OC and EC concentrations of some PM samples were measured and the thermal behavior of some samples were investigated. An automatic cryogenic online trap was designed to couple TDI and GC. Using this TDI/GC system, studies of the thermal behavior of POM samples, individual components in the sample, OC concentration measurement and characterization of n-alkanes in PM samples were conducted. A simple theoretical equation was derived both for gas saturation and evaporation tube method; and compared with experimental observations. The equilibrium vapor pressures of n-alkane C_{20}, C_{26}, C_{27} and C_{28} in a wide temperature range were measured and compared with literature data. The activity coefficients of the components in binary and ternary n-alkane mixtures were determined. Finally, the diffusion coefficients of n-alkane C_{20} and C_{28} were measured and the relationship between temperature and diffusion coefficient was investigated.

2. Theory

2.1. Thermal Analysis

Thermal Analysis is "A group of techniques in which a physical property of a substance and/or its reaction products is measured as a function of temperature whilst the substance is subjected to a controlled temperature program." (Mackenzie 1982). Depending on the sample, thermal analysis may involve melting, sublimation, evaporation, dehydration, desorption, solid-state and other reactions. In this work, the evolved gas analysis (EGA) is used. The equipment used is a thermal desorption instrument (TDI) and TDI-GC on-line coupling.

Unlike for homogeneous reactions, bulk concentration measurements can not be directly used to characterize solid-state reactions, it is replaced by an extent of conversion or fraction reacted (α). The kinetics of solid-state reaction is often expressed by a mathematical function and a temperature dependent rate constant, mostly based on the Arrhenius equation, as shown in Equation (Vyazovkin 2000) (2.1):

$$(\frac{\mathrm{d}\alpha}{\mathrm{dt}}) = k(T)\, f(\alpha) \quad \textit{and} \qquad k(T) = \mathrm{A}\exp(-\Delta\,\mathrm{E}^{a}/\mathrm{RT}) \qquad (2.1)$$

Where α is the extent of conversion at time t; *k* (T) is the temperature dependent rate constant; *f* (α) is a mathematical function which is characteristic for a specific reaction model to describe the dependence of the reaction rate on the extent of conversion; A is the pre-exponential factor for the rate expression and ΔE^a the activation energy. The concept of a reaction model connects characteristic, measured α vs t or dα/dt vs t plots with specific processes. The experimental data can be compared with a set of model plots. Based on selection of the model that reproduces the observation, kinetic parameters such as the pre-exponential factor and activation energy and the reaction model parameters, sometimes also called parameter triplet, can be estimated (Ozawa 1970; Flynn 1992).

A simple example for a reaction model can be derived for evaporation processes. Evaporation, its kinetics is zero-order, is an important process in thermal analysis. n-alkanes undergo evaporation without thermal decomposition under 673 K when carbon number (N) is less than 100 (Wall *et al.*, 1970; Vega et al.,1996). From kinetic theory, the net evaporation rate (mass per unit time and area) is derived as Equation (2.2) (Langmuir 1913a,b; 1916; Xia *et al.*, 1994).

$$\left(\frac{\Delta \mathrm{m}}{\Delta \mathrm{t}}\right)_{\mathrm{E}} = \varphi \mathrm{S}\,(\mathrm{P_s} - \mathrm{P_v})\sqrt{\mathrm{M}/(2\pi \mathrm{RT})} \qquad (2.2)$$

Where :$(\Delta m/\Delta t)_E$ - net evaporation rate; φ - evaporation coefficient, expressing the ratio of measured and calculated evaporation rates; P_s - equilibrium partial pressure of sample; P_v - partial pressure directly above sample surface; M - molar weight of the sample; R - ideal gas law constant; S - surface area of the sample. T - absolute temperature.

For desorption from surfaces the rate can be expressed by Equation (2.3) (Paserba *et al.*, 2001):

$$-\frac{\Delta\theta}{\Delta \mathrm{t}} = k\theta^n = \nu \exp\left(-\frac{\Delta E^*}{RT}\right)\theta^n \qquad (2.3)$$

Where: k is desorption rate constant; θ is the adsorbate coverage of surface; n is the reaction order; ν is a pre-exponential frequency factor for desorption; n is zero for multiple and one for monolayer coverage. ΔE^* is desorption enthalpy (ΔE^{des}, n=1) or vaporization enthalpy (ΔE^{vap}, n=0). The opposite process to desorption is adsorption which occurs when a vapor or liquid solute accumulates on a surface to form a film of the molecules. The adsorption process is usually classified as physisorption and chemisorption. In physisorption, only weak interaction exists between the adsorbate and substrate. This force is relatively small, usually equivalent to the enthalpy of condensation. Physisorption is characterized by occurrence at low temperatures, weak interaction forces, formation of multilayers, low desorption enthalpy and activation energy, reversibility. In chemisorption, the molecules attach to the surface by forming strong, often covalent bonds. The enthalpy of chemisorption is much greater than that of physisorption. Chemisorption is characterized by occurring at high temperature, strong interaction forces, formation of monolayers, high desorption enthalpy and activation energy and reversibility only at high temperature.

The evolved gases and involved processes in a thermal analysis depend on the type of carrier gas, temperature and sample composition. In this work, OC is measured in helium carrier gas on the assumption that EC is no-reactive under inert gases, and total carbon (TC) is measured by combusting the carbonaceous materials under high temperature in He/Air mixture. In part of this study the carbon in the evolved gases are oxidized catalytically to carbon dioxide, reduced to CH_4 in the presence of an excess of hydrogen and CH_4 measured by flame ionization detector (FID). This method and many similar methods described in literature (Dan et al; 2004, Minoura et al; 2006) for analysis of POM only allows determining total carbon evolved, but does not provide direct information on the chemical composition of the evolved has.

2.2.Thermodesorption-GC Coupling

Although compounds of different volatility or reactivity show different thermodesorption behavior, the limited resolution of thermodesorption does not allow compound specific analysis for complex samples such as atmospheric PM. For speciation purposes, a second compound specific analysis (2nd dimension) is needed. A suitable technique is GC. In this study evolved organic substances from thermal analysis are collected by a trap for a given time or temperature interval and then separated by GC. The sampling intervals and the frequency of the GC-analysis is fast compared to the change of signal from the TDI, similar to comprehensive 2-D GC.

The separation in normal GC analysis is conducted by one column. In traditional comprehensive 2-D GC, the separation conducted in two analytical GC columns with different selectivity, often called the first and the second dimension. In this work, however, thermal desorption is used as the first dimension which has only limited separation power and low time resolution. The transfer and focusing of sample fractions from the first dimension, which is necessary to achieve good resolution for the GC-analysis, is achieved by a cryogenic online trap which consists of a piece of GC column which can be cooled by injection of liquid nitrogen. By modulating the trap temperature, evolved gases from the TDI are alternately collected in the trap or injected onto GC-column for analysis.

2.3.Measurements of Partial Pressure and Diffusion Coefficient

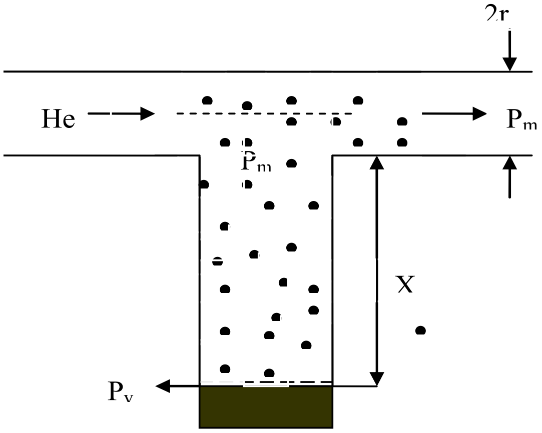

Figure 2.1. Schematic of the saturator

In the gas saturation method for measuring vapor pressure (Regnault 1845), carrier gas is passed through or over the test material. The concentration of test material in the carrier gas is determined. The equilibrium vapor pressure is obtained by choosing experimental conditions under which the pressure in the carrier gas is very close to equilibrium. This implies that the influence of mass transfer limitations on the partial pressure of the evaporating substance in the carrier gas can be neglected. A schematic depiction of possible limitations due to mass transfer is in Figure 2.1. The mass transfer processes include evaporation, diffusion and transport inside the saturator. Sample evaporates from the surface, diffuses into the carrier gas; and the carrier gas transfers the evaporated material to the detection system.

Assuming the average concentration of sample molecules in the carrier gas is C_m and the concentration gradient in the carrier gas flow is small compared to the gradient along distance x, the mass flow can be described according to the diffusion theory (Fick's law) as equation (2.4):

$$\left(\frac{\Delta \mathrm{m}}{\Delta \mathrm{t}}\right)_{\mathrm{D}} = -\mathrm{M\,D\,S}\frac{\Delta C}{\mathrm{x}} = -\mathrm{M\,D\,S}\frac{(C_{\mathrm{m}} - C_{\mathrm{v}})}{\mathrm{x}} \qquad (2.4)$$

Where: $(\Delta m/\Delta t)_D$ - diffusive mass flow rate; D - diffusion coefficient; S-sample surface area; C_m - concentration in carrier gas; C_v - vapor concentration at sample surface; x - diffusion distance from sample surface to carrier gas stream.

Within the carrier gas, transfer can be duo to flow of the carrier gas or molecular diffusion. However, for the conditions used in this work the mass transport in the carrier gas will be dominated by the carrier gas flow. Another assumption is that the carrier gas has negligible solubility in sample and thus does not change the equilibrium vapor pressure. For the carrier gas (He) and temperature (room temperature and higher) used here this condition is met. Then Equation (2.5) can be derived:

$$\left(\frac{\Delta \mathrm{m}}{\Delta \mathrm{t}}\right)_{\mathrm{R}} = \mathrm{MF}C_{\mathrm{m}} = \frac{\mathrm{MF\,P_m}}{\mathrm{RT}} \qquad (2.5)$$

Where: $(\Delta m/\Delta t)_R$ - mass flow rate removed by carrier gas; P_m – measured partial pressure of sample in carrier gas ; F - total carrier gas flow rate.

When the signal is stable, that is steady state achieved, $(\Delta m/\Delta t)_E = (\Delta m/\Delta t)_D = (\Delta m/\Delta t)_R$ and Equation (2.6) is obtained by combining Equation (2.2), (2.4) and (2.5).

$$P_m = \frac{P_s}{1+\left(\frac{x}{D} + \sqrt{2\pi M / \varphi^2 RT}\right)\left(\frac{F}{S}\right)} \qquad (2.6)$$

It was stated that φ=1 for all pure liquids, and that various theories predicting or explaining φ < 1 deserve only historical interest (Cammenga 1980). For the current experimental conditions, the biggest possible value of $(2\pi M/RT)^{1/2}$ is 3.2×10^{-2} s/m when T = 298 K and M = 394g/mol (for C_{28}). x 0.05 - 0.1 centimeter or more (refer to experimental section). For C_{28}, measured D is 0.05 cm^2/s under 2.3 atmospheres, 463 K (result section). Thus the $(2\pi M/RT)^{1/2}$ will be 30 times smaller than x/D and can be ignored. Therefore Equation (2.6) can be used to study the volatilization of pure substances and similar cases using a simplified Equation (2.7):

$$P_m = \frac{P_s}{1+\left(\frac{x}{D}\right)\left(\frac{F}{S}\right)} \qquad \text{or} \qquad \frac{1}{P_m} = \frac{1}{P_s} + \left(\frac{x}{D\,S\,P_S}\right)F \qquad (2.7)$$

From Equation (2.7), the equilibrium partial pressure can be derived from the measured partial pressure and experimental parameters. Ideally, the measured partial pressure should be effectively equal to the equilibrium partial pressure, which is the case for (x/D)(F/S)<< 1.

If the equilibrium vapor pressure is known, the measured partial pressure can be used to determine diffusion coefficients as can be seen from rearranging Equation (2.7).

$$\frac{S\left(P_S/P_m-1\right)}{F} = \frac{x}{D} \qquad \textit{or} \qquad D = \frac{x\,F}{S\left(P_S/P_m-1\right)} \qquad (2.8)$$

However, for practical applications to measure diffusion coefficients the experimental conditions have to be such that Ps/Pm is substantially larger than unity to reduce the errors resulting from measurement uncertainties.

When applied to a pure compound B and a mixture containing B, Equation (2.7) can be rewritten as Equation (2.9) and (2.10) according to Raoult's law respectively:

$$\mathrm{P}_{\mathrm{m},pure}{}^{\mathrm{B}} = \frac{\mathrm{P}_{\mathrm{s}}{}^{\mathrm{B}}}{\left(1+\dfrac{\mathrm{x\ F}}{\mathrm{D\,S}}\right)_{\mathrm{C\text{-}1}}} \quad (2.9) \quad and \quad \mathrm{P}_{\mathrm{m},mixture}{}^{\mathrm{B}} = \frac{\mathrm{P}_{\mathrm{s}}{}^{\mathrm{B}}\, x_{\mathrm{B}}\, \gamma_{\mathrm{B}}}{\left(1+\dfrac{\mathrm{x\ F}}{\mathrm{D\,S}}\right)_{\mathrm{C\text{-}2}}} \qquad (2.10)$$

γ_B is the activity coefficient; x_B is mol fraction of B in the mixture; P_s^B is the equilibrium partial pressure of pure B; $P_{m,pure}^B$ is the partial pressure of pure B measured under condition C-2; $P_{m,mixture}^B$ is the partial pressure of B above the mixture measured under condition C-1. C-1 and C-2 represents the experimental conditions (e.g. x, F, D and S). If the experimental conditions for measuring $P_{m,pure}^B$ and $P_{m,mixture}^B$ are similar, Equation (2.11) is derived from Equation (2.9) and (2.10):

$$\gamma_{\mathrm{B}} = \mathrm{P}_{\mathrm{m},mixture}{}^{\mathrm{B}} \Big/ \left(x_{\mathrm{B}}\ \mathrm{P}_{\mathrm{m,pure}}{}^{\mathrm{B}}\right) \qquad (2.11)$$

It suggests that γ_B can be derived when $P_{m,pure}^B$ and $P_{m,mixture}^B$ are determined under similar conditions without even knowing the exact values of P_s^B and (xF/DS).

3. Experiment

3.1. Thermal Desorption Instrument

3.1.1. Instrumentation

The schematic of the thermal desorption instrument (TDI) is shown in Figure 3.1. The TDI mainly consists of a sample reactor, a detection system comprised of catalysts and a FID (Varian, Inc.), flow rate and temperature controllers, and a signal processor. The sample reactor was made up of two concentric quartz tubes with three connections on one end and one on another. The two layers of the reactor were connected by a small hole. Sample was loaded into a small quartz boat and placed in the reactor close to the thermocouple. The reactor was heated by a ceramic cylindrical radiant heater (Omega Engineering, Inc.). The heating was controlled through a proportional-integral-derivative (PID) controller. Temperature control of the reactor was tested by a digital thermometer (model 8110-00, Omega Engineering, Inc.) which was placed inside the inner layer of the reactor at the same point where the sample was located. The temperatures of reactor, oxidation and reduction catalysts were monitored by thermocouples continuously. The oxidation catalyst was MnO_2 (Sigma-Aldrich) and the reduction catalyst was Nickel (Sigma-Aldrich). Helium was used as transfer gas and was always flowing through the system. Controlled by a remotely operated valve air can be introduced either at the beginning of the reactor or between the reactor and the oxidation catalyst. Hydrogen was added between the oxidation and reduction catalyst. The typical flow rates for the TDI were: Helium 25 ml /min; air 6 ml/min and hydrogen 15 ml/min. There was a split between the oxidation and reduction catalyst, which allowed adjusting the split ratio between vent and reduction catalyst by a needle valve.

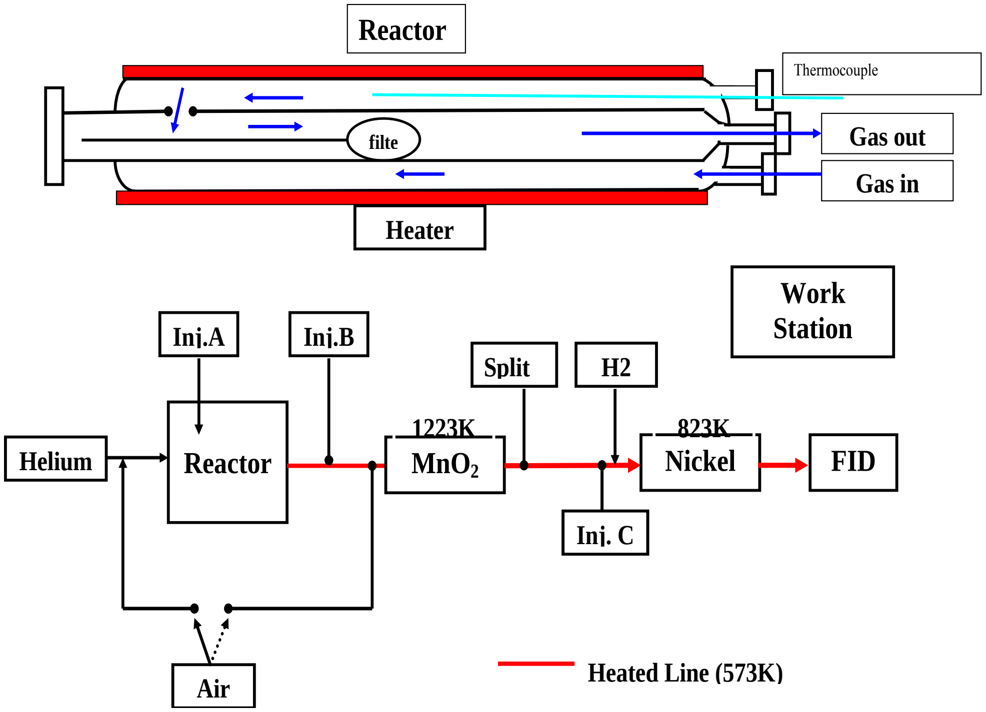

Figure 3.1. Schematic of the thermal desorption instrument (TDI).

There were three injection ports (Inj. A, B and C) as shown in Figure 3.1, which were used to test and calibrate the TDI. For quick cooling the reactor, compressed air can be introduced between the radiant heater and the reactor. The software controlling the TDI was based on Labview (International Instruments Inc.) and can fulfill the following functions: 1) temperature control of the reactor, catalyst, transfer lines and detector block; 2) data collection and storage; 3) set up, save and load methods (including reactor temperature program); 4) display data, run time, settings and actual temperatures; 5) adjust FID amplifier gain, FID offset, and control valve positions automatically.

3.1.2. Calibration and Testing

The catalysts were tested by injecting 200 μL CO_2 (1645 ppm) or CH_4 (3597 ppm) standard gases, which were prepared from pure CO_2 and CH_4, respectively and calibrated by a reference standard supplied by the Meteorological Service of Canada. It was found by comparing the signals of CO_2 and CH_4 injected at port C that CO_2 can be reduced to CH_4 effectively when the reduction catalyst temperature was above 773 K. By keeping the reduction catalyst at room temperature, it was found that CH_4 injected at port B can be completely oxidized above an oxidation catalyst temperature of 1173 K. Standard operating temperatures for the reduction and oxidation catalyst are 823 K and 1223 K, respectively. The TDI was calibrated by injecting CH_4 and CO_2 standard gases at port B and C. The split ratio was determined by comparing the responses of CH_4 or CO_2 injected at port B, C.

Various TDI methods differing in reactor temperature program and carrier gas composition are summarized in Table 3.1. The temperature program included initial temperature (IT), final temperature (FT) and heating rate (β). As shown in Table 3.1, total carbon and organic carbon were measured by TC, or OC method in which the carrier gas was a He/Air mixture and helium, respectively. After the measurement of OC, the samples were also analyzed using method TC to determine EC from the difference of the signals. Therefore, the definition of OC is the carbon evolved in a helium atmosphere below the temperature of 1173 K. The definition of EC is the carbon which survived heating in helium to 1173 K. Examples, showing the measured reactor temperatures as function of time for different methods are shown in Figure 3.2. A summary of the methods used for TDI measurements is given in Table 3.1.

Table 3.1. Summary of TDI Methods.

Method	IT	Hold T and time		FT	β	Carrier gas composition	
	K	K	min	K	K/min	T<663 K	T>663 K
TC- 30	323			1023	30	He/Air	
OC-XX*	323			1023	XX	He	
OC-XX-Air	323	663	10	1023	XX	He/Air	He
OC-XX-He	323	663	10	1023	XX	He	He
	IT	FT	β (T<553 K)		β (T>553 K)		Carrier gas
TC	323	1173	10		30		He/Air
OC	323	1173	10		30		He

XX = 5, 10, 15, 20, 30 and 40; IT and FT – initial and final temperature; β – heating rate.

A piece of filter with an area of 1.1 cm^2 was punched out from high volume PM filters and placed in the TDI reactor. Samples were run using different TDI methods. The instrumental and quartz fiber filter blanks were determined by running the TDI under TC-30 or OC-30 methods without and with placing filter pieces in the reactor. The FID signal was integrated for the whole run time interval and the blank values were calculated from CH_4 calibration data. Filters of different sizes were cut out from high volume sampler quartz fiber filters. The filters were pre-fired at 1023 K for 24 hours under a flow of 150 ml/min compressed synthetic air in an oven (muffle furnace, Fisher Scientific). The filters were sealed in a glass jar and stored in a freezer. Filters and sample boat were handled using fired (673 K) stainless steel tweezers. Examples of thermograms of a SONTAS PM sample are shown in Figure 3.3.

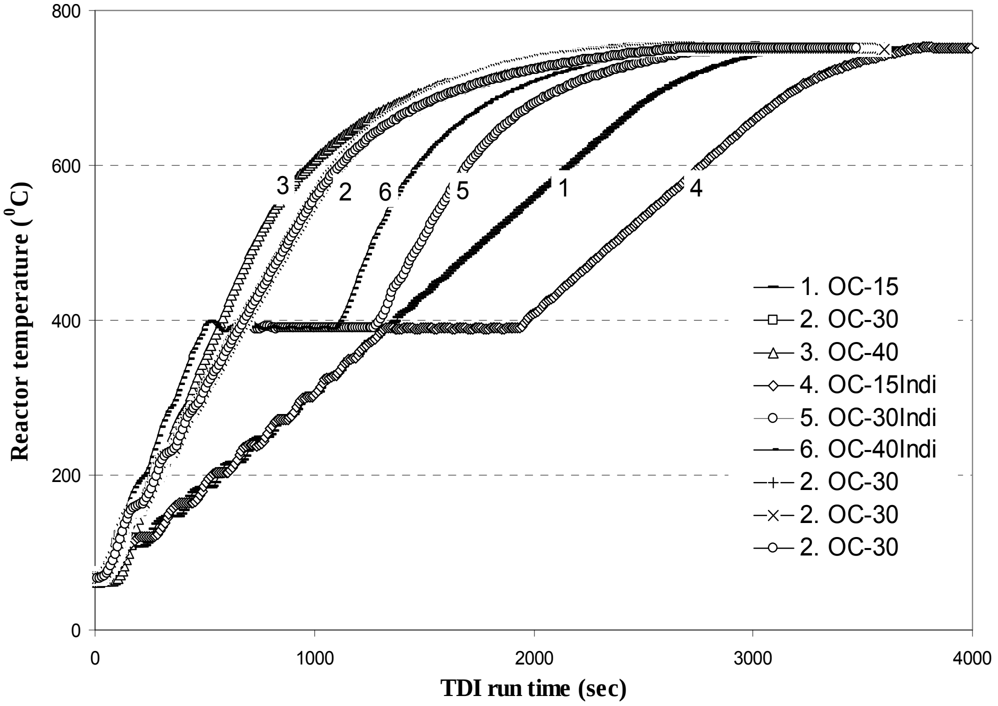

Figure 3.2. TDI temperature profiles with different heating rate and holding time at 663 K.

The TDI was tested using potassium hydrogen phthalate (KHP), mannitol, and n-alkanes solutions spiked into quartz sample boat. Some mannitol samples were measured at a transfer line temperature of 673 K and reactor temperature of 1173 K. The composition of the test solutions are shown in Table 3.2. The thermal behavior of n-alkanes, KHP, and mannitol were studied by OC-XX, OC-XX-Air and OC-XX-He. The carbon mass was calculated by:

Carbon Mass = PA/RF – B

where PA is peak area counts; RF is response factor and B is filter blank value.

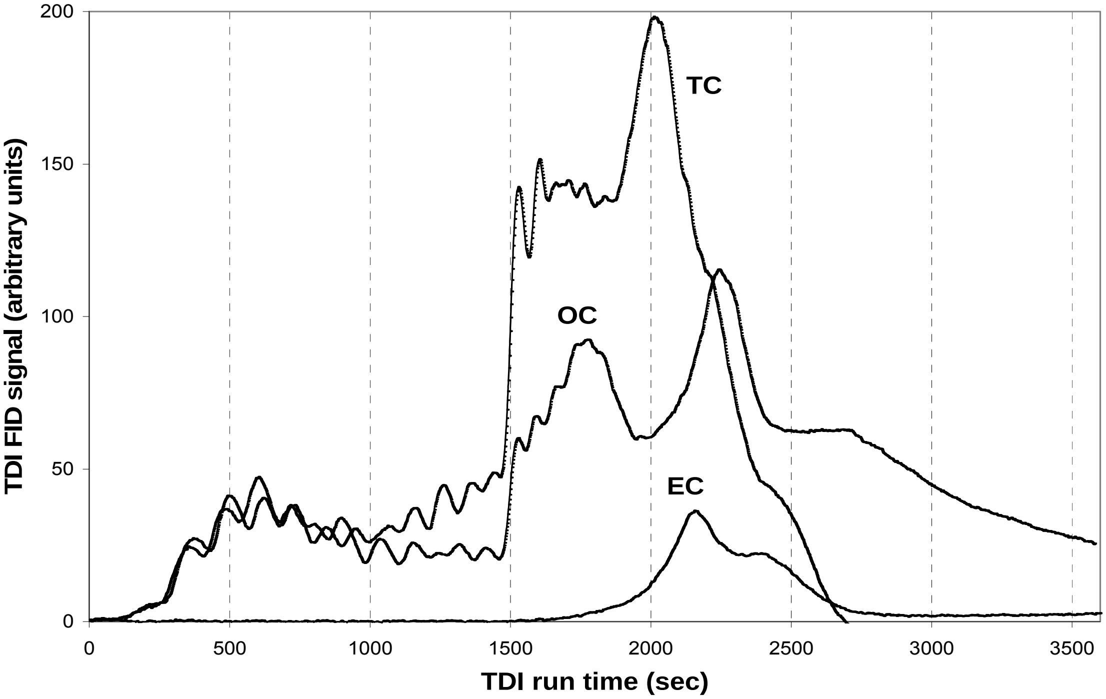

Figure 3.3. Examples of TC, OC and EC thermograms of a SONTAS PM sample.

3.1.3. Analysis of PM Samples

PM samples were collected on 8” × 10” Quartz fiber filters (Pallflex Products, Putnam, CT) using high volume air sampler equipped with PM_{10} head. Samples were collected at Hamilton during the Southern Ontario Aerosol Study (SONTAS) and at York

Gateway Tunnel, downtown Toronto in 2000. Average sampling flow rates were 1.13 m^3/min, and generally samples were collected for 24 hours. Prior to sampling, new filters were pre-fired as described above. After sampling, the filters were divided into eight parts and stored at –20°C in gas-tight glass jars. TC, OC and EC concentrations of SONTAS sample were measured. As a routine quality control, the following procedures were implemented: 1) Methane calibration after every single measurement to check the effectiveness of the catalysts and the split ratio; 2) Every few days, a test standard prepared by spiking known masses (10 to 30 micro grams) of KHP or n-alkane test mixtures on pre-fired filters was analyzed to check the carbon recovery. The atmospheric concentration of PM carbon was calculated using Equation (3.1):

$$C = A_e \left(PA/RF - B\right) \big/ \left(VA_p\right) \qquad (3.1)$$

Where: A_e- effective area of PM_{10} high volume sampler filter; A_p- area of filter part used for analysis; PA - sample peak area counts; RF - response factor; B - Carbon mass of blank filter with an area of A_p; V - sampling volume.

Table 3.2. Composition of Test Solutions.

	Concentrations of n-alkane/hexane solutions (μg C/μl)						
n-Alkane	C_{20}	C_{21}	C_{27}	M2	M3	M14	M17
C_{18}							0.0260
C_{19}							0.0270
C_{20}	1.2580			6.2901		0.0996	0.0270
C_{21}		0.4302			0.2807	0.1005	0.0270
C_{22}						0.0981	0.0260
C_{23}						0.1097	0.0280

C_{24}				0.1274	0.0340
C_{25}				0.1061	0.0280
C_{26}			0.3510	0.0945	0.0270
C_{27}	1.5430	7.7711			0.0270
C_{28}				0.0976	0.0260
C_{29}				0.0284	0.0070
C_{30}				0.1036	0.0270
C_{31}				0.0756	0.0070
C_{32}				0.1018	0.0400
C_{33}				0.0918	0.0260
C_{34}			0.4406	0.0830	0.0280

Concentrations of KHP/water and Mannitol/water solutions (μg C/μl)

KHP	Mannitol
0.2238	0.1406

3.2.TDI/GC

3.2.1. Instrumentation

The schematic of coupling the TDI with GC is shown in Figure 3-4. It allowed the combination of two separation dimensions, the first dimension -TDI and the second dimension - online GC. The split and injector B on the TDI were removed. The GC was a Hewlett Packard 5890 with flame ionization detector and electronic pressure control (EPC). Column was DB-5MS, 5m×0.25 mm i.d. (film thickness: 0.25μm, Restek Corp.). The conventional GC injector was removed. The GC-FID signal was recorded by a PC using Chemstation software (Hewlett Packard, 1995 version). The GC was connected to the TDI reactor by a 70 cm length 1/16” Silcosteel tube (Restek Corp.) heated to 603 K through a Silcosteel reducing union (Restek Corp.).

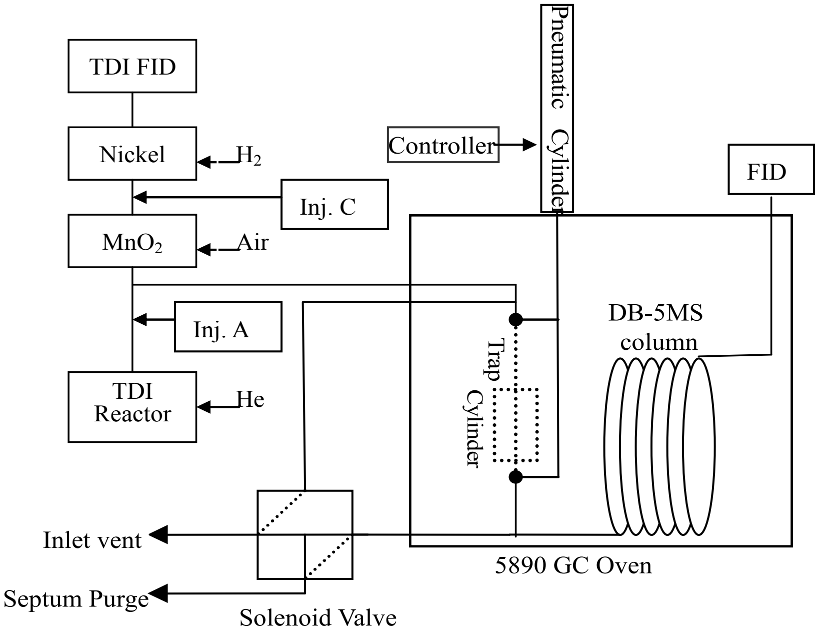

Figure 3.4. Schematic of thermodesorption-GC coupling.

An online automatic cryogenic trap which has the same function as the modulator in comprehensive 2D-GC was developed and installed at the head of the GC column. It consisted of a modified cryogenic pre-focuser (Tekran Inc.), a liquid nitrogen cooled trap, a pneumatic cylinder (BIMBA Inc.) which is operated by compressed air and controlled by solid state timers (NCC National Controls Corp.), and activated by a two position actuator with a four port valve (VICI Inc.). The trap block was made of a stainless steel cylinder (4 cm o.d. × 6 cm length) (Figure 3.5). A hole of about 1 cm diameter and 5 cm length was drilled along the axis in the center of the cylinder. The opening was sealed by soldering to form a 1 cm diameter × 4 cm long cavity inside the cylinder. A small hole was drilled at the centers of the rod's both ends and a 1/32" I.D. cupper tube was inserted and sealed. A thermal resistor was installed at the middle of the cylinder with its sensing tip close to the copper tube. The cylinder was mounted vertically inside the GC oven and a piece of DB-5MS column, which was used as online trap, was placed inside the copper tube. The fused silica tube is moved up or down (e.g. in or out of the cooled cylinder) by a pneumatic cylinder. The position of the trap and the holding time at the position was controlled by the solid state timers. Based on tests with n-alkane mixtures, the trap quantitatively focused n-alkenes when operating in a temperature range of 273 – 303 K.

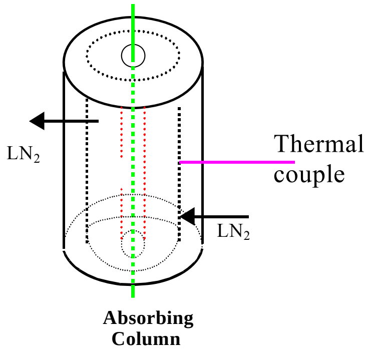

Figure 3.5. Schematic of cryogenic trap

3.2.2. Experimental Procedure

The GC was operated under constant column head pressure. The typical flow rates were F_{TDI}=65 ml/min, $F_{GC\ vent}$=16 ml/min, $F_{GC\ purge}$=2.6 ml/min and $F_{GC\ FID}$=3.0 ml/min. The TDI/GC method was set-up in such a way that for measurement of n-alkane test mixtures every collection of evolved n-alkanes from the TDI reactor throughout the entire measurement can be completely separated by GC within the given sampling interval. Therefore the TDI/GC method differs in TDI and GC oven temperature program.

An example for a TDI/GC method, Table 3.3 shows the conditions for measurements of a mixture containing 14 n-alkanes (M14, see Table 3.2). Both the TDI and GC were calibrated by methane injected at injector port A and C, and tested by test solutions of C_{21}, M3 and M14 (compositions see Table 3.2) containing 2 micro grams to 2 milligrams carbon. After a sample was placed in the TDI reactor and the cryogenic trap was cooled to the pre-set temperature, TDI, GC and the solid state timers were started simultaneously. The evolved substances transferred to the GC were collected by the trap for a given sampling interval and injected into the GC column by moving the fused silica trap out of the cooled cylinder for a short time period. The collection, and release process was automatically repeated till the end of the TDI measurement.

The TDI/GC was tested using various test solutions. As an example, the signal of 1μL of mixture M14 analyzed by the method in Table 3.3 is shown in Figure 3.6. The individual compounds were identified by their GC retention times and their masses were derived from peak area counts and the calibration.

Table 3.3. TDI/GC Method for Measurements of 14 n-Alkane Mixture.

	IT (K)	Hold time (minute)	FT (K)	β (K/min)	Timing of cryo trap Sampling (minute)	 Release (second)
TDI	313	----	553	5.0	----	----
GC	473	9	553	3.6	2.0	10

IT – initial temperature; FT – final temperature; β – heating rate.

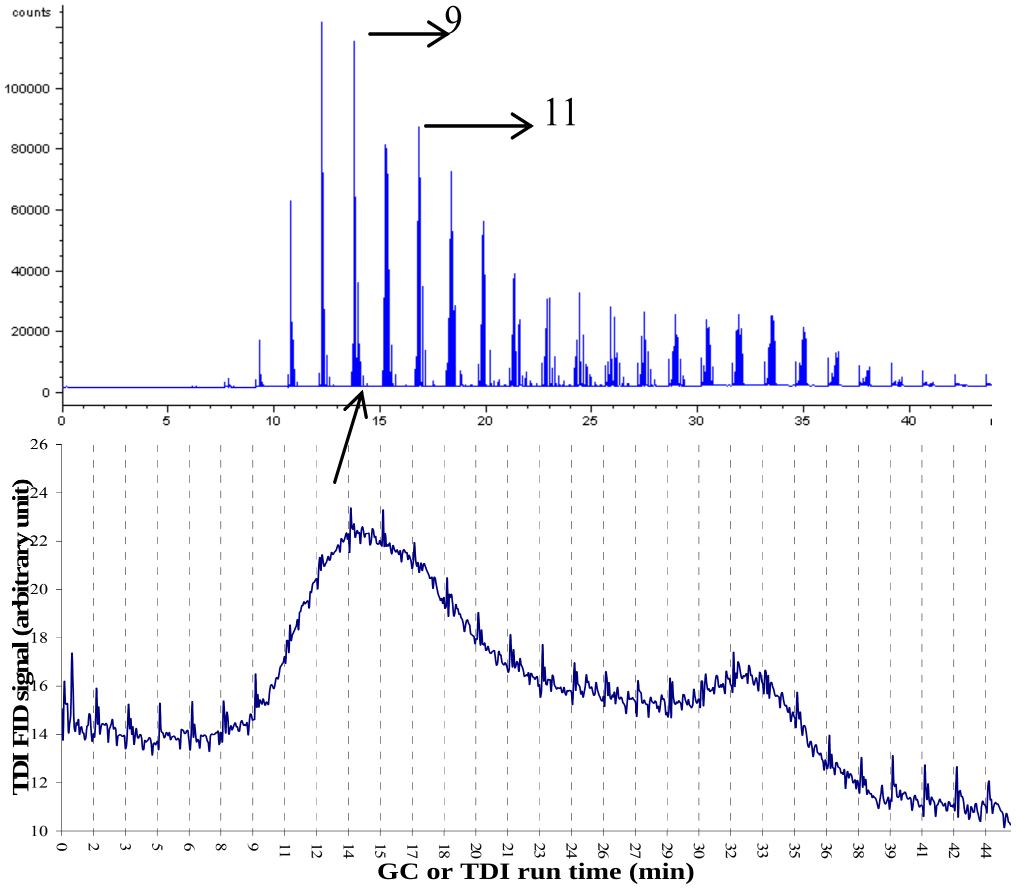

Figure 3.6. Example of GC chromatogram and TDI thermogram for measurement of 1μL of 14 n-alkane mixture.

3.2.3. Studies of n-Alkane Thermal Behavior and n-Alkanes in PM Samples

The thermal behavior of n-alkanes was studied in detail using solutions of n-alkanes (Table 3.2). Different volumes of the solutions were spiked on pre-fired quartz fiber filters (QF), small quartz glass plates or a small quartz glass boat (QG) and ambient

PM collected on quartz fiber filters. These samples were studied by the TDI/GC using the method parameters given in Table 3.3.

For studying n-alkanes in PM samples, the following changes were conducted to maximize the sensitivity: 1) no flow to the TDI FID detection system by directly connecting the TDI reactor to the online trap; 2) increasing the fraction of transfer gas ratio to the GC-FID by rising the GC column head pressure; 3) longer sampling interval (3-5 minutes) for the individual GC runs. The TDI/GC method was changed as shown in Table 3.4. The TDI/GC was calibrated by spiking different volumes of M17 on pre-fired quartz fiber filters. For the analysis of PM samples the peak area of identified n-alkanes peaks were determined for every sampling interval and converted to carbon mass using the response factors determined from the calibration. The concentrations of individual n-alkanes were calculated from the sum of the n-alkane carbon masses from all sampling intervals, the total volume of air collected on the high-volume filter and the ratio of filter area used for analysis over area of the high-volume filter.

Table 3.4. Parameters for the TDI/GC Method for Measurements of n-Alkanes in PM Samples.

	IT (K)	Hold time (minute)	FT (K)	β (K/min)	Timing of cryo trap	
					Sampling (minute)	Release (second)
TDI	313	----	553	2.0	----	----
GC	453	9	553	2.5	3.0	10

IT – initial temperature; FT – final temperature; β – heating rate.

3.3. Measurement of Partial Pressures

The instrumentation for measuring partial pressure was the same as TDI/GC shown in Figure 3.4 except that the reactor and cylindrical radiant heater were replaced by a saturator and saturator oven. As shown in Figure 3.7, the saturator was made of Quartz glass and had a length of 5”, inner diameter of ½” and wall thickness of 0.04”. The carrier gas was preheated by passing it through a 4 meter long 1/16” coiled stainless steel tube inside the saturator oven. The split flow rate at the outlet of the saturator was controlled by a needle valve. The pressure in the saturator was measured by a digital gauge (Crystal engineering Corp.). The sample boat had an inner diameter of about 6 mm and a length of about 6 cm.

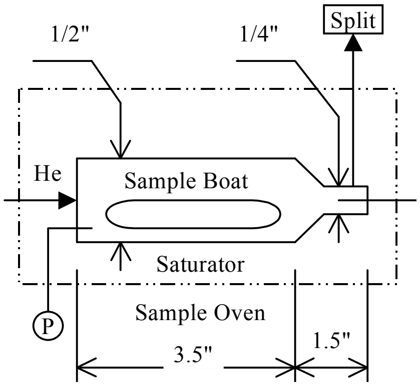

Figure 3.7. The schematic of the saturator

The saturator oven was always heated to at least 473 K for 10 minutes for the purpose of cleaning the instrument from residue contaminants. The GC-FID was calibrated by spiking eicosane or heptacosane standard solution into the sample boat (sample mass range: 0.01- 10.0 μg C). The GC oven was run isothermally at temperatures ranging from 523 K to 553 K, depending on the n-alkane studied. The sampling intervals were between 1 and 5 minutes. Except for a series of experiments to study the impact of sample size on n-alkane evaporation rate, the sample boat was always completely filled with n-alkanes.

The TDI/GC was operated in two different modes. In one mode the trap was kept at the same temperature as the GC oven. In this mode of operation the GC column acts as transfer line to the GC's FID and the measurements are not substance specific. In the second mode the trap is cooled and the partial pressure measurements are made by online chromatography. As an example, Figure 3.8 shows the FID signal as function of time for

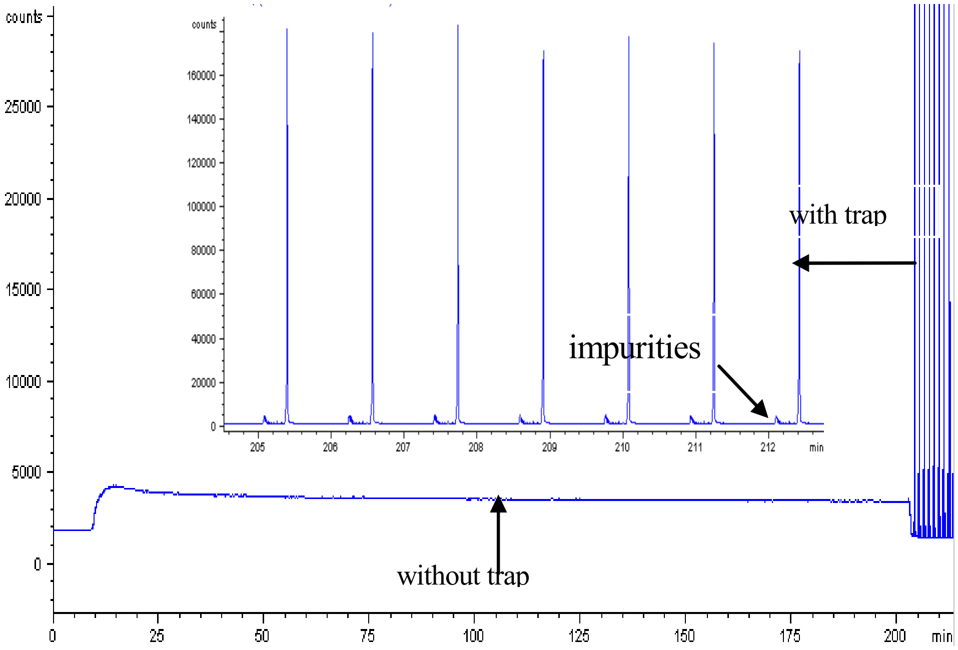

Figure 3.8. FID signal as function of time for partial pressure measurements of C_{28} at 393 K. At approximately 200 min the measurement mode was changed from continuous to trapping with GC separation. The inlay shows an enlarged view of the measurements made in GC separation mode.

measurement of the partial pressure of n-alkane C_{28} at 393 K in both modes. Partial pressure measurements were only made when the signals had stabilized and showed no detectable systematic change with time. The partial pressure was calculated as follows:

$$SR = \frac{U}{F} = \frac{U}{U + F_{SPLIT} + F_{VENT} + F_{PURGE}} \qquad (3.2) \qquad n = \frac{PA}{RF \times SR \times M} \qquad (3.3)$$

$$V = t \times F \left(\frac{P_0}{P}\right)\left(\frac{T}{T_0}\right) \qquad (3.4) \qquad P_m V = n R T \qquad (3.5)$$

where: SR - split ratio to GC FID; F_{SPLIT} - flow rate of the split; PA - peak area counts; T - saturator temperature; V - carrier gas volume during time t; t - sampling or averaging interval; F - total carrier gas flow rate measured at P_0 and T_0; P_0 and T_0 - atmospheric pressure and temperature in the laboratory; P – total pressure in the saturator; P_m - partial pressure; RF-response factor determined by calibration. The peak area is determined by either integrating the chromatographic peak for the substance which is studied (on-line GC mode) or integrating the baseline corrected FID signal for time period (continuous mode) t. For each isothermal experiment the partial pressure measurement was repeated 7 times.

In a series of experiments the dependence of n-alkane partial pressure on sample size and carrier gas flow rate was investigated. The GC/TDI conditions for these experiments are listed in Table 3.5. Different masses (0.14 to 100 milligrams) of pure C_{27}

were loaded into the sample boat and the n-alkane partial pressures were measured by method 1. For these measurements the saturator temperature was changed continuously in a temperature program. Studies of the dependence of the partial pressure on gas flow rate in the saturator were conducted for C_{20} (method 2), C_{27} and C_{28} (method 3). These measurements were conducted isothermally with the sample boat completely filled with n-alkanes.

The partial pressures of several n-alkanes were measured by TDI/GC using a temperature program for the saturator oven. The temperature program was started after the partial pressure was stable at the initial temperature. The different temperature programs are listed in Table 3.6. Partial pressures were determined by method 1 to 9 for C_{20}, 10 to 12 for C_{27} and 13 to 14 for mixtures of C_{27} and C_{28}, respectively. Mixtures of n-alkanes were studied isothermally (method 15).

The n-alkane mixtures were prepared by placing some ten (23 to 69) mg of more than one n-alkanes (C_{26}, C_{27}, C_{28}) into the sample boat. The exact masses of the individual n-alkanes were determined with an analytical balance. The partial pressures of the n-alkanes were measured using method 15 at temperatures of 433 K, 443 K and 453 K, respectively. A summary of the n-alkanes studied and the temperatures for which partial pressure measurements were conducted is presented in Table 3.7.

Table 3.5. Parameters of TDI/GC Methods for Partial Pressure Measurements.

TDI/GC method	Saturator oven IT (K)	FT (K)	β (K/min)	GC Oven Temp.(K)	F (ml/min)	Timing of cryo trap collection (min)	release (second)
1	303	473	2.0	523	22.0	1.0	10
2	----	373	----	503	17.0 to 231	1.1	10
3	----	433	----	523	8 to 161	2.0	10

IT – initial temperature; FT – final temperature; β – heating rate; F - total carrier gas flow rate.

Table 3.6. TDI/GC Methods and Oven Temperature Programs.

TDI/GC method	Saturator oven IT (K)	FT (K)	β (K/min)	GC oven Temp.(K)	F (ml/min)	Timing of cryo trap collection (min)	release (second)
1	358	413	0.1	503	11.7	2.0	10
2	358	413	2.0	503	11.7	2.0	10
3	358	413	5.0	503	11.7	2.0	10
4	413	358	-0.1	503	11.7	2.0	10
5	413	358	-2.0	503	11.7	2.0	10
6	413	358	-5.0	503	11.7	2.0	10
7	313	298	-0.1	503	11.7	2.0	10
8	298	318	0.1	503	11.7	2.0	10
9	313	338	0.1	503	11.7	2.0	10
10	316	354	0.1	503	10.7	3.0	10
11	353	316	-0.1	503	10.7	3.0	10
12	433	382	-0.1	503	10.7	5.0	10
13	398	448	0.1	503	22.0	3.0	10
14	398	423	0.1	503	22.0	5.0	10
15		*		503	22.0	3.0	10

IT – initial temperature; FT – final temperature; β – heating rate. *:the final temperature is 433, 443 and 453 K, respectively; F - total carrier gas flow rate.

Table 3.7. Samples and Temperature Ranges for Measurements.

Sample	Temperature (K)	Sample	Temperature (K)
C_{20}	298-473	C_{28}	393-493
C_{26}	373-473	C_{27}, C_{28} mixture	433, 443, 453
C_{27}	316-433	C_{26}, C_{27}, C_{28} mixture	433, 443, 453

3.4 Measurement of Diffusion Coefficients

For measuring diffusion coefficient, the tubular saturator was replaced by a quartz glass "T" piece as shown in Figure 3.9. Both the tubes of the "T" had an outer diameter of ½". The dead end tube of the "T" piece was filled to varying levels with n-alkane C_{20} or C_{28} and the apparent diffusion distance (x^a), which is the distance from the sample liquid surface to the edge of the horizontal tube. The n-alkane partial pressures were measured under isothermal conditions as well as using temperature programs for different diffusion distances and flow rates. A summary of the operating conditions is given in Table 3.8.

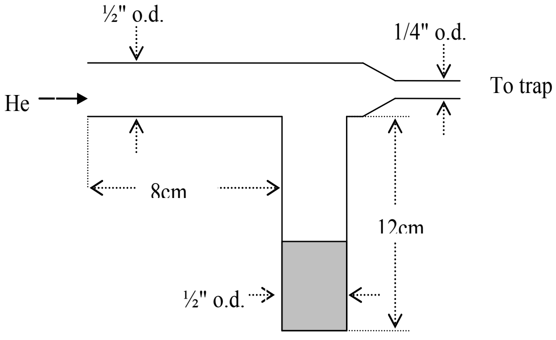

Figure 3.9 "T" type saturator

Table 3.8. TDI/GC Methods for Measuring Diffusion Coefficient.

TDI/GC method	Saturator oven				GC		Timing of cryogenic trap	
	IT (K)	FT (K)	β (K/min)	x (cm)	oven Temp.(K)	F (ml/min)	collection (min)	release (second)
C_{20}	---	423	---	0.85 to 9.50	523	8 to 140	1.1	10
C_{28}	---	463	---	1.40 to 6.45	523	19 to 88	1.1	10
C_{20}	440	464	0.2	9.40	523	21.4	1.1	10

IT – initial temperature; FT – final temperature; β – heating rate; F - total carrier gas flow rate.

4. Result

The following subchapters contain examples for the conducted measurements and tests and a summary of the most important results of the different types of experiments performed. A detailed presentation of the results is given in the attached data CD.

4.1 TDI Performance and Applications

4.1.1. TDI Calibration

Calibration curves showing the TDI-FID peak area counts against injected carbon mass for six calibrations conducted between July 15 and Aug. 26 2001 are presented in Figure 4.1. A comparison of the calibration with injections of CH_4 and CO_2 at port B and C is shown in Table 4.1.

Table 4.1. Comparison of the TDI Calibration with Injections of CH_4 and CO_2 at Injection Ports B and C.

	Sample injection			Correlation equation parameters					
Species	ppm	Port	μL	a (Counts/μg C)	b (Counts)	RE %	R^2	n	Recovery %
CH_4	3597	B	50-400	9.92×10^3	20	0.6	0.9990	27	96
CO_2	1645	B	50-400	10.6×10^3	-5	0.2	0.9998	17	103
CO_2	1645	C	10-200	10.6×10^3	-1	0.3	0.9992	36	102
CH_4	3597	C	5-200	10.3×10^3	-15	0.4	0.9993	37	Reference

Temperatures for the reduction and oxidation catalyst are 823 K and 1223 K, respectively.

Peak area counts (PA) = a m + b, m= injected carbon mass; RE: relative error of the slope.

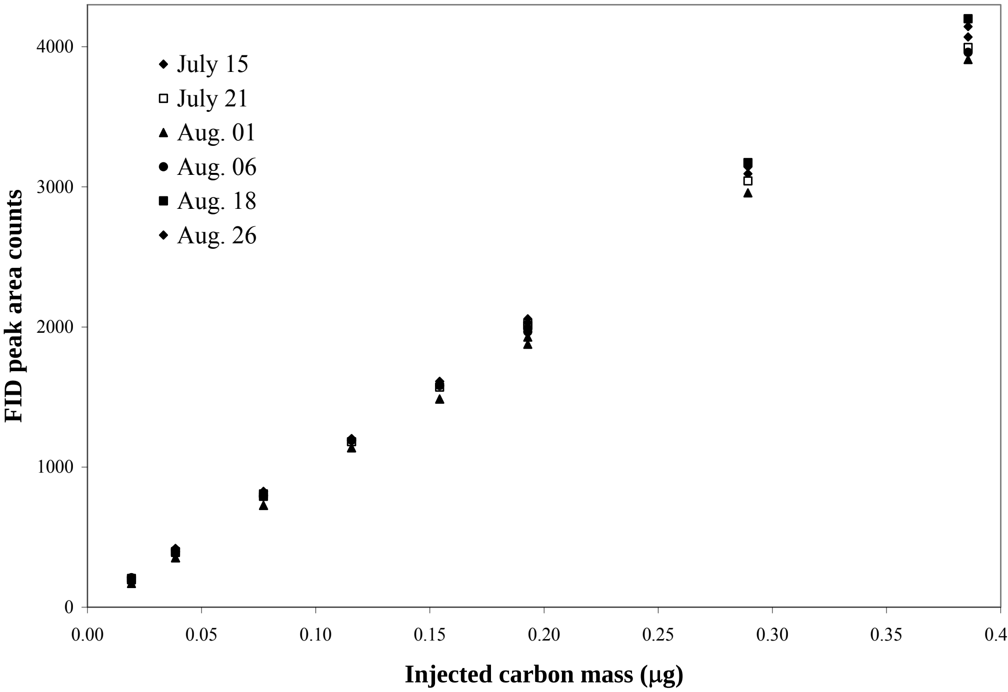

Figure 4.1. Calibration curves for the TDI system using injections of 10-200μL of a mixture containing 3597 ppm CH_4 (0.02-0.39 μg carbon) at port C. The average slope of

the linear regression line for the 6 calibrations is 1.05×10^4 counts/μg C. Relative standard deviation of the response factor is 3%.

4.1.2. Blank Values and Accuracy of Calibration

The blank values were calculated from integrated peak area counts of the FID signal and the CH_4 calibration data, as described in Experimental section 3.1.2. The measured blank values for various conditions are shown in Table 4.2.

Table 4.2. Summary of Blank Values.

Method	Blank type	Average carbon mass (μg)	STDEV μg	RSD %	n
OC	Pre-fired filter	2.6	0.6	24.3	17
OC	Unfired filter	18.4			1
OC	No filter	1.1	0.3	24.2	2
TC	Pre-fired filter	1.8	1.0	53.8	19
TC	Unfired filter	13.6	0.1	0.9	2
TC	No filter	0.8	0.3	33.3	7
TC	Field blank filter	2.6	0.7	26.3	17

A comparison of measured carbon masses by the TC and OC methods with spiked carbon masses is shown Figure 4.2 for different materials. Results from linear regressions are shown in Table 4.3. No linear regression was calculated for OC- Mannitol because the data clearly deviate from linearity.

Table 4.3. Summary of TDI Test Result.

Compound		Mass range	Regression parameter				Error		Slope
	Method	µg C	a	b (µg)	R^2	n	a	b (µg)	RE a, %
KHP	TC-30	1.1—93	0.99	-0.38	0.996	32	0.02	0.73	1.8
Mannitol		1.4—84	0.84	2.40	0.982	33	0.03	1.28	3.2
Alkane mixture		0.01—65	1.06	0.83	0.990	77	0.02	0.45	2.0
KHP	OC-30	2.2—97	1.07	-2.55	0.992	41	0.03	1.63	2.8
Alkane mixture		0.9—70	0.99	0.36	0.997	42	0.01	0.43	1.0

(Measured carbon mass) = a × (spiked carbon mass) + b; RE: relative error.

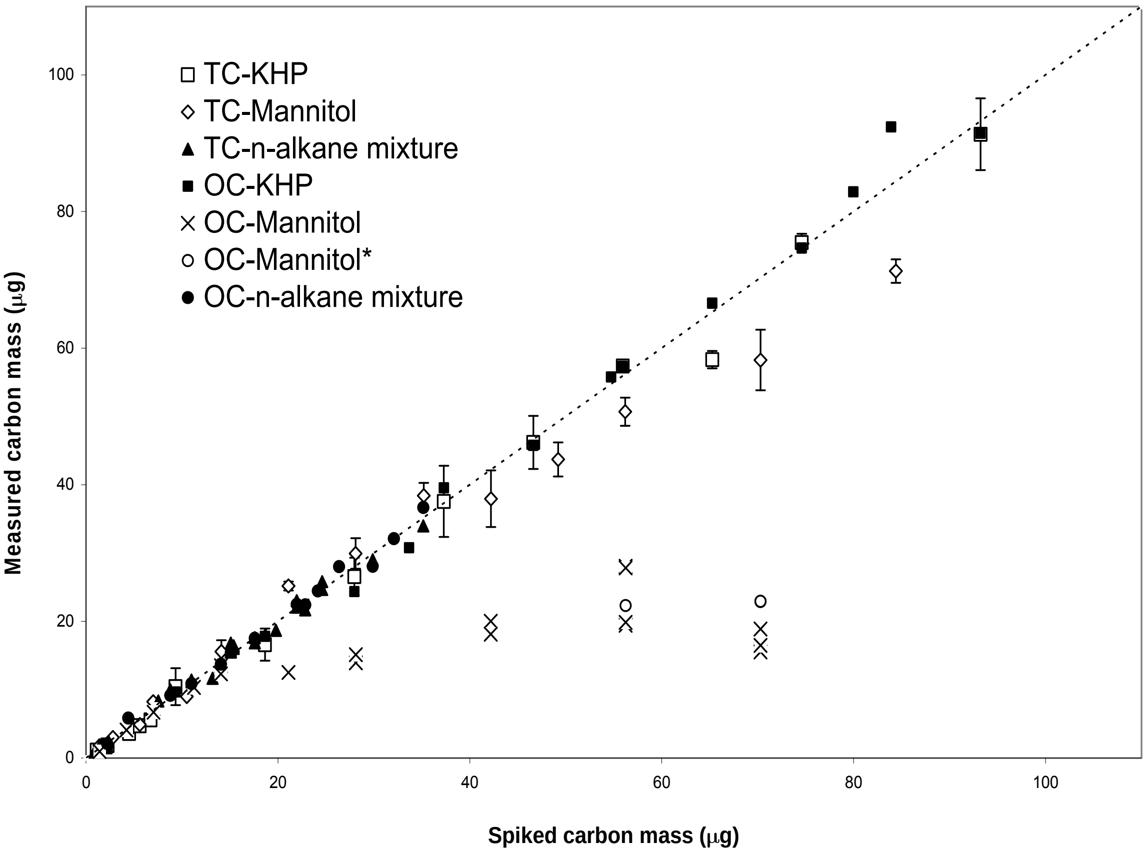

Figure 4.2. Comparison of carbon mass measured and mass spiked on filter.

4.1.3. Thermal Behavior of Individual Samples

The thermograms for 3 individual n-alkanes (C_{21}, C_{26} and C_{34}) spiked on filters and analyzed using the TDI OC method (Table 3.1) are shown in Figure 4.3. As an example, the plot of FID signal against reactor temperature for individual measurements of C_{34} samples run by TDI OC-5, -10 and -20 methods are shown in Figure 4.4. Examples for thermograms obtained for 37.3 micro grams KHP spiked on filters using OC-XX-Air methods are shown in Figures 4.5, 4.6 and 4.7. The results of measurements of KHP samples spiked on filters using different versions of the OC-method are summarized in Table 4.4. Results from repeat analysis of two samples collected in a railway overpass in the centre of Toronto using different OC-methods are shown in Table 4.5.

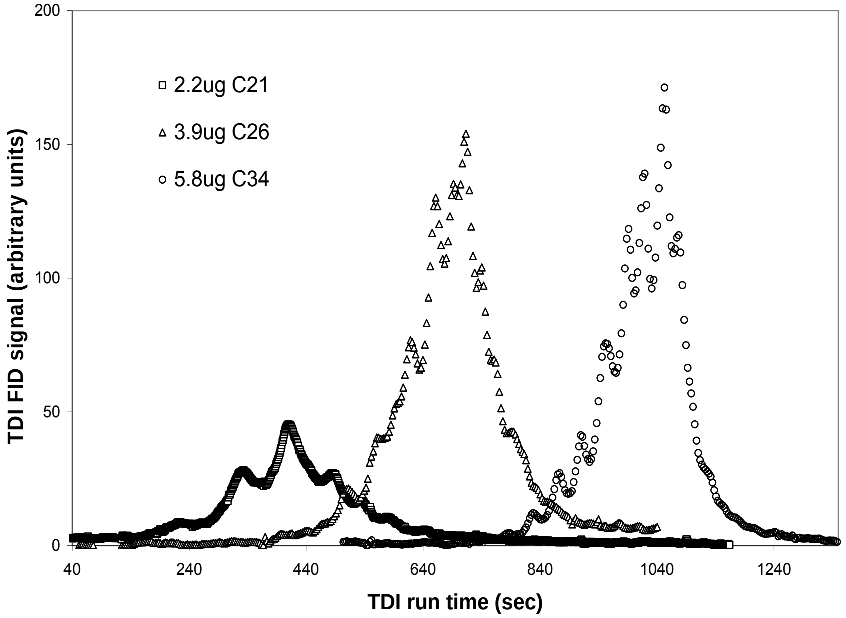

Figure 4.3. Thermograms of individual n-alkane C_{21}, C_{26} and C_{34} analyzed using TDI OC-10 methods under identical experimental conditions.

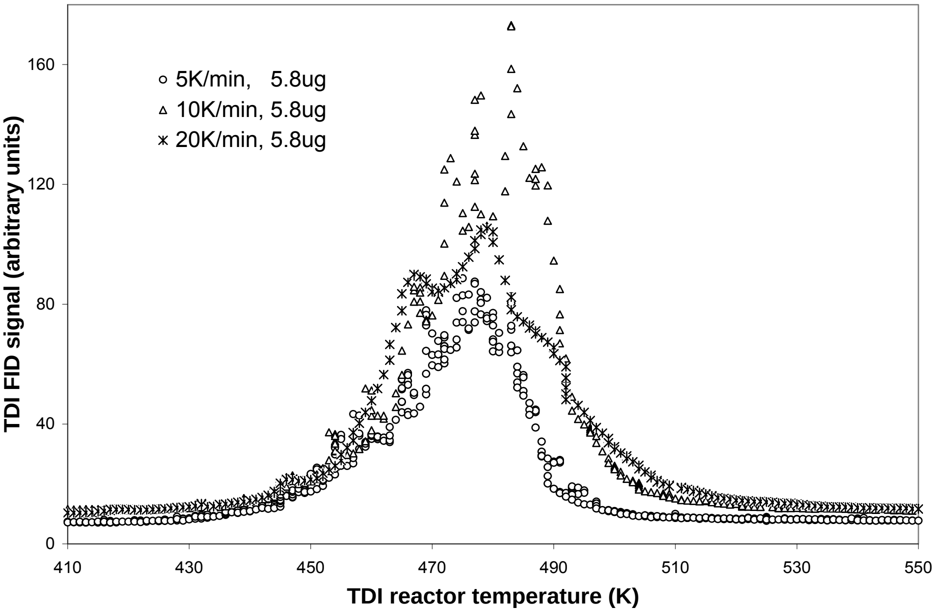

Figure 4.4. Dependence of FID signals on heating rate for C_{34}.

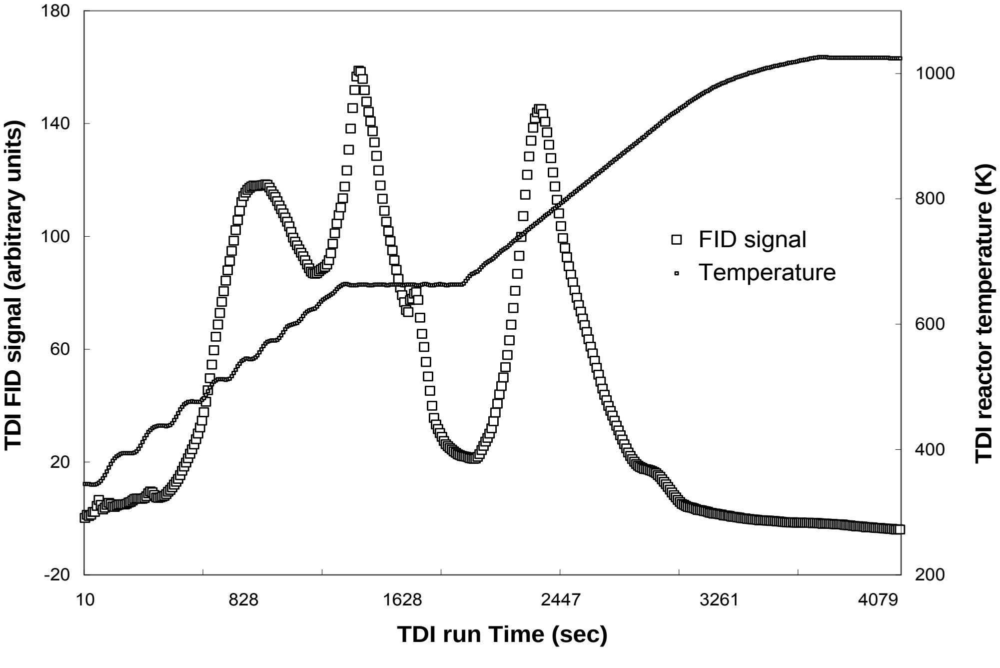

Figure 4.5. Thermogram of 37.3 μg KHP using method OC-15-Air.

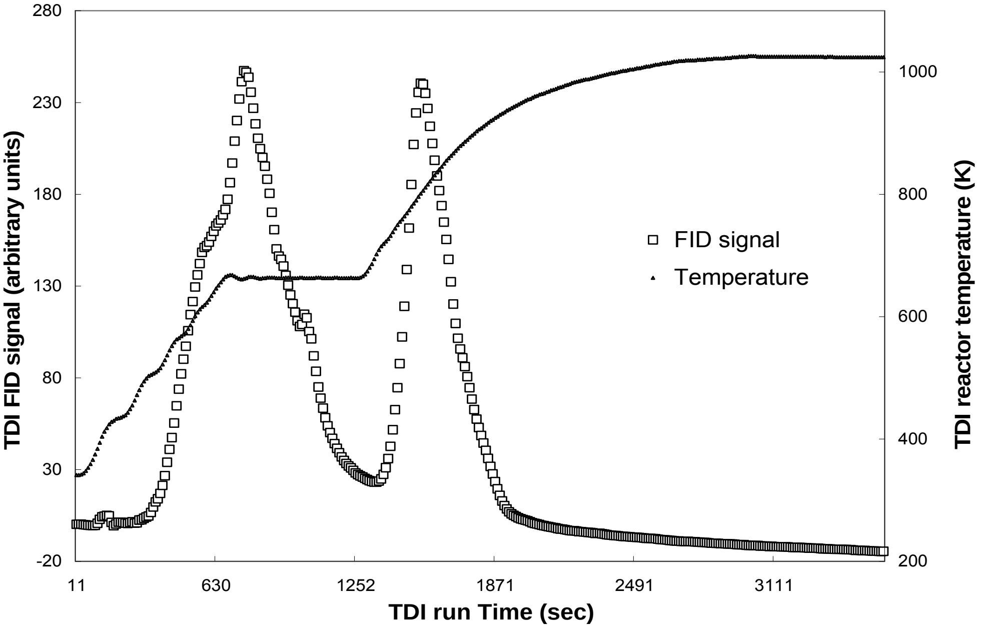

Figure 4.6. Thermogram of 37.3 μg KHP using method OC-30-Air.

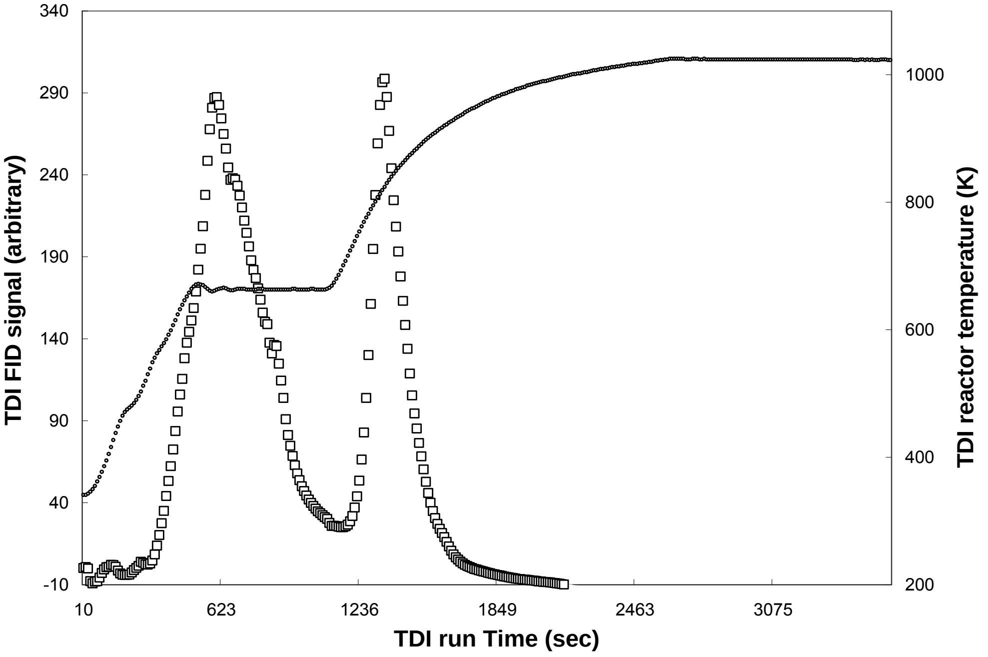

Figure 4.7. Thermogram of 37.3 μg KHP using method OC-40-Air.

Table 4.4. Comparison of Spiked Carbon Masses for KHP with Measurements Using Different OC Methods.

	Spiked	Measured		Spiked	Measured
Method	KHP mass (μg)		Method	KHP mass (μg)	
OC-15	37.3	33.0	OC-30-Air	46.6	46.6
OC-15-Air	37.3	40.0	OC-30-Air	55.9	55.7
OC-15-He	37.3	35.1	OC-30-Air	55.9	56.8
OC-30	37.3	33.7	OC-30-Air	58.9	56.4
OC-30	37.3	34.0	OC-30-Air	58.9	56.7
OC-30-Air	4.5	4.3	OC-30-Air	65.3	63.8
OC-30-Air	9.3	9.9	OC-30-Air	65.3	63.2
OC-30-Air	18.6	18.8	OC-30-He	37.3	35.7
OC-30-Air	28.0	28.4	OC-30-He	37.3	35.1
OC-30-Air	37.3	37.2	OC-40	37.3	36.8
OC-30-Air	37.3	37.1	OC-40	37.3	36.1
OC-30-Air	37.3	34.9	OC-40-Air	37.3	36.6
OC-30-Air	42.1	41.9	OC-40-He	37.3	35.7

Y= (0.97±0.02)m+(-0.04±0.89) R^2 = 0.989; Y= Measured carbon mass, m: Spiked carbon mass

Table 4.5. Result of Analysis of Two Samples Using Different OC Methods.

Method	Sample A (μg)	Method	Sample A (μg)	Method	Sample B (μg)
OC-15	20.6	OC-30	20.4	OC-30-He	99.1
OC-15-Air	19.7	OC-30-Air	21.2	OC-30-He	106.0
OC-15-Air	19.9	OC-30-He	17.5	OC-30	108.0
OC-15-Air	21.5	OC-40	21.0	OC-30	108.1
OC-15-He	17.8	OC-40-Air	20.4	OC-30-Air	108.2
OC-15-He	21.4	OC-40-He	20.0	OC-30-Air	115.9
Average	20.1±1.3μg, RSD=6.5%.			107.6±5.4μg, RSD=5.0%.	

Y= (0.97±0.02) m+(-0.04±0.89), R^2 = 0.989; Y= Measured carbon mass, m: Spiked carbon mass.

4.1.4. TC, OC and EC Concentrations of PM Samples

The TC, OC and EC concentrations of a number of samples collected during SONTAS were determined by thermal desorption analysis (details of methods see Experimental section, Table 3.1). The results are summarized in Table 4.6. For a subset of the samples repeat measurements were conducted and the results are given in Table 4.7. A comparison of the results of TC measurements with the sum of OC, EC carbon is given in Figure 4.8.

Table 4.6. Comparison of TC with OC and EC Concentrations for SONTAS Samples.

Sampling		Sample name No.	TC	OC	EC
Date DD/MM/YY	Duration Hours		Concentration (μg/m^3)		
23-24/06/00	22:35	1	9.9	6.6	3.8
24-25/06/00	27:46	2	6.5	4.1	1.4
25-26/06/00	19:35	3	6.2	5.2	1.0
26-27/06/00	26:26	4	5.8	4.5	0.8
28-29/06/00	23:55	5	5.5	2.3	2.3
27-28/07/00	22:40	6	6.8	5.0	0.3
29-30/06/00	23:35	7	4.3	4.0	0.3
30/06-01/07/00	17:20	8	4.2	3.3	0.3
01-02/07/00	11:42	9	5.5	4.2	0.7
01-07-00	27:55	10	5.4	3.2	0.7
01-07-00	4:00	11	6.1	5.3	0.3
01-07-00	4:00	12	5.8	5.0	0.3
02-07-00	3:41	13	6.3	5.9	0.7
02-07-00	3:52	14	5.5	5.2	0.8
02-07-00	3:40	15	6.2	6.0	0.4
02-03/07/00	18:28	16	5.3	4.7	0.8
04-05/07/00	24:11	17	4.4	3.8	0.6
03-04/07/00	23:43	18	5.2	3.8	1.2
05-06/07/00	25:01	19	4.9	4.3	0.4
06-07/07/00	22:15	20	4.2	3.7	0.4
07-08/07/00	25:05	21	4.3	3.4	0.8
08-09/07/00	21:25	22	3.2	2.7	0.3
09-10/07/00	23:23	23	3.9	3.5	0.3
10-11/07/00	24:09	24	4.7	4.4	0.3
11-12/07/00	23:40	25	6.3	5.7	0.5
12-13/07/00	24:11	26	7.8	6.7	1.0

Table 4.7. Reproducibility of TC, OC and EC Measurements.

Sample	TC (μg/m^3)			OC (μg/m^3)				EC (μg/m^3)			
name,No.	Aver.	RSD%	n	Value	Aver.	RSD%	n	Value	Aver.	RSD%	n
				6.9				3.9			
1	9.9	8.8	7	6.4	6.6	6.8	2	3.7	3.8	3.8	2
				3.3				0.4			
8	4.2	6.8	5	3.4	3.3	3.4	2	0.2	0.3	31.2	2
7	4.3	5.9	6		4.0	9.0	5		0.3	26.5	6
17	4.4	3.9	6		3.8	6.3	6		0.6	9.8	4
26	7.8	2.3	4		6.7	11.6	7		1.0	81.8	6

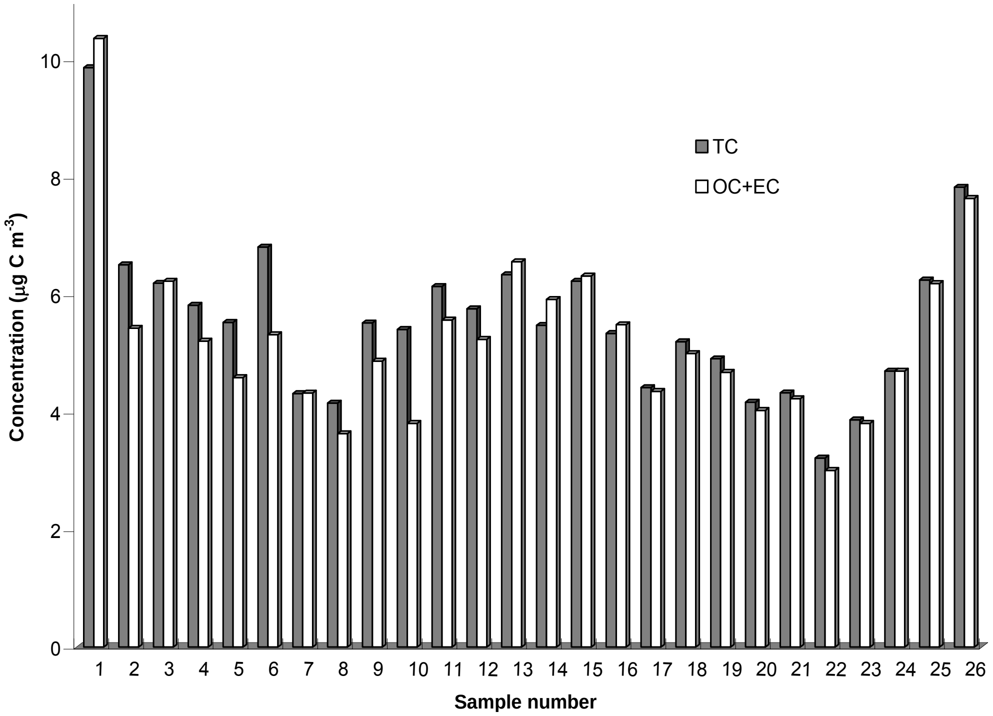

Figure 4.8. Comparison of the concentrations of TC and the sum of OC, EC.

4.2. TDI/GC

4.2.1. Performance

Coupling the on-line GC to the TDI changed the TDI calibration due to changes in the fraction of evolved material entering the TDI detection system. Figure 4.9 shows the CH_4 calibration curves for the TDI detection system using injector A, which is located before the split, and injector C, which is placed between split point and detection system. From the ratio of the slope of the calibration curves, the split ratio between TDI detection system and on-line GC is calculated. Figure 4.10 shows the calibration curve for the GC-FID. It should be noted that the response factor for the TDI detection system substantially differs from that of the GC-FID because the two FIDs were different models. An example for repeat measurements of carbon mass flow of material evolving from the TDI reactor under constant conditions is given in Table 4.8. Examples for the separation of n-alkanes evolving from a mixture of n-alkanes in the TDI reactor are shown in Figure 4.11.

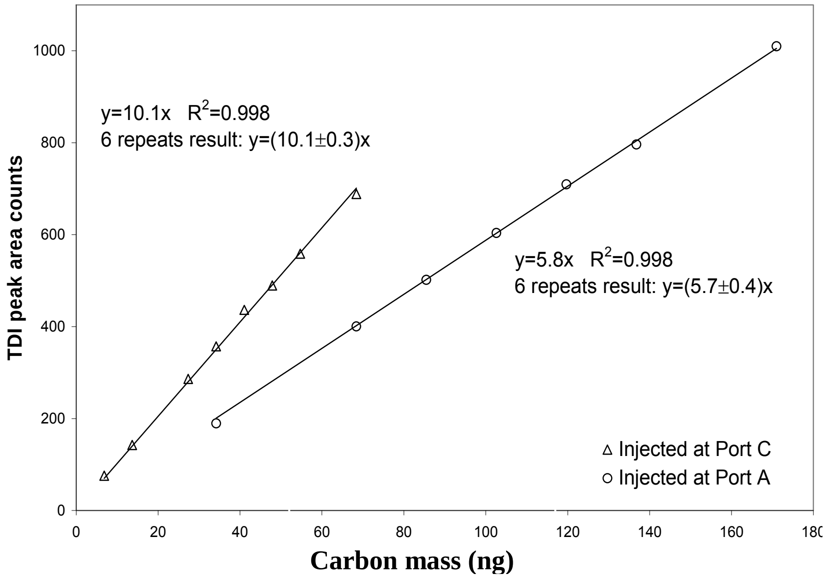

Figure 4.9. CH_4 calibration curves of the TDI detection system. The average results of 6 repeat calibrations are shown.

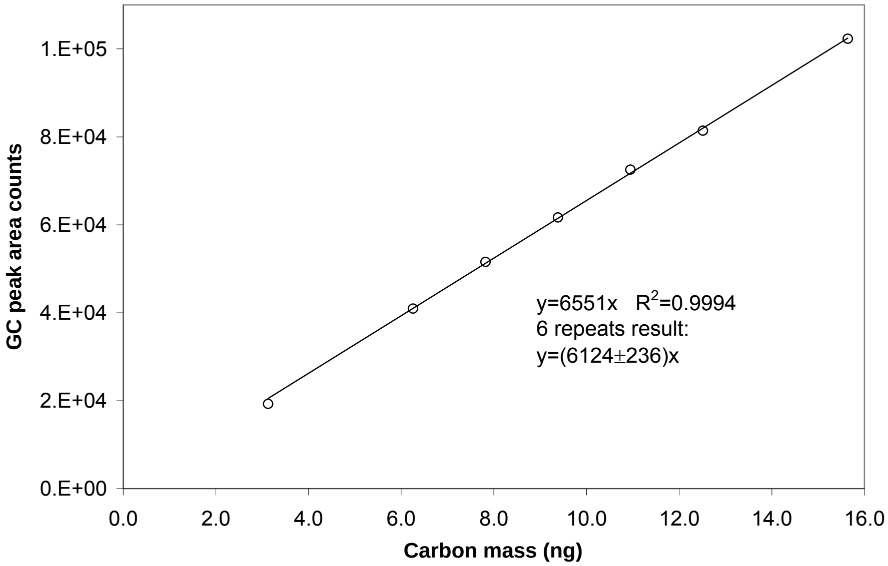

Figure 4.10. CH_4 calibration curve of GC-FID.

Table 4.8. Result of 7 Repeat Measurements of C_{28} (TDI-reactor at 393 K) in the Gas Flow from the TDI Reactor Using Continuous Detection as Well as On-line GC Separation.

	Continuous measurement			GC-separation		
	Area*	Signal height	MF** (ng/s)	Peak area	Peak height	MF (ng/s)
	531238	1672	3.25	121319	188919	3.23
	541546	1670	3.32	122601	184322	3.26
	544444	1675	3.33	121784	186718	3.24
	534983	1640	3.28	121464	181990	3.23
	540080	1632	3.31	121243	184054	3.23
	536399	1641	3.29	121879	182473	3.25
	544049	1632	3.33	120771	180883	3.22
Average	538963	1652	3.30	121580	184194	3.24
STDEV	4931	20	0.03	581	2814	0.02
RSD%	0.9	1.2	0.91	0.5	1.5	0.48

*Integration time interval is 5 minutes; **MF= Carbon mass flow.

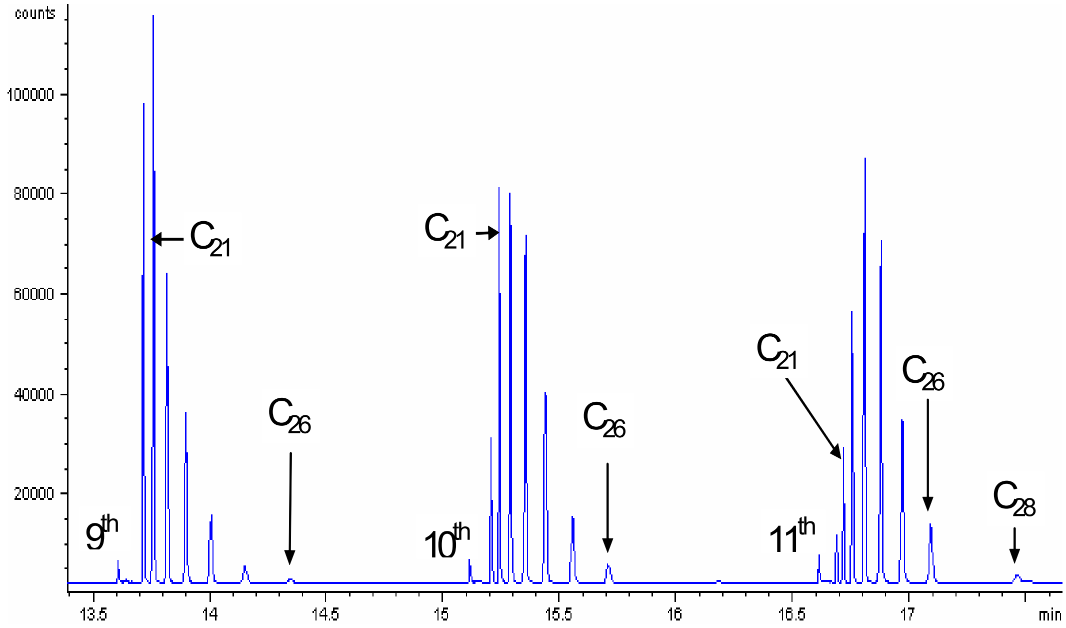

Figure 4.11. Chromatograms of sampling interval 9 to 11 for measurement of a 14 n-alkane mixture.

A comparison of carbon mass measured by the TDI detection system and the on-line GC in parallel for several n-alkanes and n-alkane mixtures is shown in Figure 12. An example for a measurement of an n-alkane mixture showing evolved carbon mass for individual n-alkanes determined by on-line GC as well as total carbon mass measured by the TDI detection system as function of run time is shown in Figure 4.13. Figure 4.14 shows the measured partial pressures of C_{21}, C_{24}, C_{27} and C_{32} in a 17 n-alkane mixture as function of TDI reactor temperature for four repeat runs.

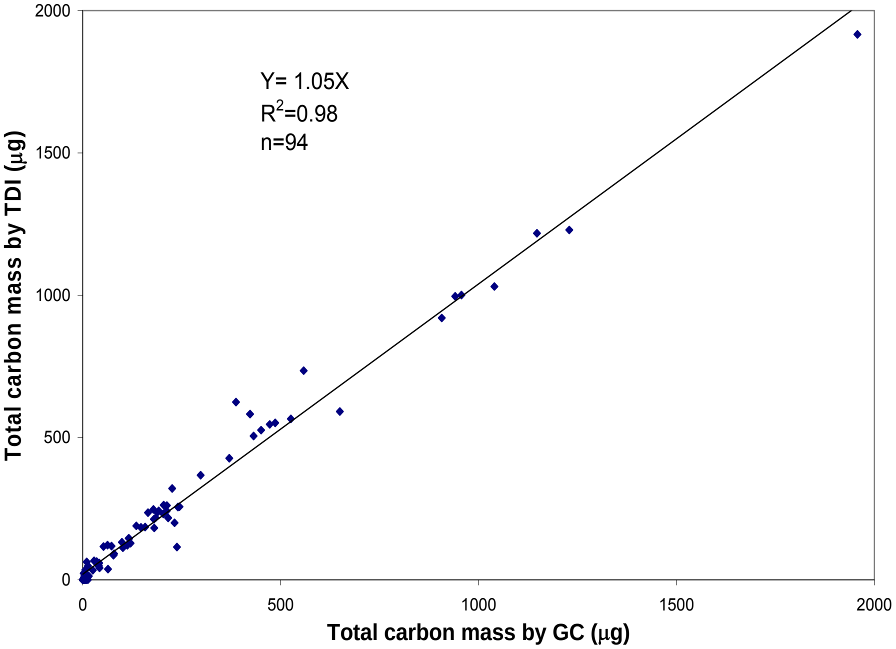

Figure 4.12. Comparison between measured total carbon mass by TDI and GC.

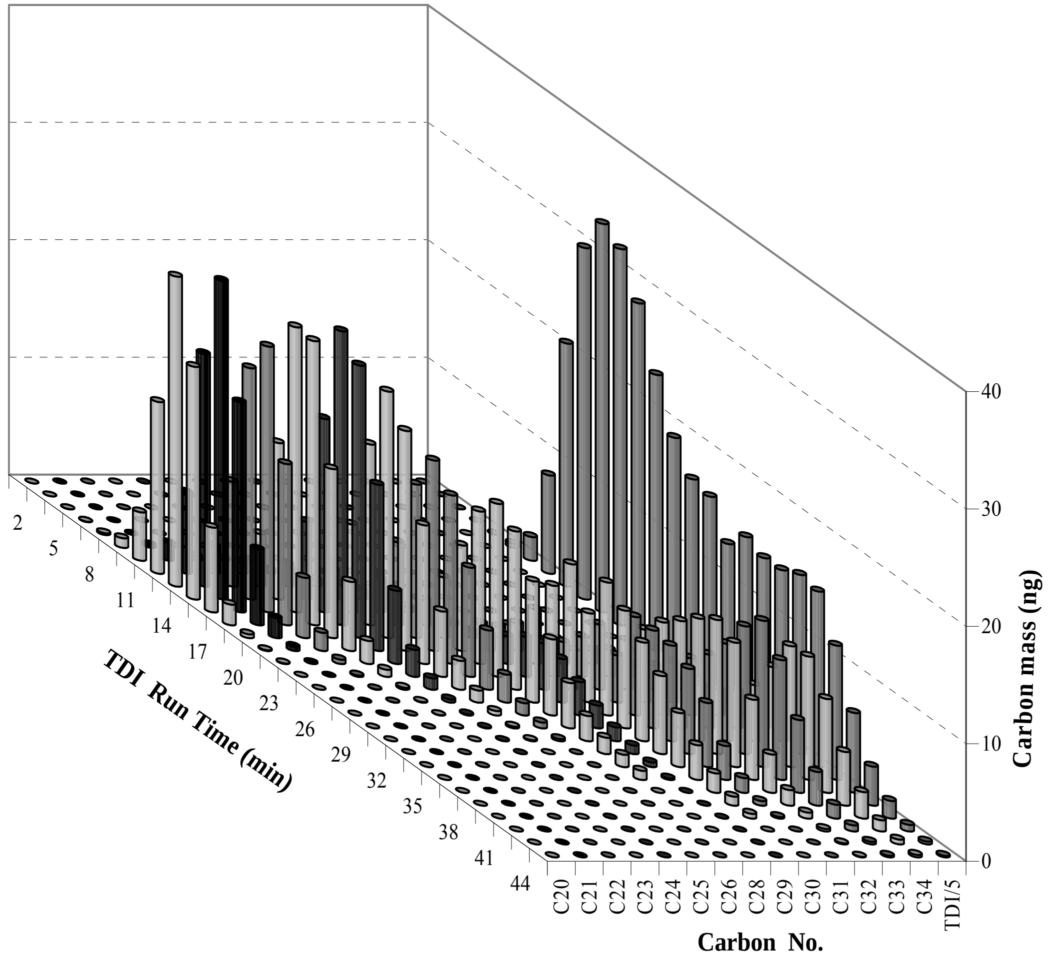

Figure 4.13. Comparison of measured n-alkane carbon mass by GC separation and total carbon mass by the TDI detection system.

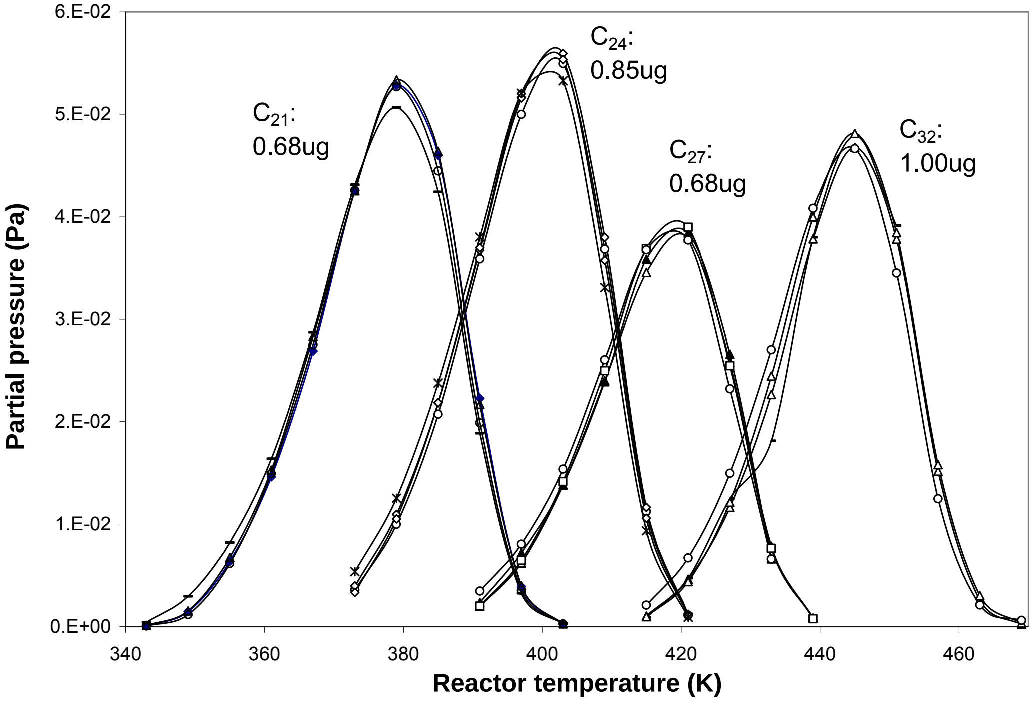

Figure 4.14. Partial pressures for repeat measurement of selected n-alkanes in a 17 n-alkane mixture. The spiked total carbon mass is 11 μg. The mol fractions of n-alkanes C_{21}, C_{24}, C_{27} and C_{32} in the mixture are 0.073, 0.080, 0.057 and 0.071, respectively.

4.2.2. Studies of n-Alkane Thermal Behavior

Examples for the thermal behavior of small samples of pure n-alkanes and n-alkane mixtures spiked on different types of surfaces are shown in Figures 4.15 to 4.19. The behavior of different masses of C_{20} spiked on quartz fiber filters and into a quartz boat respectively, is shown in Figure 4.15. Figure 4.16 presents results from measurements of C_{20} and C_{27} as pure substances and a C_{20}/C_{27} mixtures spiked on quartz glass. The thermal behavior of pure C_{27} and C_{27} in two different n-alkane mixtures spiked on quartz fiber filters is shown in Figure 4.17. The partial pressures as function of temperature for selected n-alkanes evolving from n-alkane mixtures spiked on quartz glass, clean quartz fiber filters and quartz fiber filters with PM samples are shown in Figures 4.18 and 4.19.

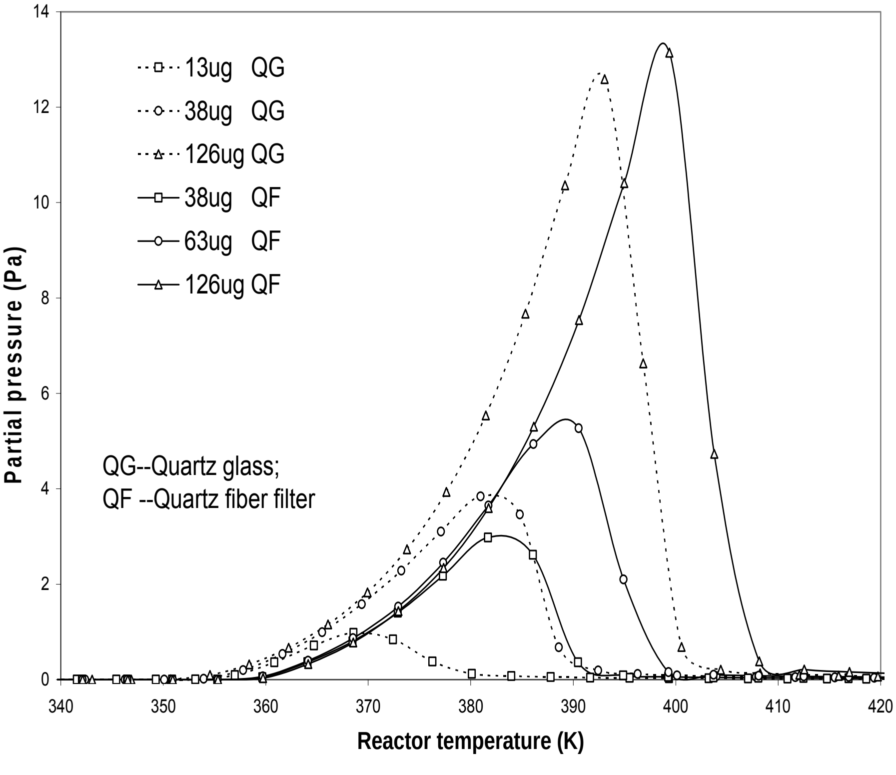

Figure 4.15. Dependence of measured C_{20} partial pressure on sample mass and surface type.

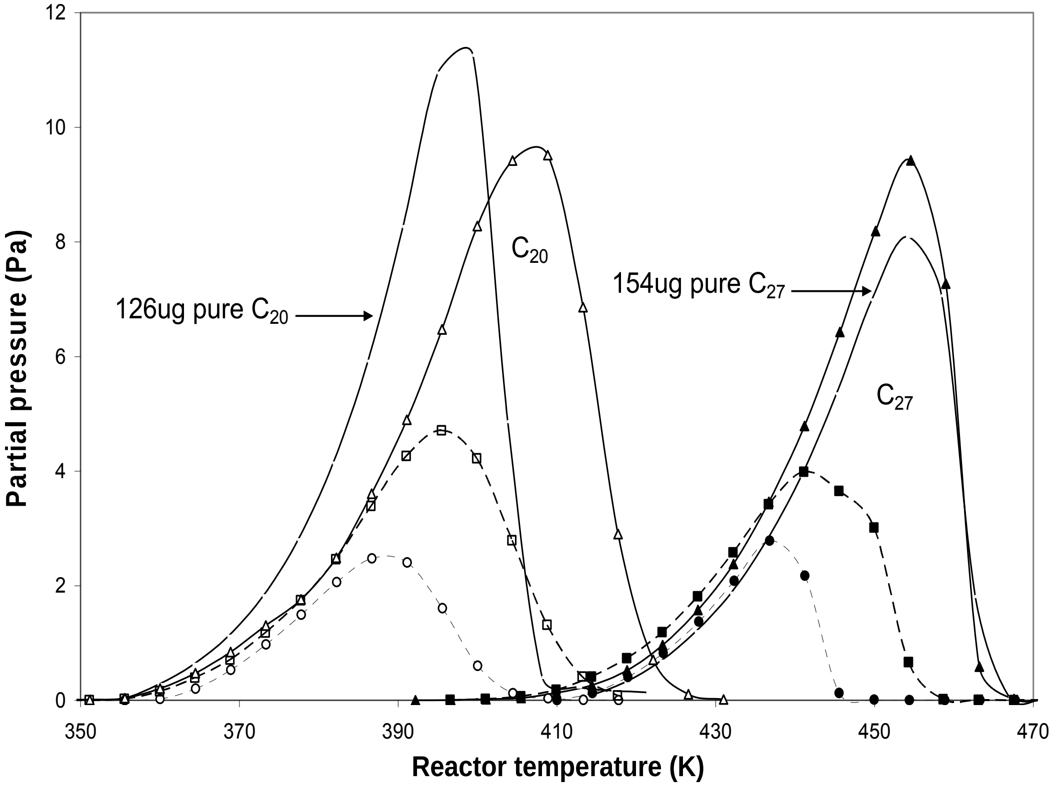

Figure 4.16. Measured partial pressures for pure samples of C_{20} and C_{27} and binary mixtures of C_{20} and C_{27}. Solid line: spiked solution contains 126 μg C_{20} and 154 μg C_{27}. Broken line: spiked solution contains 63 μg C_{20} and 77 μg C_{27}. Dashed line: spiked solution contains 38 μg C_{20} and 46 μg C_{27}.

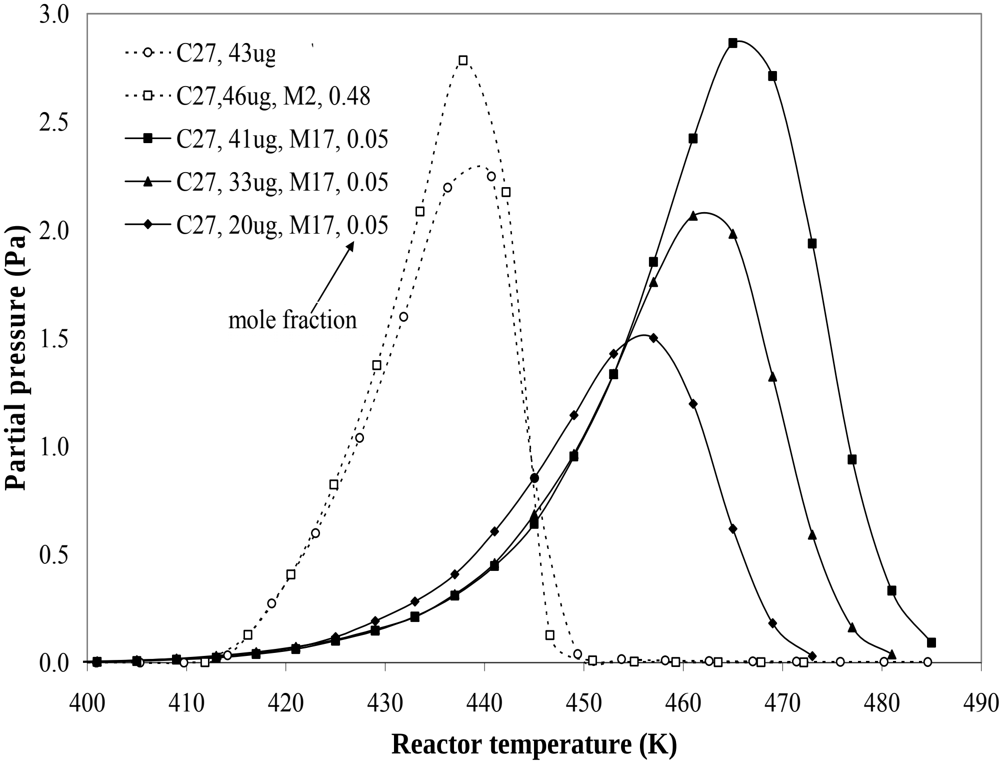

Figure 4.17. Partial pressures of C_{27} for samples of the pure substance and C_{27} in different mixtures and different masses of the same mixture spiked on quartz fiber filters.

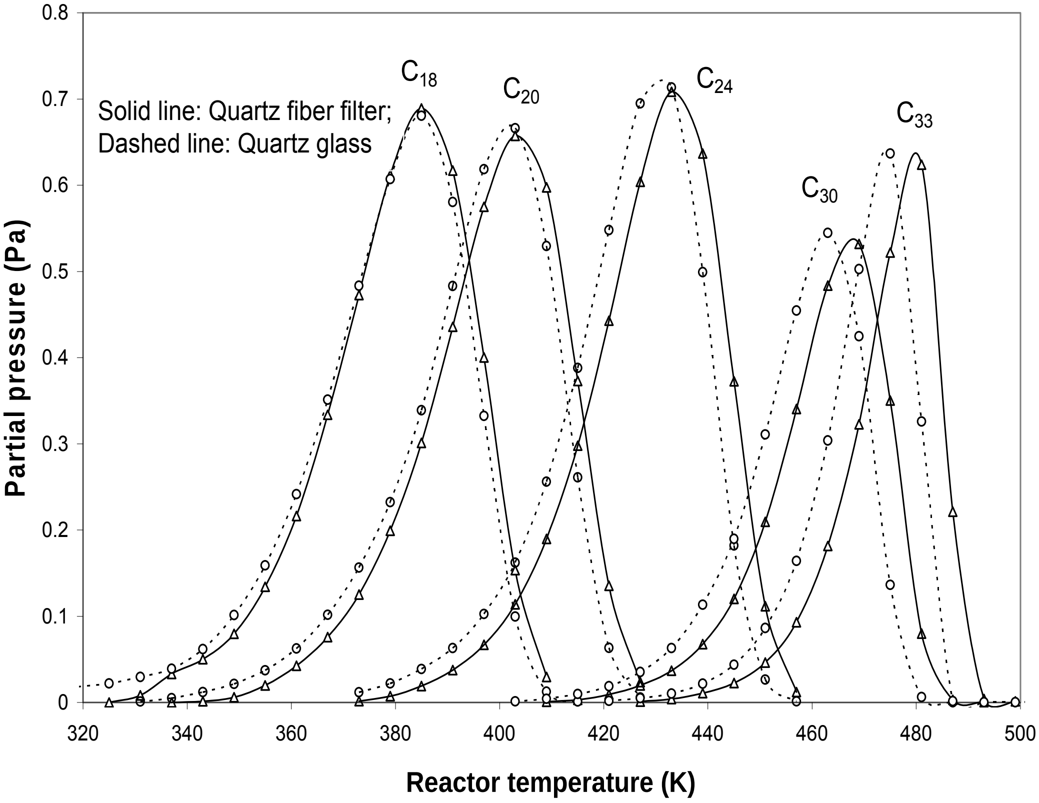

Figure 4.18. Dependence of measured partial pressures on temperature for selected n-alkanes evolving from mixtures of n-alkanes spiked on quartz fiber filters and quartz glass. The spiked total carbon mass is 176 μg. The mol fractions of n-alkanes C_{18}, C_{20}, C_{24}, C_{30} and C_{33} in the spiked mixture are 0.081, 0.075, 0.080, 0.050 and 0.044, respectively.

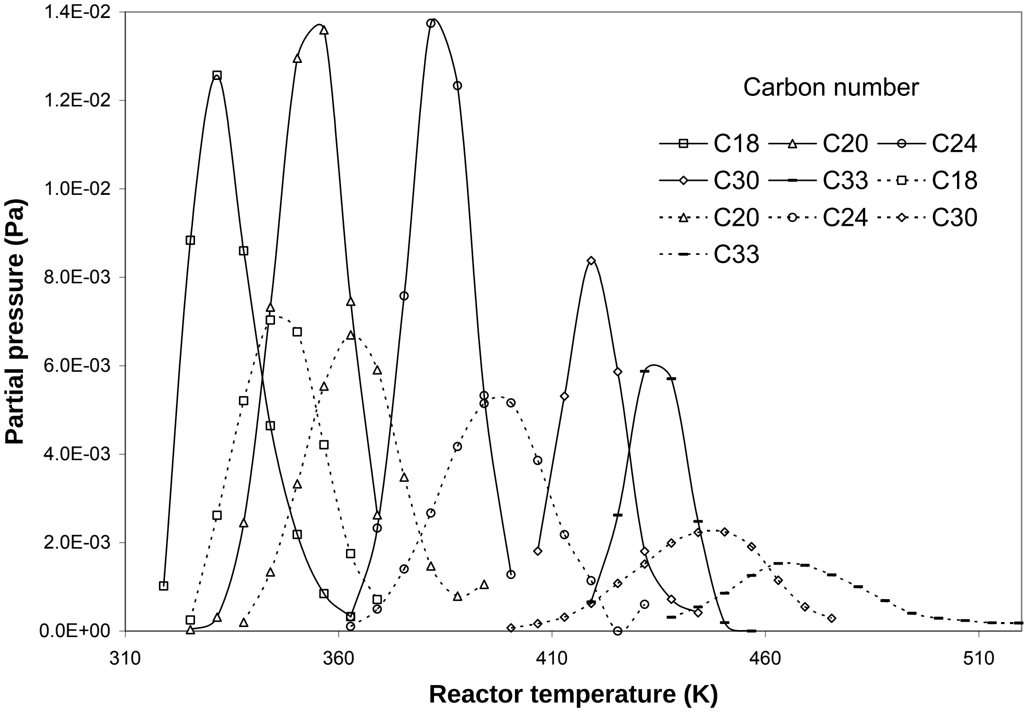

Figure 4.19. Partial pressures against temperature for selected n-alkanes evolving from mixtures of n-alkanes spiked on quartz fiber filters and PM samples on quartz fiber filters. Solid line: 4.4 µg n-alkanes spiked on clean quartz fiber filter. Dashed line: 2.2 µg n-alkanes spiked on quartz fiber filter with PM sample. The mol fractions of n-alkanes C_{18}, C_{20}, C_{24}, C_{30} and C_{33} in the mixture are 0.081, 0.075, 0.080, 0.050 and 0.044, respectively.

4.2.3. Studies of n-Alkanes in PM Sample

Examples of calibration curves using 17 n-alkane mixtures for analysis of n-alkanes in PM samples are shown in Figure 4.20. The chromatographs of sampling interval number 9 and 29 from the analysis of a PM sample (Sample No. 19 collected as part of the SONTAS campaign in southern Ontario) are shown in Figure 4.21. The GC peak area counts for the n-alkane peaks for every sampling interval are shown in Figure 4.22. Figures 4.23 and 4.24 show the partial pressures of n-alkanes with even and odd carbon number respectively as function of reactor temperature for a SONTAS PM sample. A summary of total n-alkane peak areas measured in several samples from SONTAS campaign is given in Table 4.9.

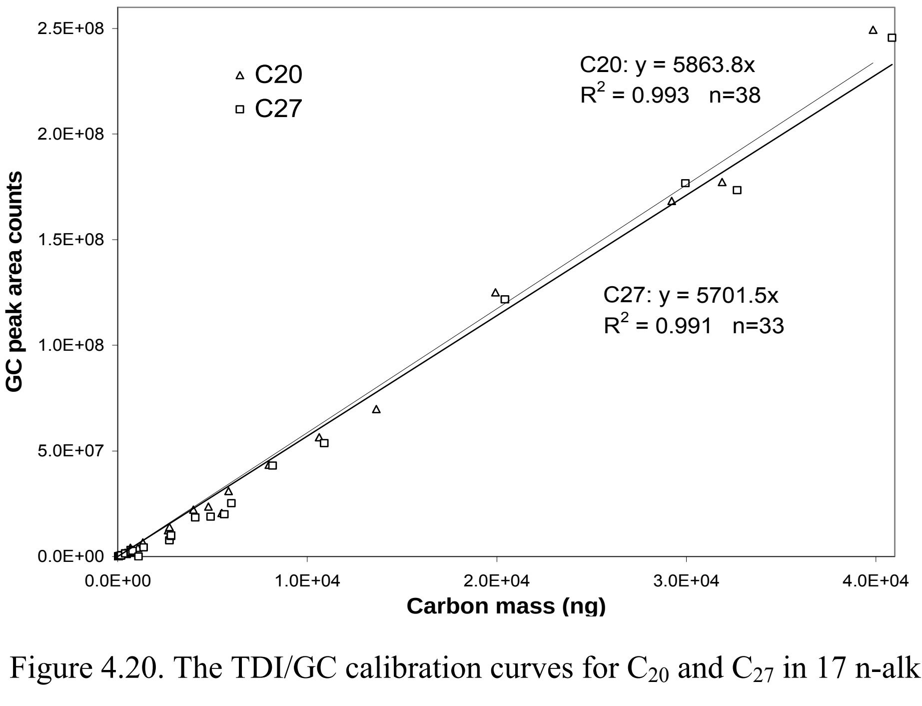

Figure 4.20. The TDI/GC calibration curves for C_{20} and C_{27} in 17 n-alkane mixture.

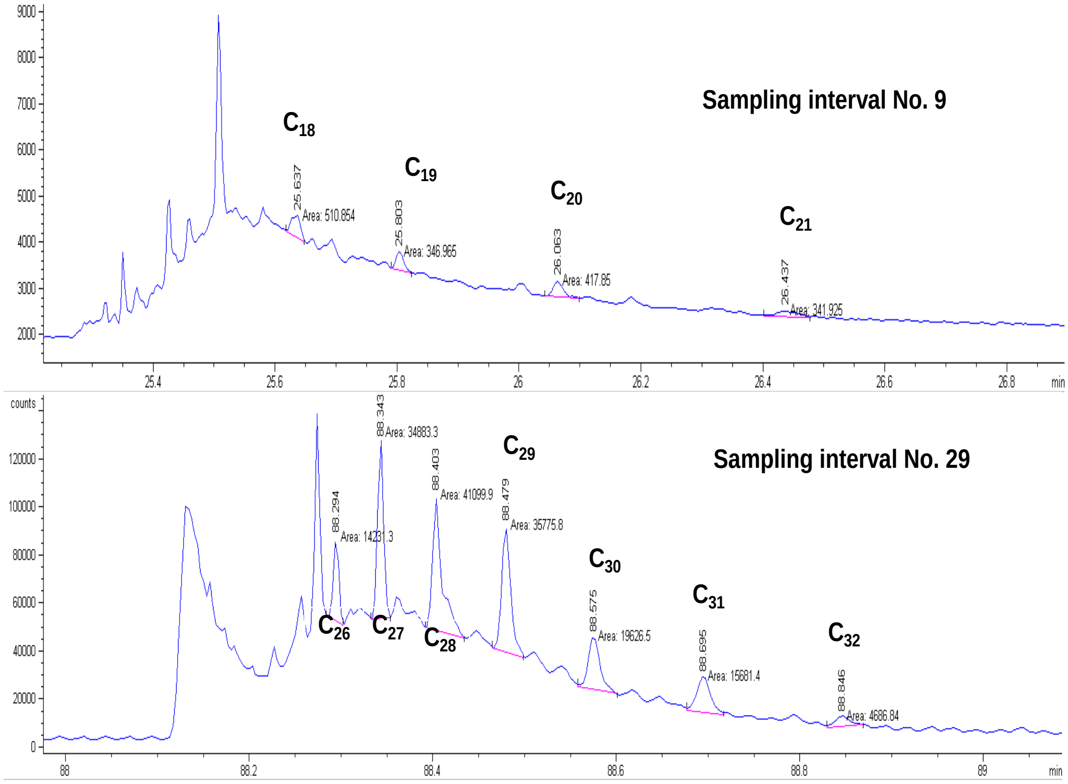

Figure 4.21. Example chromatograms for sampling interval number 9 and 29 for a sample collected during SONTAS. The TDI oven average temperatures for sampling interval number 9 and 29 are 363 K and 488 K, respectively. The analyzed PM filter area is 10.6 cm^2.

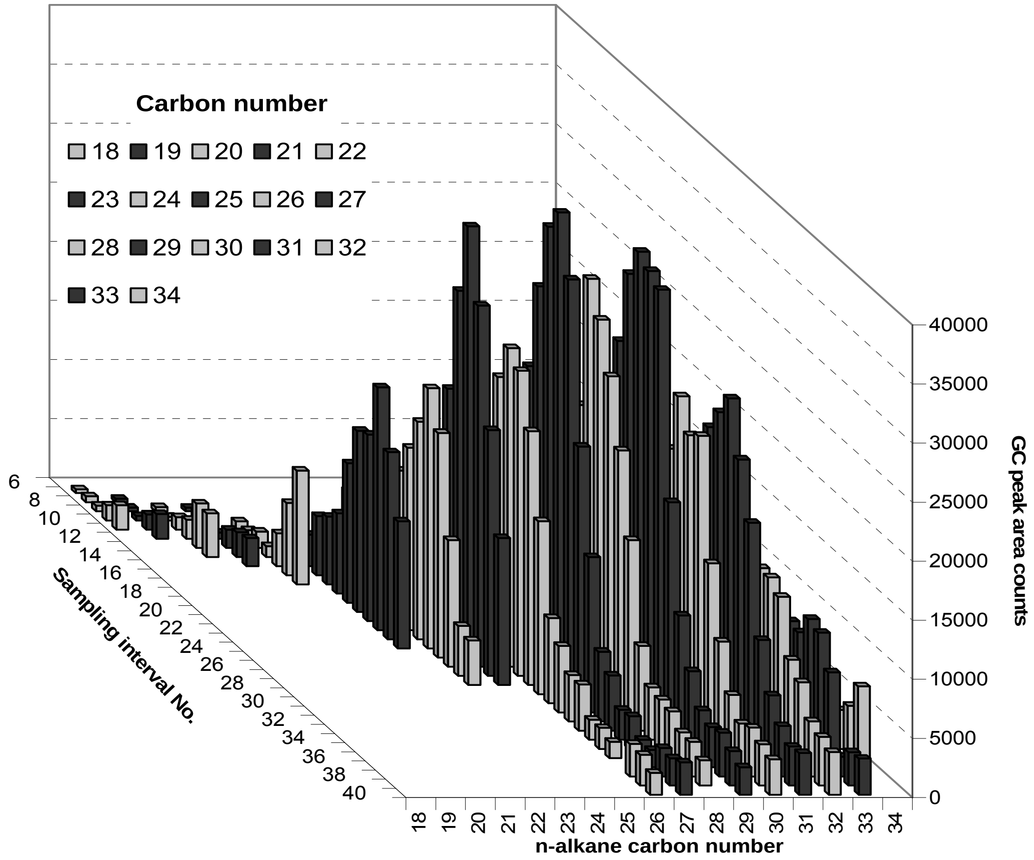

Figure 4.22. Dependence of peak area counts measured for n-alkanes as function of sampling interval for a TDI/GC analysis of a SONTAS PM sample. The sampling interval is 3.1 minutes. The TDI oven temperature is increased linearly from 313 K to 556 K.

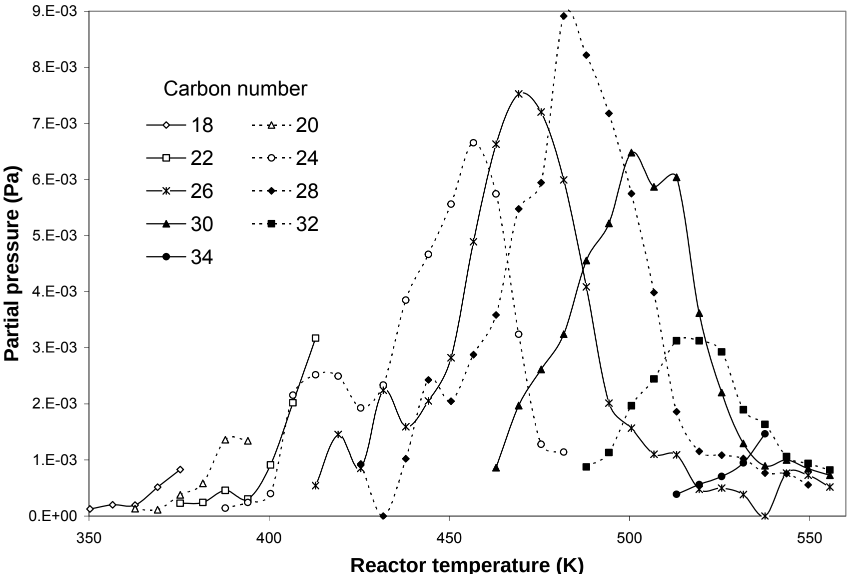

Figure 4.23. Partial pressures of n-alkanes with even carbon number for a SONTAS PM sample as function of reactor temperature.

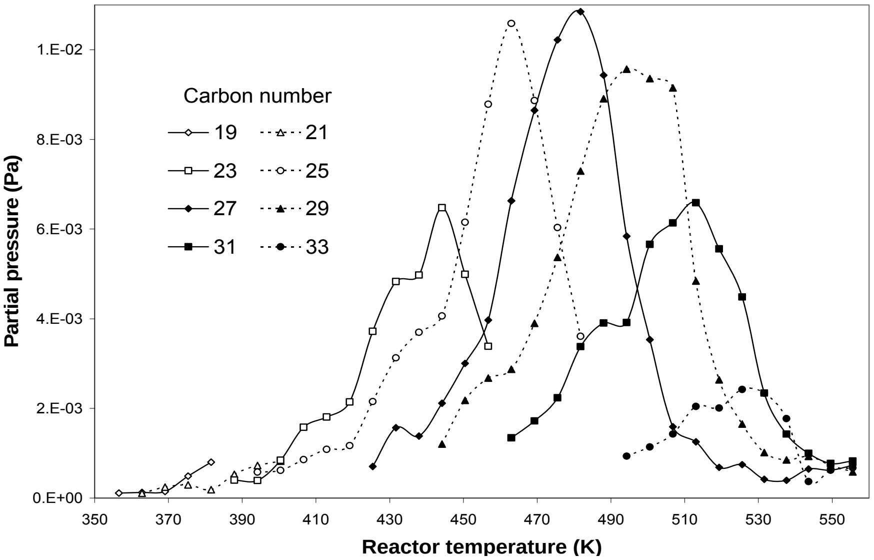

Figure 4.24. Partial pressures of n-alkanes with odd carbon number for a SONTAS PM sample as function of reactor temperature.

Table 4.9. Total n-Alkane Peak Area Counts Measured in Several Samples.

Sample	Total peak area per cm^2 of filter area								
I.D.	C_{18}	C_{19}	C_{20}	C_{21}	C_{22}	C_{23}	C_{24}	C_{25}	C_{26}
12	200	69	526	494	365	586	326	528	103
13	178	121	525	653	758	1045	558	1503	438
14	186	80	542	646	752	844	722	1118	553
15	663	860	2208	2380	1748	2639	1331	3583	2319
16	394	663	880	614	163	982	401	862	1780
17	287	356	1029	1077	1516	4155	6951	16446	10408
18		8	222	20	16	5			
19	409	415	1020	795	2102	10647	13852	19969	19289
26	942	300	2960	547	823	2036	1761	6464	4137
26	661	447	3231	633	641	989	1351	4776	2912
I.D.	C_{27}	C_{28}	C_{29}	C_{30}	C_{31}	C_{32}	C_{33}	C_{34}	
12	271	1058	472	127	447	97			
13	551	1940	1412	1254	1060	189			
14	624	886	3410	605	2633				
15	3390	3123	5168	4425	2565				
16	1947	5771	3332	976	845				
17	18082	23281	17537	10675	14495	4924	2358	809	
18	102	790	763	516	829	227			
19	26329	23860	28534	18490	20660	9119	6749	1796	
26	6585	8343	8428	3073	7647	1308	619	629	
26	6106	6415	8615	3010	7252	3233	1253		

4.3. Measurements of Partial Pressures

4.3.1. Partial Pressure and Carrier Gas Flow Rate

The calibration curves of individual n-alkane C_{20} and C_{27} by the TDI/GC continuous mode for measuring the partial pressures of n-alkanes are shown in Figure 4.25. The dependence of the inverse of the partial pressure for C_{20}, C_{27}, and C_{28} as function of flow rate through the saturator is shown in Figure 4.26. The dependence can be divided in two parts. For low flow rates the measured partial pressures are independent of the flow rates and for higher flow rates the inverse of the partial pressures are proportional to the flow rates. Partial pressures measured under isothermal conditions and at low flow rates (11 to 32 ml/min) are presented in Table 4.10 to 4.13 for n-alkanes C_{20}, C_{26}, C_{27} and C_{28}.

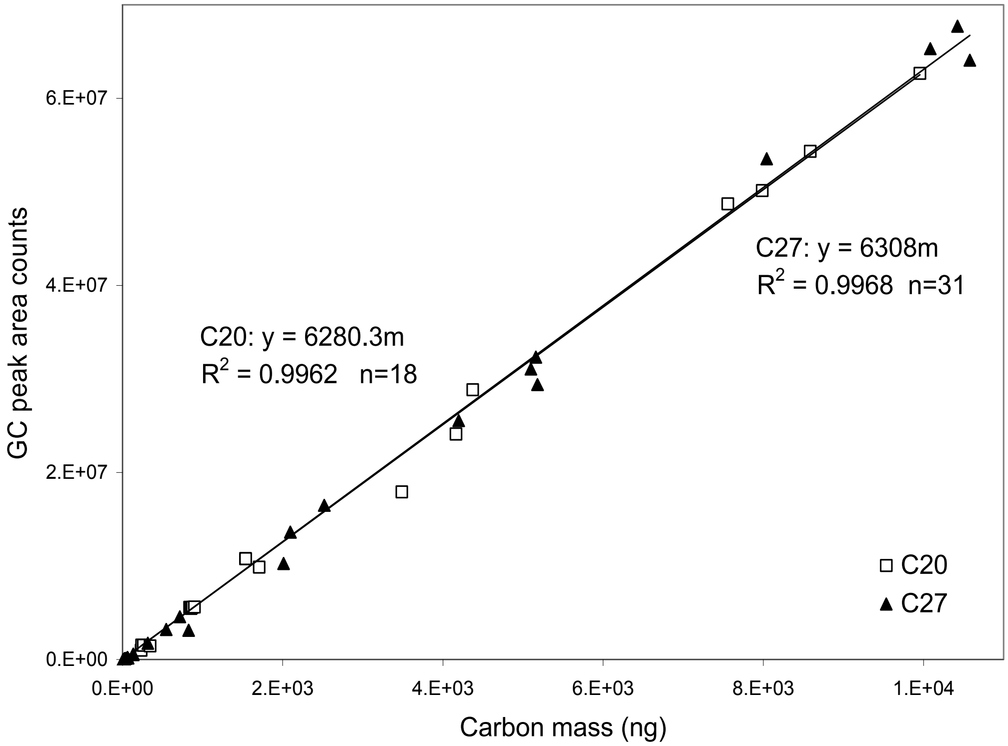

Figure 4.25. Calibration curves of GC-FID for individual n-alkanes C_{20} and C_{27} using the TDI/GC continuous mode.

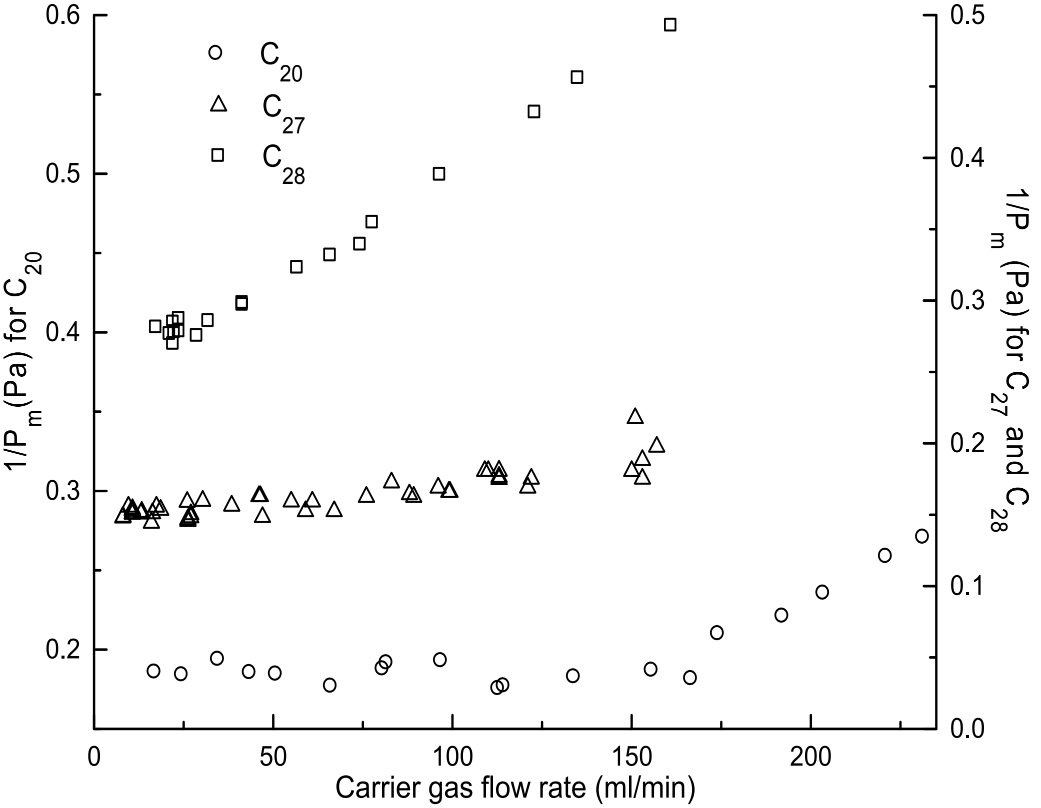

Figure 4.26. Dependence of the inverse partial pressure of n-alkane on carrier gas flow rate at 373 K for C_{20} and 433 K for C_{27}, C_{28}.

Table 4.10. Partial Pressures Measured Isothermally for C_{20}.

Temp. K	Pressure Pa	STDEV Pa	n	RSD %	Temp. K	Pressure Pa	STDEV Pa	n	RSD %
298.2	1.14E-03		1		373.2	5.84E+00	2.5E-01	14	4
299.2	2.30E-03	3.4E-05	2	1	383.0	1.26E+01	1.1E-01	3	1
300.2	3.25E-03		1		383.2	1.21E+01	1.1E+00	10	9
303.2	4.26E-03	1.5E-03	6	34	388.2	1.95E+01		1	
308.2	8.79E-03	1.9E-03	4	21	393.0	2.23E+01		1	
311.2	1.20E-02	9.0E-06	2	0	393.2	2.54E+01	2.3E+00	13	9
313.2	1.55E-02	3.2E-03	12	21	398.2	3.05E+01	8.0E-02	2	0
315.2	1.99E-02		1		403.0	4.95E+01		1	
318.2	2.83E-02	2.2E-03	2	8	403.2	4.95E+01		1	
323.2	5.54E-02	9.7E-03	6	18	413.0	8.69E+01		1	
333.2	1.44E-01	1.1E-02	8	7	413.2	8.18E+01	5.5E-01	2	1
343.2	4.43E-01	7.0E-02	8	16	418.2	1.08E+02		1	
353.0	8.21E-01	8.5E-03	2	1	423.2	1.63E+02		1	
353.2	9.31E-01	1.1E-01	14	12	428.2	1.86E+02		1	
358.0	1.57E+00		1		433.2	2.79E+02		1	
363.0	2.35E+00		1		443.2	4.61E+02		1	
363.2	2.54E+00	4.7E-02	3	2	453.2	7.63E+02		1	
368.0	3.03E+00	3.1E-01	3	10	463.2	1.25E+03		1	
373.0	5.31E+00	1.5E-01	3	3	473.2	2.09E+03		1	

Table 4.11. Partial Pressures Measured Isothermally for C_{26}.

Temp. K	Pressure Pa	STDEV Pa	n	RSD %	Temp. K	Pressure Pa	STDEV Pa	n	RSD %
373.2	7.19E-02	8.7E-04	7	1.2	423.2	6.45E+00	2.7E-02	7	0.4
378.2	8.91E-02	2.7E-03	7	3.0	433.2	1.27E+01	7.6E-01	7	6.0
383.2	2.33E-01	1.6E-03	7	0.7	443.2	2.48E+01	1.5E-01	7	0.6
393.2	6.08E-01	5.4E-03	7	0.9	453.2	4.48E+01	3.0E-01	7	0.7
403.2	1.27E+00		1		463.2	7.96E+01	3.7E-01	7	0.5
413.2	3.01E+00	1.8E-02	7	0.6	473.2	1.36E+02	7.6E-03	7	0.0
418.2	4.12E+00	1.7E-02	7	0.4					

Table 4.12. Partial Pressures Measured Isothermally for C_{27}.

Temp. K	Pressure Pa	STDEV Pa	n	RSD %	Temp. K	Pressure Pa	STDEV Pa	n	RSD %
333.2	2.79E-04	3.6E-05	3	13	393.0	3.67E-01	7.1E-02	9	18
339.7	7.34E-04	7.4E-05	3	10	393.5	3.18E-01		1	
340.1	7.69E-04	9.8E-05	3	13	403.4	6.32E-01	1.6E-01	10	25
340.4	8.02E-04	9.0E-05	3	11	408.2	8.46E-01	0.0E+00	2	0
343.2	1.25E-03	1.9E-04	5	15	413.2	1.30E+00	1.2E-01	3	9
349.6	2.69E-03	5.1E-04	3	19	418.2	1.97E+00	3.6E-02	3	2
349.9	2.76E-03	5.0E-04	3	18	423.2	2.78E+00	8.3E-02	2	3
350.3	2.89E-03	4.8E-04	3	17	430.0	5.75E+00		1	
360.1	9.89E-03	1.7E-04	2	2	430.5	5.85E+00		1	
360.4	1.05E-02		1		433.0	7.34E+00	3.7E-01	24	5
369.6	2.90E-02		1		433.2	5.63E+00	9.0E-02	3	2
369.9	2.99E-02		1		443.2	1.11E+01	1.2E+00	2	11
370.3	3.13E-02		1		453.2	2.13E+01	1.5E+00	2	7
382.5	9.79E-02		1		463.2	3.91E+01	4.2E+00	2	11
383.2	1.04E-01	6.9E-03	3	7	473.2	7.20E+01	5.5E+00	2	8
383.5	1.11E-01		1						

Table 4.13. Partial Pressures Measured Isothermally for C_{28}.

Temp. K	Pressure Pa	STDEV Pa	n	RSD %	Temp. K	Pressure Pa	STDEV Pa	n	RSD %
393.0	1.39E-01	1.0E-02	2	7	438.0	8.18E+00	2.9E-02	7	0.4
403.0	3.13E-01	1.2E-01	2	39	443.0	9.20E+00	4.8E-02	7	0.5
408.0	6.88E-01	2.0E-03	7	0	453.0	1.76E+01	9.2E-02	7	0.5
413.0	6.17E-01	3.0E-03	7	0	458.0	3.06E+01	1.6E-01	7	0.5
418.0	1.78E+00	1.9E-03	7	0	463.0	3.33E+01	7.3E-03	7	0.0
423.0	1.95E+00	5.7E-03	7	0	473.0	5.93E+01	3.8E-01	7	0.6
428.0	2.73E+00	1.6E-02	7	1	483.0	1.02E+02	5.0E-01	7	0.5
433.0	4.13E+00	1.2E-01	25	3	493.0	1.71E+02	2.0E-01	7	0.1

4.3.2. Partial Pressure Measurement Using Oven Temperature Programming

Measurements of n-alkane partial pressures running linear temperature programs of the saturator are shown in Figures 4.27 to 4.32. Figure 4.27 shows the measured partial pressures of C_{27} as function of temperature for different loadings of the saturator with C_{27} by method 1 in Table 3.5. The influence of the heating rate in temperature programmed measurements of the partial pressures of C_{20} is shown in Figure 4.28. The dependencies of partial pressure on temperature for C_{20} and C_{27} using a very slow temperature programming of the saturator oven are shown in Figures 4.29 to 4.32.

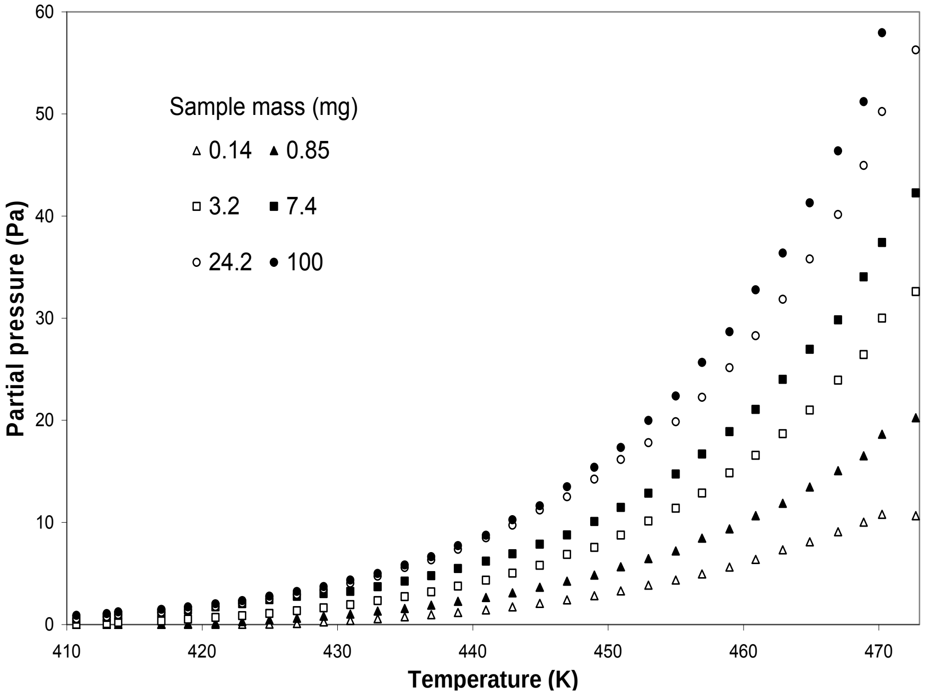

Figure 4.27. Dependence of measured partial pressure on sample mass for C_{27}.

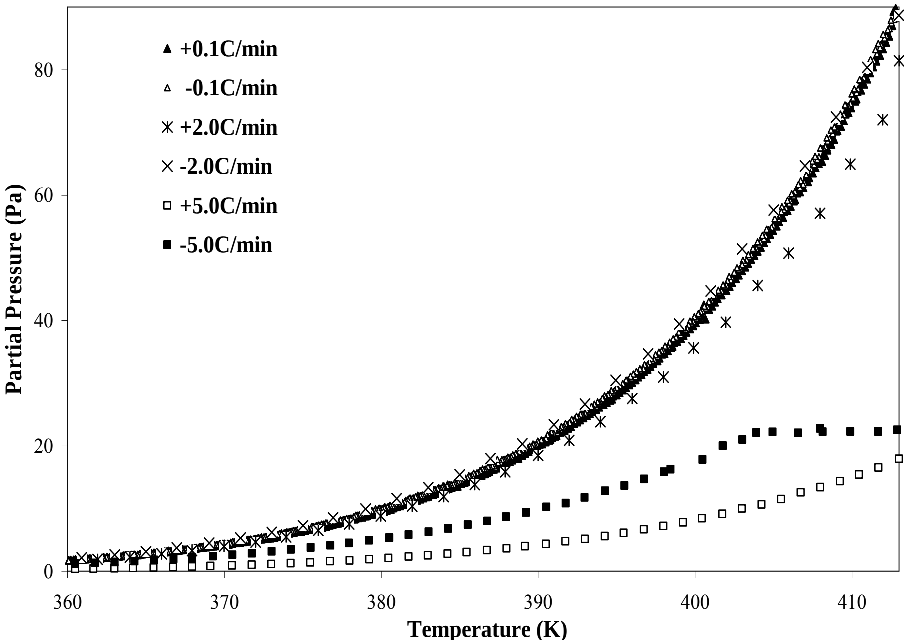

Figure 4.28. The influence of the heating rate on measured partial pressures for C_{20}.

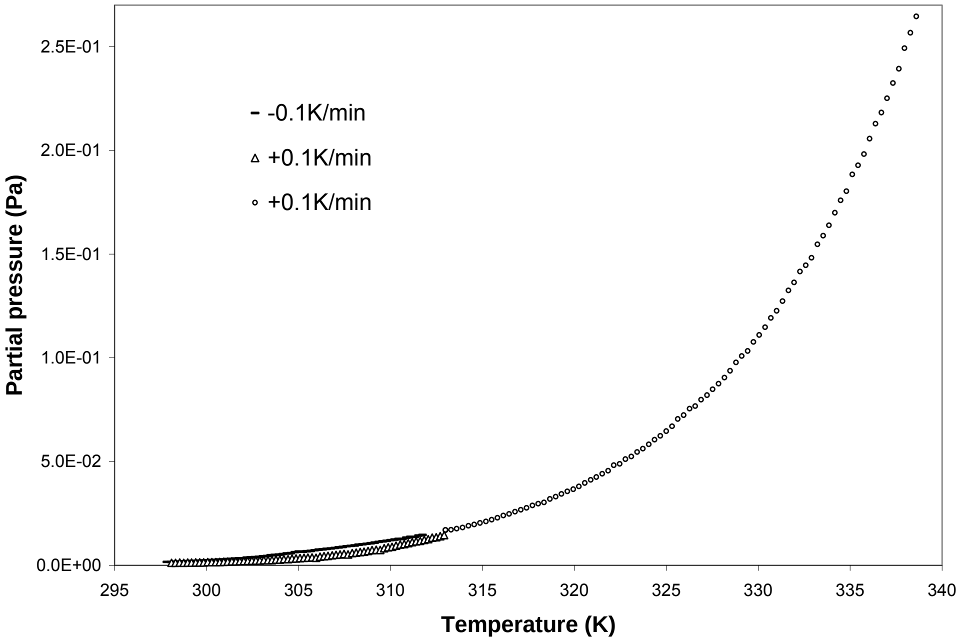

Figure 4.29. Measured partial pressure by temperature program for C_{20}.

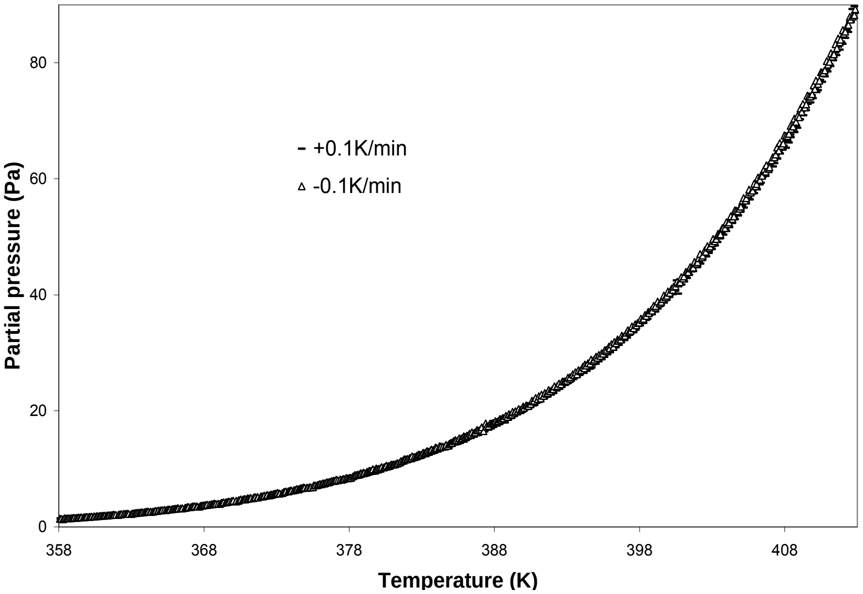

Figure 4.30. Measured partial pressure by temperature program for C_{20}.

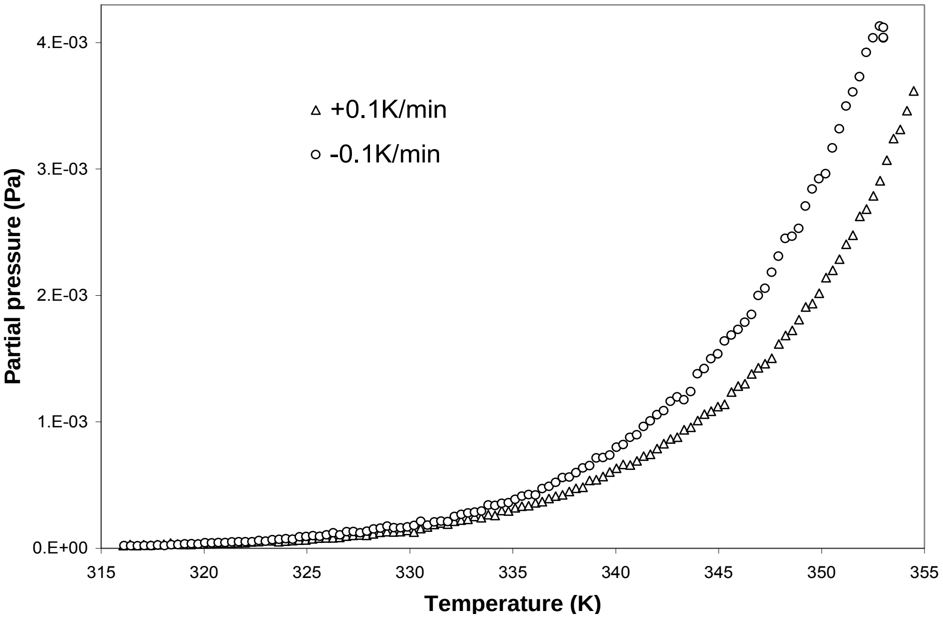

Figure 4.31. Measured partial pressure by temperature program for C_{27}.

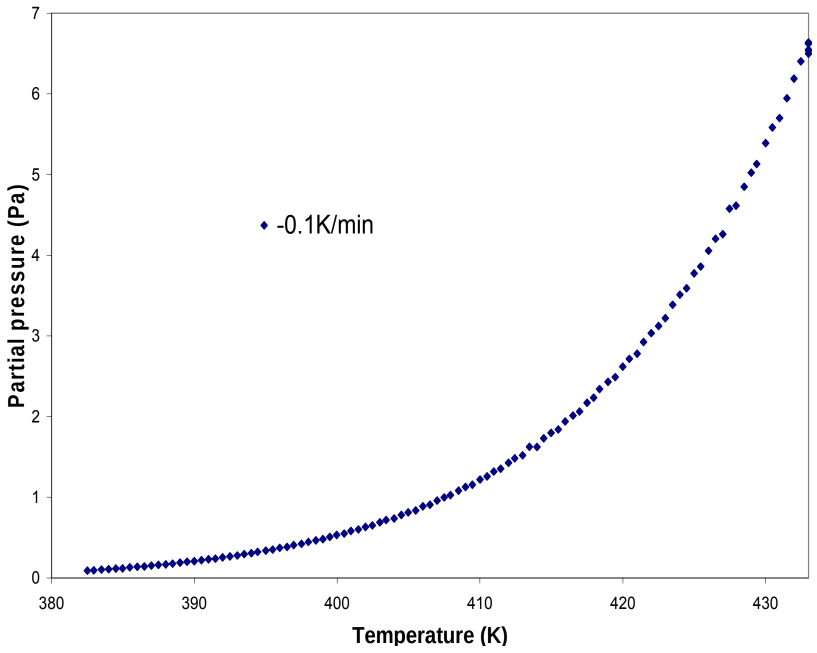

Figure 4.32. Measured partial pressure by temperature program for C_{27}.

4.3.3. Measurement of Partial Pressures Above Mixtures of n-Alkanes

The FID signal for measurements of a ternary mixture (C_{26}, C_{27} and C_{28}) by continuous and on-line GC modes for saturator temperatures of 433, 443 and 453 K, and an enlarged part of a chromatogram for 433 K is shown as Figure 4.33. The dependencies of the partial and total partial pressures of C_{27} and C_{28} in binary mixtures at 433 K as function of the composition of the mixture are shown in Figure 4.34. The partial pressures of C_{26}, C_{27} and C_{28} in binary and ternary mixtures for different saturator temperatures and different sample compositions are summarized in Table 4.14.

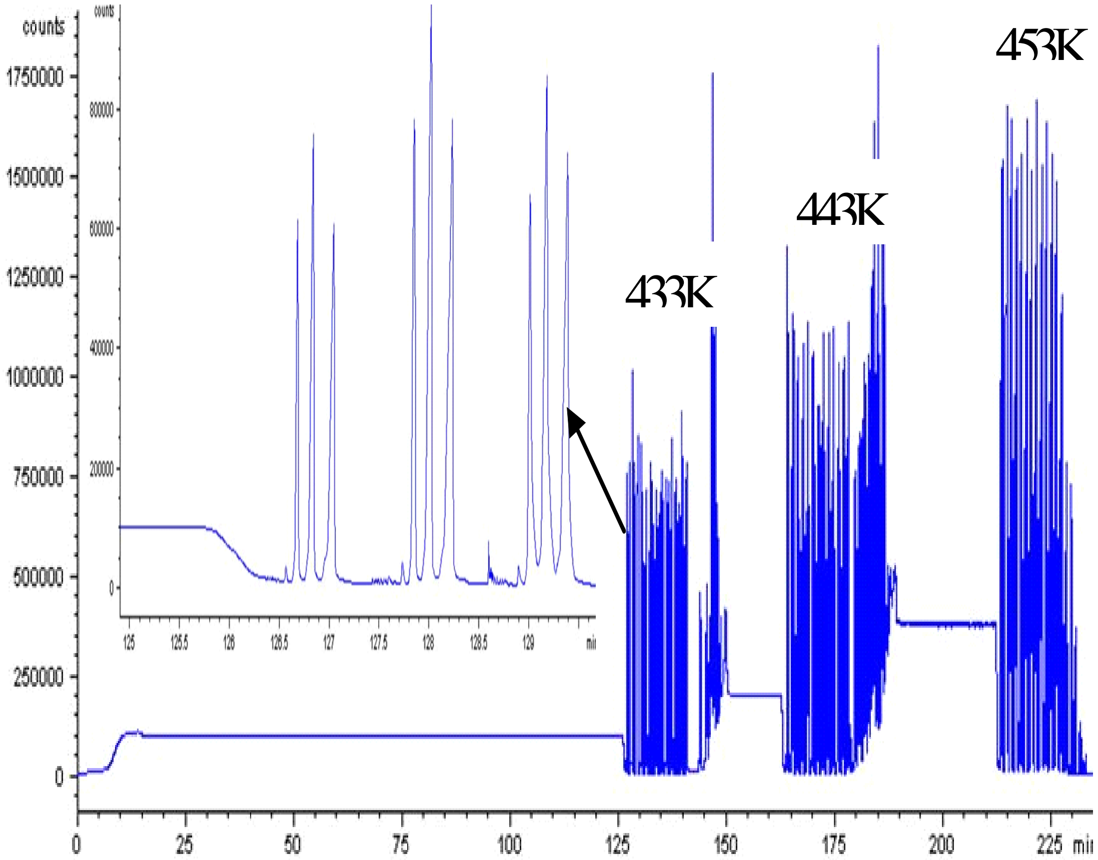

Figure 4.33. Chromatogram of a ternary mixture at saturator temperature of 433, 443 and 453 K.

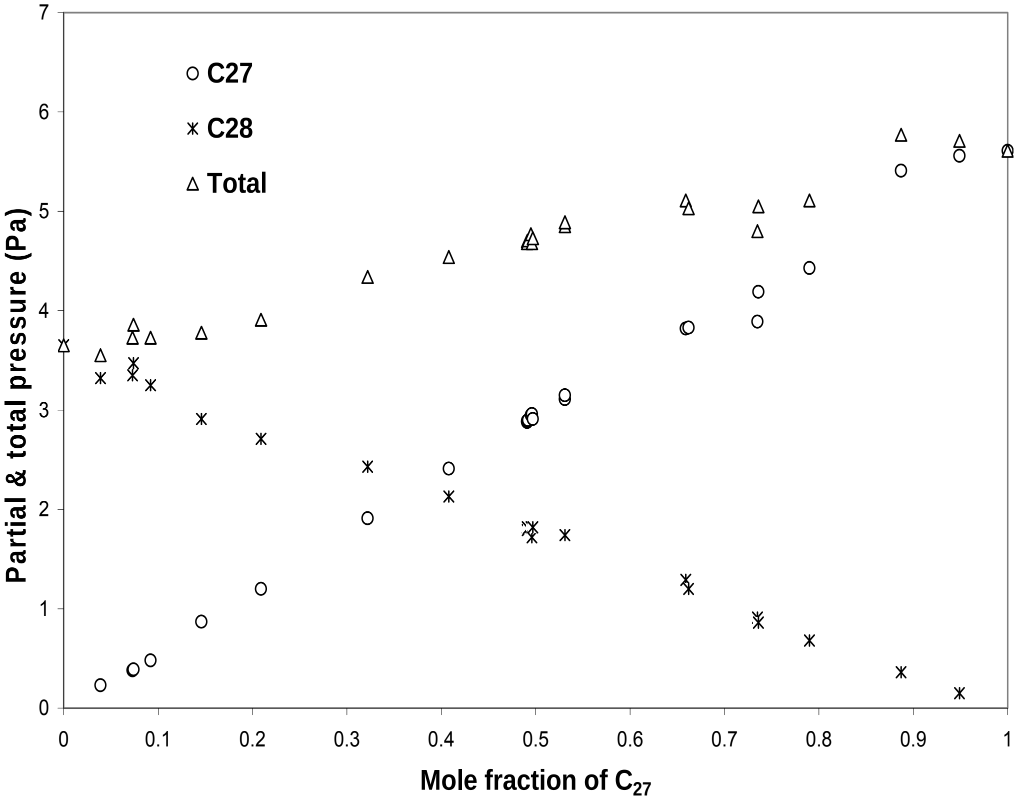

Figure 4.34. Dependencies of the partial and total partial pressures of C_{27} and C_{28} in binary mixtures at 433 K as function of C_{27} mol fraction.

Table 4.14. Result of the Partial Pressures and Compositions of C_{26}, C_{27} and C_{28} in Binary and Ternary Mixtures.

Mol Fraction			C_{26}		C_{27}		C_{28}		Total P_m	Temp.
C_{26}	C_{27}	C_{28}	P_m (Pa)	STDEV (Pa)	P_m (Pa)	STDEV (Pa)	P_m (Pa)	STDEV (Pa)	Pa	K
0.050	0.462	0.487	0.54	0.02	2.76	0.1	1.75	0.2	5.05	433
0.112	0.332	0.556	1.25	0.02	2.10	0.1	2.05	0.2	5.40	433
0.112	0.332	0.555	1.25	0.01	2.12	0.06	2.10	0.1	5.48	433
0.113	0.332	0.555	1.20	0.02	2.02	0.05	1.97	0.1	5.19	433
0.114	0.333	0.553	1.24	0.03	2.07	0.1	2.00	0.2	5.31	433
0.144	0.416	0.441	1.49	0.04	2.46	0.2	1.58	0.2	5.52	433
0.275	0.387	0.338	3.22	0.04	2.14	0.06	1.14	0.04	6.50	433
0.363	0.199	0.438	4.22	0.02	1.22	0.02	1.47	0.05	6.90	433
0.367	0.199	0.435	4.59	0.06	1.20	0.07	1.45	0.09	7.24	433
	0.490	0.510			5.77	0.6	3.67	0.6	9.44	443
	0.489	0.511			5.90	0.4	3.76	0.4	9.65	443
0.051	0.463	0.486	1.10	0.08	5.50	0.6	3.57	0.6	10.18	443
0.113	0.333	0.554	2.42	0.04	4.16	0.2	4.17	0.3	10.75	443
0.143	0.415	0.441	2.78	0.1	4.92	0.3	3.15	0.3	10.85	443
0.275	0.387	0.338	6.17	0.1	4.30	0.09	2.39	0.05	12.85	443
0.362	0.199	0.439	7.93	0.05	2.41	0.04	2.99	0.1	13.33	443
	0.489	0.511			10.60	0.6	7.45	1.3	18.05	453
0.050	0.462	0.488	1.61	0.08	10.25	0.4	7.16	0.6	19.02	453
0.113	0.332	0.555	3.93	0.3	7.91	0.5	8.21	0.6	20.05	453
0.142	0.415	0.442	4.48	0.3	8.82	0.8	5.78	0.7	19.08	453
0.273	0.387	0.339	9.15	0.9	8.07	0.3	5.47	0.8	22.68	453
0.361	0.199	0.441	12.28	1.2	5.19	0.9	6.43	1.2	23.89	453

4.4. Measurement of Diffusion Coefficients

Measured partial pressures for different diffusion distances x and carrier gas flow rates are tabulated in Tables 4.15 and 4.16 for C_{20}, C_{28} at 423 K and 463 K, respectively. As an example, the diffusion coefficient of C_{20} calculated from Equation (2.8) as function of carrier gas flow rates for every apparent diffusion distance is shown in Figure 4.35. For $x > 4$ cm and $F < 0.5$ mL s^{-1} the calculated diffusion coefficient does not depend on x or F. For x = 9.4 cm and F = 21.4 ml/min, the diffusion coefficients of C_{20} between 440 K and 464K derived from partial pressures measured using a temperature program with 0.2 K/min heating rate are listed in Table 4.17.

Table 4.15. Dependence of Measured Partial Pressures on x and F* for C_{20} at 423 K.

x	F*	P_m (Pa)		x	F*	P_m (Pa)	
cm	ml/s	Average	STDEV	cm	ml/s	Average	STDEV
0.85	0.26	3.00E+01	1.4E-01	6.40	0.28	4.70E+00	7.2E-03
0.85	0.32	2.77E+01	5.0E-01	6.40	0.39	3.39E+00	9.1E-03
0.85	0.46	2.19E+01	9.3E-02	6.40	0.39	3.46E+00	7.1E-03
0.85	0.60	1.84E+01	3.1E-02	6.40	0.48	2.75E+00	5.3E-03
0.85	0.76	1.61E+01	2.9E-02	6.40	0.49	2.76E+00	5.8E-03
0.85	0.92	1.48E+01	5.0E-02	6.40	0.58	2.33E+00	5.4E-03
0.85	1.16	1.20E+01	3.7E-02	6.40	0.61	2.16E+00	5.6E-03
0.85	1.44	1.05E+01	2.2E-02	6.40	0.67	1.99E+00	4.9E-03
1.40	0.08	4.41E+01	3.3E-01	6.40	0.76	1.71E+00	5.3E-03
1.40	0.13	3.54E+01	1.1E-01	6.40	0.79	1.72E+00	3.2E-03
1.40	0.24	2.39E+01	7.0E-02	6.40	0.97	1.34E+00	2.7E-03
1.40	0.39	1.52E+01	5.1E-02	6.40	1.00	1.35E+00	4.8E-03
1.40	0.61	1.07E+01	5.7E-02	8.50	0.186	5.10E+00	1.9E-02
1.40	0.96	7.51E+00	2.4E-02	8.50	0.308	3.13E+00	9.0E-03
1.40	1.29	5.87E+00	1.5E-02	8.50	0.413	2.34E+00	4.0E-03
4.65	0.23	8.08E+00	2.5E-02	8.50	0.501	1.90E+00	5.8E-03
4.65	0.23	8.09E+00	1.9E-02	8.50	0.598	1.56E+00	2.7E-03
4.65	0.34	5.66E+00	3.7E-02	8.50	0.691	1.36E+00	2.4E-03
4.65	0.44	4.26E+00	1.3E-02	9.50	0.178	4.86E+00	2.8E-02
4.65	0.59	3.25E+00	1.4E-02	9.50	0.247	3.52E+00	1.7E-02
4.65	0.68	2.76E+00	9.4E-03	9.50	0.340	2.60E+00	6.7E-03
4.65	0.78	2.30E+00	1.4E-02	9.50	0.444	1.95E+00	6.2E-03
6.40	0.18	7.03E+00	2.7E-02	9.50	0.563	1.51E+00	4.7E-03
6.40	0.28	4.87E+00	7.4E-03	9.50	0.660	1.22E+00	3.6E-03

F*: flow rate at saturator temperature and pressure.

Table 4.16. Dependence of Measured Partial Pressures on x and F* for C_{28} at 463 K.

x	F*	P_m (Pa)		x	F*	P_m (Pa)	
cm	ml/s	Average	STDEV	cm	ml/s	Average	STDEV
1.40	0.27	4.24E+00	1.3E-02	3.60	0.35	9.68E-01	8.1E-03
1.40	0.33	3.73E+00	9.4E-03	3.60	0.46	7.51E-01	5.3E-03
1.40	0.42	3.09E+00	5.1E-03	3.60	0.57	6.05E-01	1.6E-03
1.40	0.50	2.73E+00	2.2E-03	3.60	0.69	4.92E-01	9.8E-03
1.40	0.50	2.73E+00	3.8E-03	3.60	0.79	4.18E-01	5.5E-03
1.40	0.59	2.36E+00	3.5E-03	3.60	0.91	3.58E-01	2.5E-03
1.40	0.79	1.83E+00	2.4E-03	3.60	0.99	3.19E-01	2.3E-03
2.30	0.29	2.07E+00	8.1E-03	4.65	0.25	9.32E-01	5.0E-03
2.30	0.29	2.05E+00	1.1E-03	4.65	0.34	7.19E-01	2.8E-03
2.30	0.34	1.82E+00	7.3E-03	4.65	0.44	5.72E-01	2.2E-03
2.30	0.44	1.44E+00	4.2E-03	4.65	0.56	4.61E-01	1.9E-03
2.30	0.59	1.04E+00	1.1E-03	4.65	0.68	3.88E-01	2.4E-03
2.30	0.59	1.04E+00	1.8E-03	4.65	0.80	3.35E-01	1.5E-03
2.30	0.80	7.89E-01	8.4E-04	4.65	0.88	3.05E-01	1.1E-03
2.80	0.29	1.58E+00	7.2E-03	5.50	0.25	8.63E-01	7.5E-03
2.80	0.39	1.23E+00	1.5E-02	5.50	0.37	5.73E-01	2.0E-03
2.80	0.39	1.22E+00	5.6E-03	5.50	0.49	4.33E-01	1.9E-03
2.80	0.47	9.94E-01	7.0E-03	5.50	0.62	3.33E-01	2.1E-03
2.80	0.59	8.36E-01	4.4E-03	5.50	0.73	2.82E-01	5.1E-04
2.80	0.70	7.11E-01	4.3E-03	5.50	0.85	2.43E-01	1.3E-03
2.80	0.84	6.21E-01	6.4E-03	5.50	0.96	2.14E-01	1.0E-03
3.60	0.22	1.35E+00	7.6E-03				

F*: flow rate at saturator temperature and pressure.

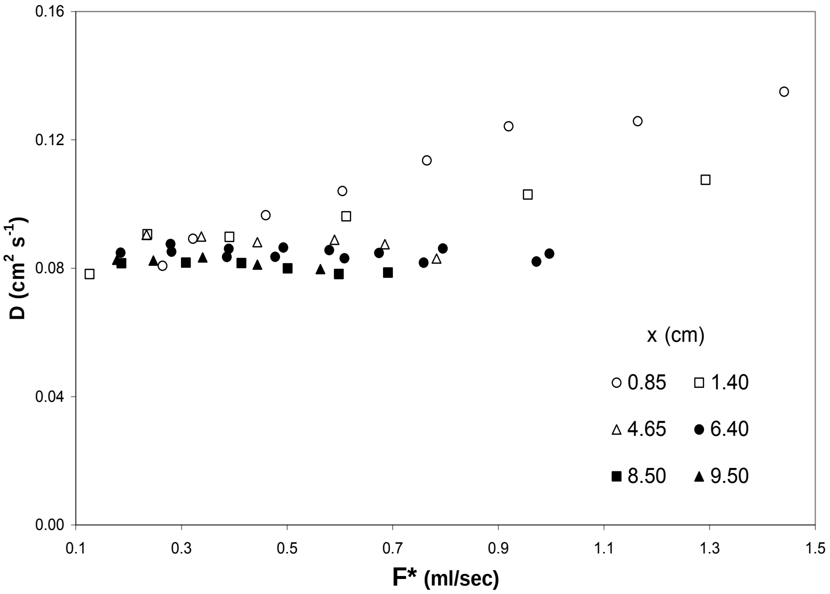

Figure 4.35. Diffusion coefficient at 423 K and 2.3 atmospheres as function of carrier gas flow rate for C_{20}.

Table 4.17. Dependence of Measured Diffusion Coefficients on Temperature for C_{20} at 2.3 Atmospheres He.

T (K)	D (cm^2 s^{-1})	T (K)	D (cm^2 s^{-1})	T (K)	D (cm^2 s^{-1})	T (K)	D (cm^2 s^{-1})	T (K)	D (cm^2 s^{-1})
439.8	1.05E-01	444.5	1.07E-01	449.1	1.09E-01	453.8	1.09E-01	458.7	1.11E-01
440.0	1.04E-01	444.7	1.07E-01	449.3	1.08E-01	454.0	1.10E-01	458.9	1.12E-01
440.2	1.05E-01	444.9	1.06E-01	449.6	1.09E-01	454.2	1.10E-01	459.1	1.12E-01
440.4	1.05E-01	445.1	1.07E-01	449.8	1.09E-01	454.5	1.10E-01	459.4	1.11E-01
440.7	1.05E-01	445.3	1.07E-01	450.0	1.09E-01	454.7	1.10E-01	459.6	1.12E-01
440.9	1.05E-01	445.6	1.07E-01	450.2	1.09E-01	454.9	1.10E-01	459.8	1.12E-01
441.1	1.05E-01	445.8	1.07E-01	450.5	1.09E-01	455.1	1.10E-01	460.0	1.12E-01
441.3	1.05E-01	446.0	1.08E-01	450.7	1.09E-01	455.6	1.11E-01	460.2	1.12E-01
441.6	1.05E-01	446.2	1.07E-01	450.9	1.09E-01	455.8	1.11E-01	460.5	1.12E-01
441.8	1.06E-01	446.5	1.07E-01	451.1	1.09E-01	456.0	1.10E-01	460.7	1.12E-01
442.0	1.05E-01	446.7	1.08E-01	451.4	1.08E-01	456.2	1.10E-01	460.9	1.12E-01
442.2	1.05E-01	446.9	1.07E-01	451.6	1.09E-01	456.5	1.11E-01	461.1	1.12E-01
442.5	1.05E-01	447.1	1.08E-01	451.8	1.09E-01	456.7	1.10E-01	461.4	1.12E-01
442.7	1.06E-01	447.3	1.07E-01	452.0	1.09E-01	456.9	1.11E-01	461.6	1.13E-01
442.9	1.05E-01	447.6	1.08E-01	452.2	1.09E-01	457.1	1.11E-01	461.8	1.13E-01
443.1	1.05E-01	447.8	1.08E-01	452.5	1.09E-01	457.4	1.11E-01	462.5	1.14E-01
443.3	1.06E-01	448.0	1.09E-01	452.7	1.09E-01	457.6	1.11E-01	462.7	1.14E-01
443.6	1.06E-01	448.2	1.08E-01	452.9	1.09E-01	457.8	1.11E-01	462.9	1.13E-01
443.8	1.05E-01	448.5	1.08E-01	453.1	1.09E-01	458.0	1.11E-01	463.1	1.13E-01
444.0	1.06E-01	448.7	1.09E-01	453.4	1.10E-01	458.2	1.11E-01	463.4	1.14E-01
444.2	1.06E-01	448.9	1.08E-01	453.6	1.09E-01	458.5	1.12E-01	464.0	1.14E-01

5. Discussion

5.1. Characterization and Test of the TDI

Based on the tests of the TDI detection systems it can be concluded that the TDI detection system allows quantitative determination of organic substances reaching the oxidation catalyst. The results in 4.1 demonstrate that CH_4, which is one of the most difficult organic compounds to be oxidized, is completely oxidized by the TDI oxidation catalyst, and CO_2 is reduced to CH_4 efficiently by the TDI reduction catalyst. The CH_4 calibration is stable over time and the recoveries for CH_4 or CO_2 injected at different injection ports are near unity (96-103%) compared to the calibration using methane injections into the TDI reactor. The recoveries of KHP and n-alkanes for both the TC-30 and OC-30 methods are close to one with good linearity ($R^2 > 0.99$) and the relative errors of the recoveries are in the range of 1.0-2.8%, which indicates that the TDI calibration is accurate.

Overall, the test results show that the recoveries for all test substances are near unity when the sample masses are less than 20 μg (Refer to Figure 4.2). For measurements of TC the comparison shows a nearly quantitative recovery over a range of nearly 100 μg. Only the recovery of mannitol strongly depends on both the TDI method and sample masses. The recovery is 84% in the mass range of 1.4 – 84 micrograms under TC-30 method, and less than 30% when the sample mass is larger than 20 micrograms when using OC-30 method. The possible reasons for the low recovery of mannitol is wall loss, incomplete reaction or charring. Higher transfer line and final reactor temperature did not improve the recovery for large sample mass of mannitol (Table 5.1). It suggests that wall loss or incomplete reaction is not the reason and the low recovery is most likely caused by charring. This is also compatible with the finding that the recovery is decreasing with increasing sample mass.

Table 5.1. Mannitol Recovery under Different TDI Method and Experimental Conditions

TDI method	Transfer line Temperature K	Reactor final Temperature K	Spiked Mannitol mass (µg)							
			1.4	7.0	14.1	21.1	28.1	42.2	56.2	70.3
			Recovery (%)							
TC	573	1023	129	118	110	119	107	90	90	83
OC	573	1023	68	99	92	59	52	45	42	24
OC	673	1173							22	23

In summary the tests indicate that the upper limit of the linear range for TC measurements is around 80 µg, for OC about 20 µg. The detection limit is determined by the variability of the blank values given in Table 4.2, that is 0.6 µg and 1.0 µg for OC and TC measurements, respectively. The standard deviation found for TC measurements of field blanks is 0.7 µg. This results in detection limits of approximately 2 µg to 3 µg. In order to convert these detection limits and linear ranges into atmospheric detection limits, the sample volume as well as the fraction of the high volume filter which is used for TDI measurements has to be considered. During the SONTAS campaign samples were collected for 24 h at a flow rate of 1.13m^3/min, which amounts to a total sample volume of about 1500 m^3. The TDI measurements typically use a piece of filter with a diameter of 0.83 cm, which is 0.1% of the area of the high volume filter used for sample collection. This corresponds to about 2.1 m^3 of air collected on the filter aliquot used for TDI analysis. Based on this volume, the variability of the blank values results in a lower limit of detection in the range of 1$\mu g/m^3$ to 1.5$\mu g/m^3$. The upper end of the linear range is 30$\mu g/m^3$ and 8 $\mu g/m^3$ for TC and OC measurements, respectively. This is adequate for TC measurements in ambient air, with the exception of extremely polluted areas and marine background air. For OC measurements the upper end of the linear range is above most of the values measured during the SONTAS campaign, although a few data are slightly higher (Table 4.6. and Figure 4.8.). The data in Table 4.6 and Figure 4.8 demonstrate that the TC measurements are generally consistent with the values obtained from OC and EC measurements. Since the reproducibility of the measurements is usually better than 10% the methodology overall is suitable for measurements of TC and OC in ambient particulate matter. Furthermore, adjusting the sample volume or the sampling time allows to some extent to adjust of the linear range for sampling at highly polluted or extremely clean sampling sites. It should be noted that increasing the size of the filter aliquot used for TDI analysis will have little impact on the detection limit and linear range. It is unlikely that the extent of charring will change with the size of the filter and the variability of the blank is predominantly due to residual carbon on the pre-fired filters (Table 4.2).

While overall the various tests show that the TDI methods allows TC measurements with an accuracy of about 10%, the occurrence of charring results in difficulties to estimate the accuracy of differentiating between OC and EC. The measurements of KHP, mannitol, and n-alkane samples demonstrate that the extent of charring is highly substance dependent and therefore difficult to predict for the complex composition of ambient samples, in spite of the good reproducibility obtained for repeat OC and EC measurements in the same sample. This problem has been reported in literature and for many OC and EC measurement techniques the OC/EC differentiation is not so much a true chemical identification, but a definition based on instrumental methods and the thermal behavior of the individual samples (for more details see 5.2).

The thermal behavior of test samples was studied by different TDI methods. For the OC-15-Air, OC-30-Air, OC-40-Air and OC-15-He, OC-30-He, OC-40-He methods, the hold temperature was chosen to be 663 K since it is reported that elemental carbon can survive under this temperature in the presence of oxygen (Lin et al., 1988 a, b; Gelinas et al., 2001; Nguyen et al., 2004). For the OC-15, OC-30, OC-40 methods, the thermogram of KHP contains one predominant peak at about 800 K and two small peaks (Figure 5.1). It can also be seen from Figure 5.1 that the peaks systematically shift to lower temperatures when using lower heating rates. For the OC-15-Air, OC-30-Air, OC-40-Air methods, major peaks appear at lower temperature (Figures 4.5-4.7). A summary of the thermal behavior of KHP for the different methods is given in Table 5.2.

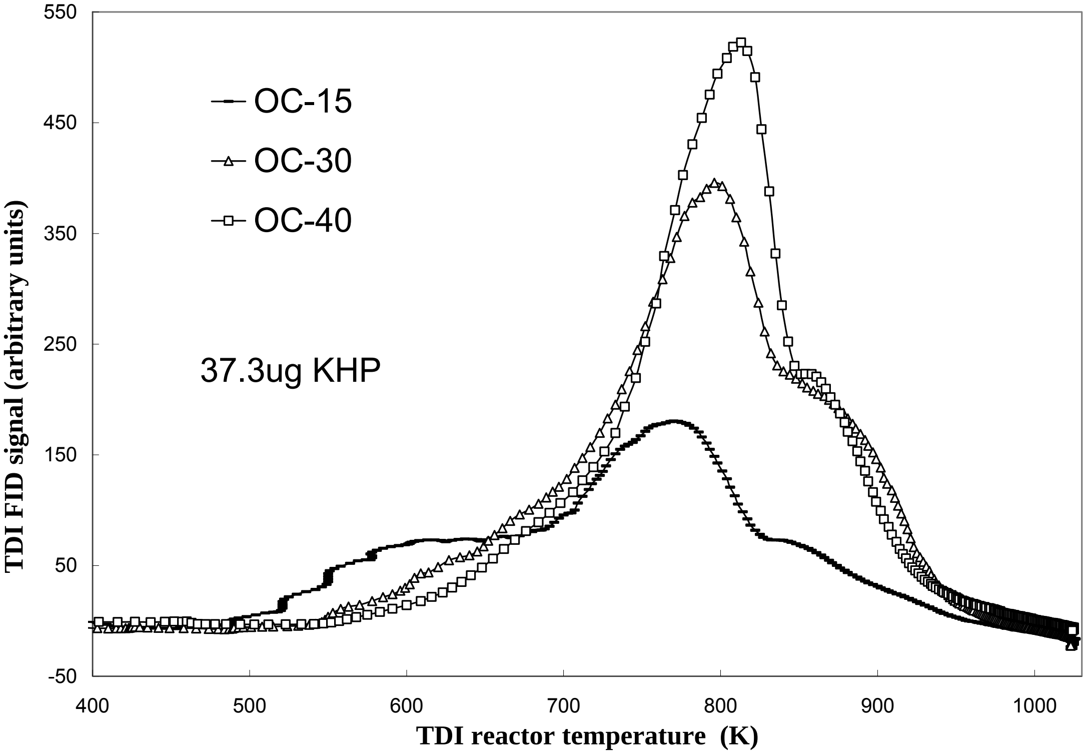

Figure 5.1. Thermograms of 37.3 μg KHP using method OC-15, OC-30 and OC-40. It should be noted that when using a T scale as x-axis, the peak areas below the curves depend on the heating rate due to the different time intervals represented by a given temperature interval.

The background corrected signals for the time intervals corresponding to TDI oven temperatures below 663 K, at 663 K hold and above 663 K, the FID signal of KHP samples were integrated and are summarized in Table 5.1. They repreaents the recoveries of KHP in different temperature ranges, integration time intervals and peak maximum temperatures (the last peak for the OC-15-Air, OC-30-Air, OC-40-Air and OC-15-He, OC-30-He, OC-40-He methods). The experimental conditions of the OC-15, OC-30, OC-40 and OC-15-He, OC-30-He, OC-40-He methods are the same below 663 K, respectively and the recoveries for these two kinds of methods are almost the same for the same heating rate. Below 663 K the highest recoveries were observed for the slowest heating rate. This is consistent with the general observation that for lower heating rates; a greater degree of decomposition degree is found for a given temperature interval (Newkirk 1960).

Table 5.2. KHP Recovery Result and Peak Maximum Temperature Using Different TDI OC methods.

TDI method	Below 663 K		Hold at 663 K		Above 663 K			Temperature (K)	
	%	Interval (s)	%	Interval (s)	%	Interval	Peak height	Peak maximum.	Peak starting point
OC-15	23	998	---	---	74	2690	180	780	493
OC-30	7	540	---	---	90	2378	396	801	543
OC-40	3	165	---	---	94	2481	522	813	606
OC-15-Air	36	880	27	598	34	1478	145	770	443
OC-30-Air	17	412	42	601	37	2303	240	811	503
OC-40-Air	8	221	53	602	36	1698	300	823	574
OC-15-He	23	821	20	606	54	2160	160	777	493
OC-30-He	7	341	34	602	56	2322	303	811	543
OC-40-He	2	130	37	595	57	2477	447	823	606

% – Recovery = Measured carbon mass/spiked carbon mass; Interval – integration time interval.

With oxygen in the carrier gas, the peaks start at lower temperature and the recovery is higher for the same heating rate below 663 K. The evolved carbon masses during the 663 K hold period is related to the carbon masses evolved below 663 K or the heating rate. More carbon evolved below 663 K, less carbon will be evolved during the 663 K hold period. The recoveries above 663 K are almost the same for the same carrier gas regardless of the heating rate for the OC-15-Air, OC-30-Air, OC-40-Air and OC-15-He, OC-30-He, OC-40-He methods. For the same heating rate and different methods, the peak maximum temperatures do not change extensively. However, for the same method and different heating rates, the temperature shift is significant (20–60 K). This behavior is predicted by the kinetic theory of solid-state reactions (Ozawa 1970). Above results imply that the thermodesorption behavior of KHP is primarily determined by thermal decomposition with some oxidation happening at temperatures below 663 K in the presence of oxygen.

The pyrolysis of KHP consists of the following steps: 1) The decomposition of KHP around 493-653 K produces dipotassium phthalate, water and phthalic acid anhydride, which has a boiling point of 558 K and does not pyrolyze below 973 K (Brown et al., 1967); 2) Around 723-853 K the decomposition of dipotassium phthalate yields potassium carbonate, charring products and volatile compounds; 3) Further decomposition results in products of charring at higher temperatures; and 4) Potassium carbonate decomposition between 1143-1163 K. The potassium carbonate and charring derived materials can react to yield carbon monoxide around 973 K. It was reported that in nitrogen and air, the first step of decomposition is similar (Newkirk et al., 1962; Belcher et al., 1960). When 200 milligrams of KHP were heated in air and its weight loss was measured by thermogravimetry, four major peaks were found at about 573, 773, 973 and 1123 K corresponding to above 4 processes (Smalley et al., 1977). It was observed in this work that the first and second step of KHP decomposition begins at 443-543 K and 733-823 K, respectively, which is in agreement with the literature. However, the percentage of carbon released at lower temperatures is not the same in helium and helium/air mixtures and no peaks were found above 973 K. Furthermore; no signal corresponding to potassium carbonate decomposition in the temperature range of 1143-1163 K as described in literature was observed. Above disagreements of the observations of this work from the literature can be caused by the following reasons: 1) the sample mass is generally 200–500 milligrams for thermogravimetry studies, and in this work it is a few ten micrograms; 2) the heating rate is 0.5-5 K/min in above literature, but between 15 and 40 K/min in this work; 3) KHP is spiked on quartz fiber filters in this work, whereas metal sample holders (platinum) are often used for thermogravimetry. The experimental results show that for KHP carbon recovery is near 100% independent of the method used. No significant difference is found for a confidence interval of 95% (Student t-test).

5.2. TC, OC and EC Concentrations of PM Samples Measured by the TDI

The maximum and starting temperatures of peaks in OC thermograms for the same PM sample only slightly change for different heating rates. As an example the thermograms for a PM sample collected under a railway overpass in the centre of Toronto are shown in Figure 5.2. The evolved carbon mass percentage for different temperature range using different TDI OC methods are shown in Table 5.3. It indicates that the heating rates do not affect the evolved carbon mass significantly for helium carrier gas below 663 K or in the 663 K hold period. With oxygen in the carrier gas, more carbon is evolved both for the interval below 663 K and 663 K hold, but the extent is much smaller than that for KHP. For all heating rates, the evolved carbon mass above 663 K is always dominating; it indicates that most of the sample components are refractory.

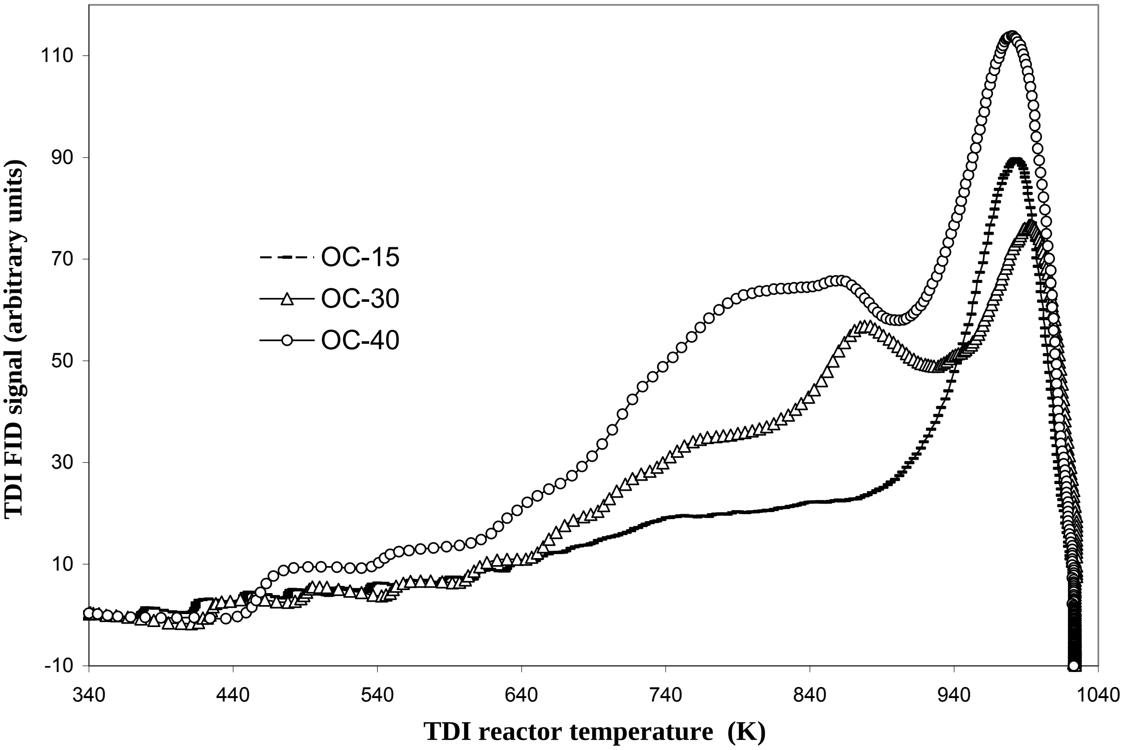

Figure 5.2. Thermograms of a PM sample using OC-15, OC-30 and OC-40 method.

It should be noted that when using a T scale as x-axis, the peak areas below the curves depend on the heating rate due to the different time intervals represented by a given temperature interval.

Table 5.3. Evolved Carbon Mass Percentage using Different TDI OC Methods for Aliquots from the Same High-volume Filter. .

Method	Below 663 K		Hold at 663 K		Above 663 K	
	%	Interval (s)	%	Interval (s)	%	Interval (s)
OC-15	8	1000	—	—	92	2810
OC-30	4	504	—	—	96	2792
OC-40	3	320	—	—	97	2500
OC-15-Air	18	1050	9	600	74	2468
OC-30-Air	11	510	14	594	75	2243
OC-40-Air	8	287	14	607	78	2293
OC-15-He	7	961	5	601	88	2323
OC-30-He	4	425	6	589	89	2310
OC-40-He	4	322	8	600	89	2264

%-Measured carbon mass in the interval/measured total carbon mass; Interval-integration time interval.

For SONTAS PM samples measured by TC methods, all the thermograms span an extremely wide temperature range (350-1100 K) and most of the carbon is evolved in the temperature range of 520-1020 K (See Figure 5.3). It was reported that EC combustion starts beyond 758 K in oxidative condition and completes around 923-933 K (Cadle *et al.*, 1980; Iwatsuki *et al.*, 1998). Obviously the carbonaceous materials in SONTAS PM samples cannot be completely burnt at above reported temperature, and it indicates that more refractory substances are contained in the samples. For every sample, the signals below the temperature of 490 K under TC and OC method are almost the same, which suggests that the carbon evolved below this temperature is from evaporation. Comparing to TC thermograms, troughs are always formed around 833-893 K on OC thermograms. It suggests that some components are refractory in this temperature range, but can be oxidized at higher temperatures. Different from TC result, OC thermograms show strong signals at higher temperature (peaked at about 970 K), the signal then decreases slowly and the FID signal does not return to baseline at the final oven temperature for OC method. This shows that the carbon release for highly refractory substances is a slow process even at high temperatures.

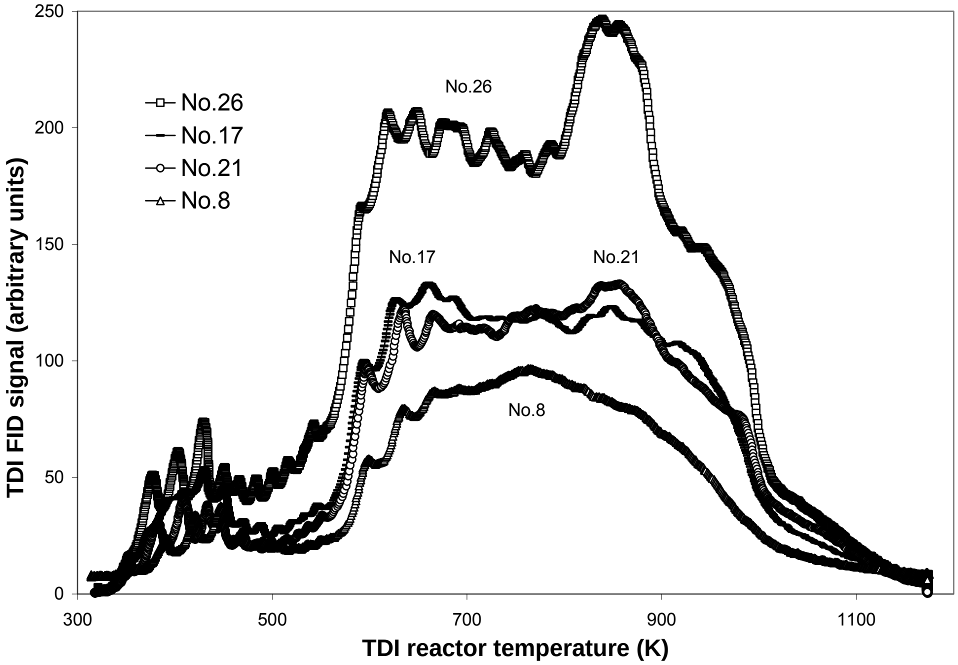

Figure 5.3. Thermograms of some SONTAS PM samples using TDI TC method.

When identical size aliquots of a PM sample filter was run repeatedly using OC method (Table 3.1), the thermograms below 763 K are almost the same, but become variable at higher temperature (See Figures Figure 5.4 and 5.5). Considering the highly reproducible TC result (Refer to Table 4.7), this variability is most likely not due to the sample inhomogeneity. After the analysis of OC, the sample was analyzed by TC method to determine EC concentrations. From the thermograms of EC, it is noted that below 720 K no carbon evolved which survived after OC run, indicating that material formed by charring does in the presence of oxygen not evolve carbon below this temperature. Most likely the charring of OC happens above 760 K and the produced/native chars decompose at higher temperature. It is found that if more carbon evolved during measurements of OC after 760 K, accordingly less EC will be measured. The variable OC thermograms suggest that the production/decomposition of char substances cannot be controlled by thermal desorption and the separation between OC and EC is not reproducible.

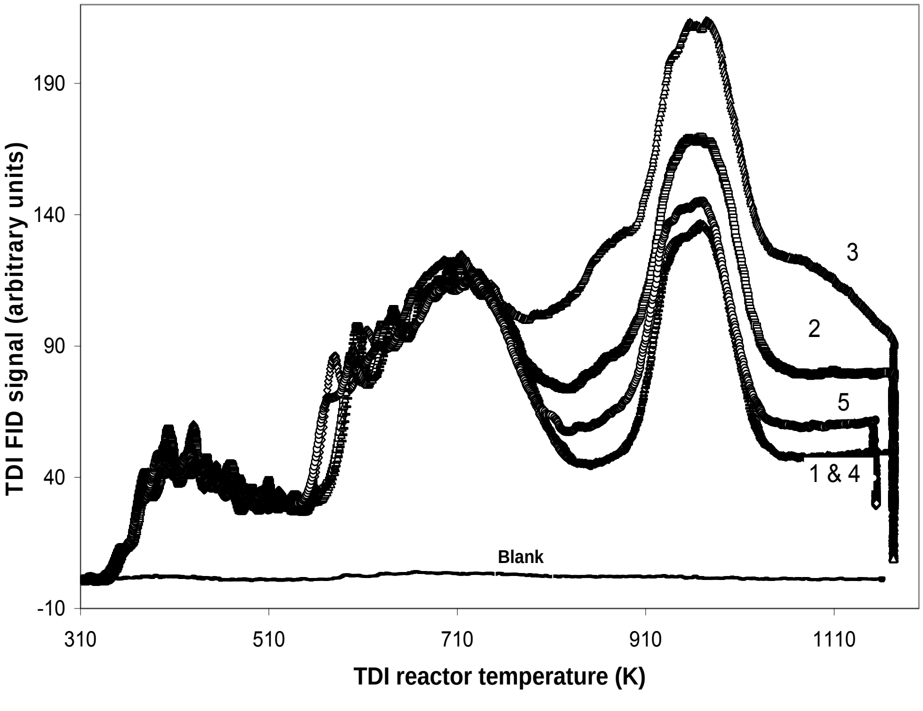

Figure 5.4. OC thermograms of SONTAS PM sample No. 26. The numbers inside the figure represent different repeat analysis under the same experimental conditions.

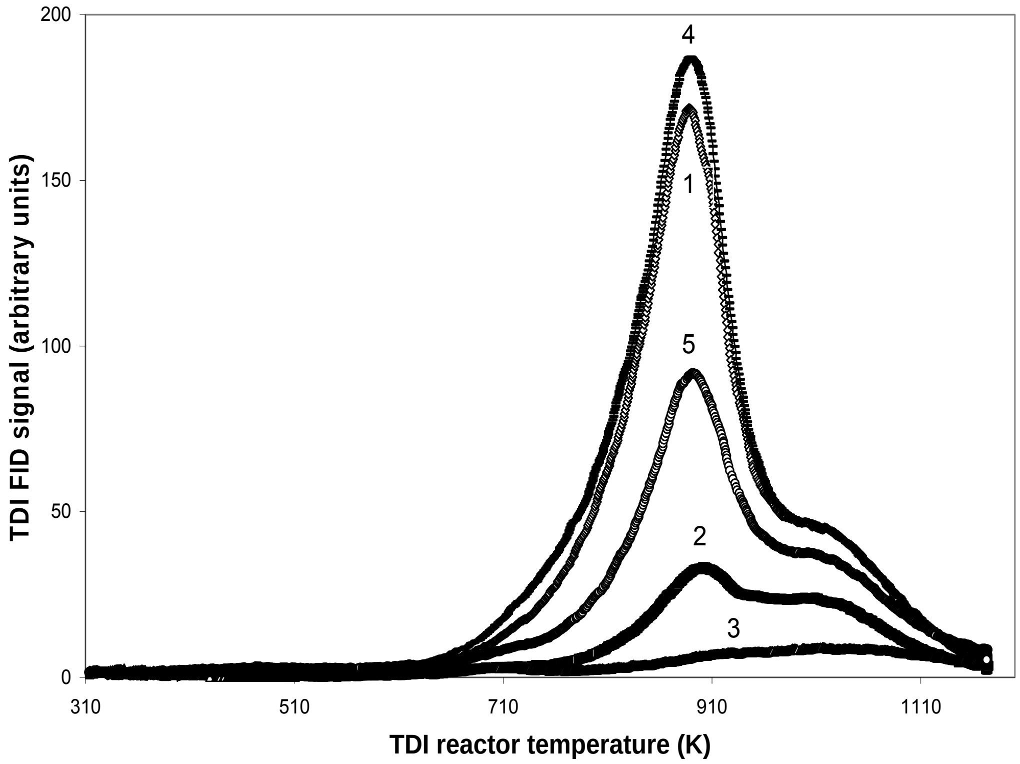

Figure 5.5. EC thermograms of SONTAS PM sample No. 26. The Arabic numbers inside the figure are corresponding to that in Figure 5.4 and represent different EC analysis under the same experimental conditions.

The concentration range, average and concentrations from literature for TC, OC and EC are summarized in Table 5.4. On averagely, TC consisted of 81% OC and 13% EC for SONTAS PM samples. The difference in budget of 6 % suggests that charring in the absence of oxygen results in the formation of a small fraction of refractory material which is not oxidized when using the EC method. The concentrations of TC, OC and EC of SONTAS samples are in the typical ranges of urban PM samples. In this work, TC, OC and EC were measured in separate runs; the TC and (OC+EC) concentrations are in good agreement (Figure 4.8). The variable OC, EC concentrations for some samples indicate that the differentiation between OC and EC is problematic. The largest relative uncertainties result for EC since EC in effectively all ambient PM samples is substantially lower than OC.

Table 5.4. Summary of TC, OC and EC Concentrations.

	TC, OC and EC result		From Reference		
	Range	Aver.	Range (μg C m^{-3})		
	μg C m^{-3}		1	2	3
TC	3.2 - 9.9	5.6		5-9	
OC	2.2 - 6.6	4.5	4.5-19	3-6	3-4
EC	0.3 - 3.8	0.8	1.3-3.8	1-3	0.3-1.1

1- Seinfeld et al., 1998; 2- Viana et al; 2006; 3- Jones et al., 2005.

The difficulty to separate OC and EC is because of the complexities of PM sample components and their thermal properties. First, the charring temperature of OC is compounds dependent and the yield of char is affected by many factors, such as sample mass, heating rate, duration of isothermal periods, type of carrier gas and temperature. Second, chars as well as native EC can decompose or react with oxygen at different temperatures (Leifeld 2007; Ohta *et al.*, 1984, 1996; Gelinas *et al.*, 2001; Nguyen et al., 2004) and trace salt (Na- and K-) content can eventually lower the thermal oxidation temperature of soot catalytically (Lin *et al.*, 1988 a, b). Third, some OC, such as a certain fractions of water soluble organic carbon and humic acids, lignin (HULIS, called Brown Carbon as well), behave thermally similar to EC which makes the split between OC and EC even more difficult (Krivacsy *et al*., 2001; Yu *et al*., 2002; 2004; Andreae *et al*., 2006).

In the past three decades, researchers developed many thermal desorption methods to measure PM OC and EC, including: 1) Removing OC thermally and defining the remaining carbon as EC. (Wolff *et al*. 1982; Ohta *et al*., 1984, 1996; Kuhlbusch *et al*.1995,1998; Lavanchy *et al*., 1999; Gustafsson *et al*.,1997,2001; Gelinas 2001; Lin *et al*., 2001; Hitzenberger *et al*.2006); 2) Measuring OC as carbon evolved in a defined temperature range, and defining the residue carbon as EC (Cadle et al., 1990; Countess 1990; Turpin et al., 1990; Stevens et al., 1992; Rubli et al., 2000; Dan et al., 2004; Minoura et al., 2006); 3) Thermal/optical methods including thermal/optical reflectance (-TOR) and thermal/optical transmittance (-TOT) to correct for charring. Many comparisons among different PM carbon measurement methods were conducted, the measured TC concentrations usually agree well, but the problematic issue of differentiating between OC and EC always causes erratic results (Cadle *et al*., 1982; Japar *et al*., 1984; Countess *et al*., 1990; Turpin *et al*., 1990; Liousse *et al*., 1993; Birch 1998; Birch *et al*., 1999; Lavanchy *et al*., 1999; Chow *et al*., 2001; Currie *et al*., 2002; Yang, *et al*., 2002; Chen *et al*., 2004; Chow *et al*., 2004; Park *et al*., 2005; Andreae *et al*., 2006; Hitzenberger *et al*., 2006; Reisinger *et al*., 2008).

In this work, OC is defined as carbon evolved between 321 K and a final temperature of 1173 K and without oxygen in carrier gas. The reproducibility of OC measurements is on average slightly better than 10 % (Table 4.7), which is sufficient to determine OC in atmospheric PM. However, when comparing OC and TC measurements, there is little additional information, which can be extracted. On average the SONTAS OC data in Table 4.6 is 18% lower than the TC values, which compares reasonably well with the finding that the measured EC values contribute nearly 13% to TC. Similarly, the value of EC/(TC-OC) is on average 0.9, close to the ideal value of 1. However, as can be seen from the individual data in Table 4.6, the individual data for measured EC values differ significantly from EC values calculated from the difference between TC and OC. This is not surprising, since the EC measurements have large relative uncertainties of up tot 80% and, as a consequence of error propagation the uncertainty of the difference between TC and OC has relative uncertainties averaging around 70%

5.3. Equilibrium Vapor Pressure and Diffusion Coefficient

The results of the vapor pressure data in Tables 4.10-4.15 show that the relative standard deviation of vapor pressure measurements is nearly always better than 10%. Similarly, the results of measurements using continuous detection mode and GC-separation mode gave effectively identical results (Table 4.8). In addition to the reproducibility, the bias due to calibration errors, wall losses and errors in the variables used to calculate equilibrium vapor pressures or diffusion coefficients will contribute to the uncertainty of the final data. The uncertainties of the response factors as well as the deviations between different calibration and measurement methods (Figures 4.9, 4.10 and 4.12, Table 4.) are in most cases between 3% and 5%.

The impact of wall losses is more difficult to estimate. Figure 5.6 shows the change of the measured vapor pressure as function of time. It is evident that for very small vapor pressures it takes several hours to obtain a stable signal. It seems reasonable that the stabilization of the signal occurs when the active surface sites are all occupied and therefore wall losses will no longer have a major impact on the result once the signal is stable. Since isothermal data are all derived from measurement made at a time when no further systematic change in signal intensity could be seen, it is assumed that these measurements are not significantly biased by wall losses. For temperature programmed partial pressure measurements the impact of wall losses will depend on the heating rate (see Chapter 5.3.2).

From the noise of the FID signal, the detection limit for TDI/GC measurements is estimated to be 10^{-6} Pa. However, the lower limit for reliable vapor pressure measurements was found to be in the 10^{-5} Pa range, for lower partial pressures the time to achieve a constant signal would have been too long.

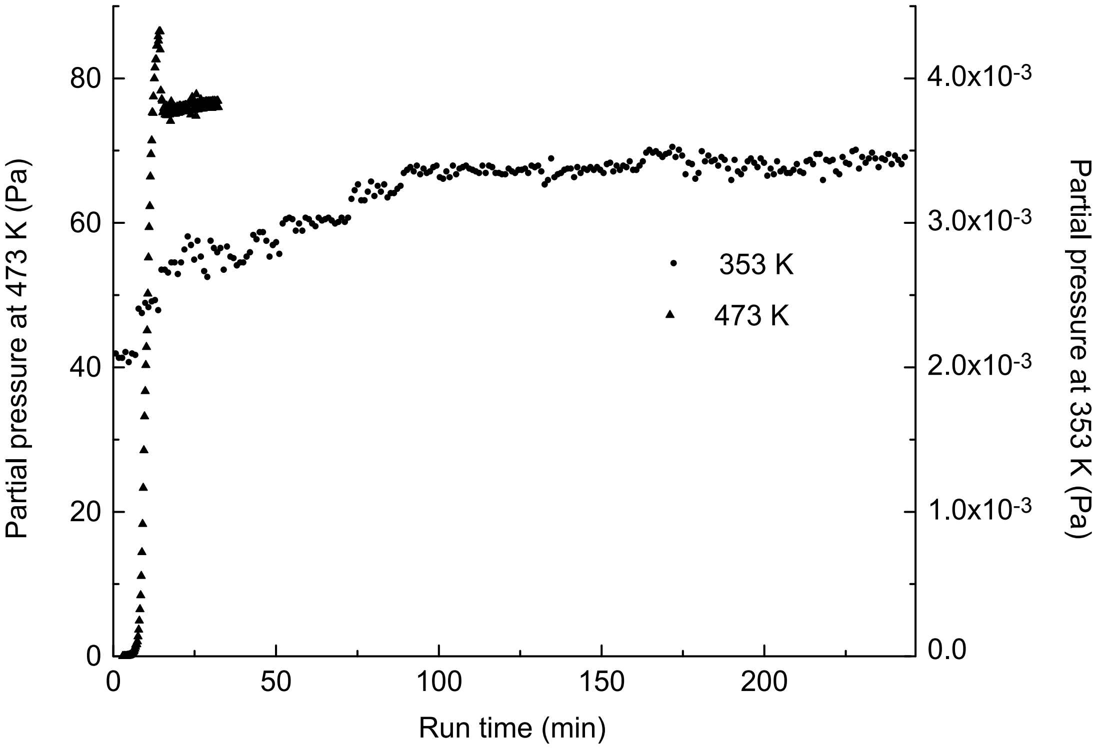

Figure 5.6. The change of the measured vapor pressure as function of time

In this work the determination of vapor pressures and diffusion coefficients is based on Equation (2.7).

$$P_m = \frac{P_s}{1+\left(\frac{x}{D}\right)\left(\frac{F}{S}\right)} \qquad \text{or} \qquad \frac{1}{P_m} = \frac{1}{P_s} + \left(\frac{x}{D\,S\,P_S}\right)F \qquad (2.7)$$

Depending on the values of (xF/DS) the following regimes can be distinguished: 1) (xF/DS) << 1 and $P_m \cong P_s$. In this case, the equilibrium partial pressure is measured without the need to know the exact values of x, D and S. It is the theoretical base of gas saturation technique and its consequence is that, as mentioned in literature (Eggertsen et al., 1969; Sinke 1974; Hales et al., 1981; Westcott et al., 1981; Sonnefeld et al., 1983; Verevkin 2004; Vasiltsova et al., 2005), that the flow rate should be low and the sample surface large in order to ensure that the measured vapor pressure is identical to the equilibrium partial pressure; 2) $(xF/DS) \cong 1$. It is expected from Equation (2.7) that a plot of inverse P_m as function of F is linear with the intercept being $1/P_s$, and the slope being $(x/DSPs)$. The equilibrium partial pressure can be derived from the slope or intercept if x, D and S can be determined accurately; 3) $(xF/DS) >>1$ and $P_m = P_s\ DA/(xF)$. In this regime, the curve of inverse P_m as function of F is linear with the intercept being close to zero and slope being $(x/DSPs)$. In this last case the equilibrium vapor pressure cannot be derived from partial pressure measurements because the extrapolation to F=0 will result in a too large uncertainty of any calculated y-axis intercept.

It should be noted that Equation (2.7) does not consider the influence of flow rate on turbulence or the possibility that the flow rates are too high to allow effectively uniform distribution of the evaporating substance in the gas phase. In the following part of discussion this problem will be studied in more detail.

5.3.1. Measurement of Partial Pressure under Isothermal Conditions

The dependence between the inverse of measured partial pressures and flow rate (Figure 4.26) shows two distinctive features, a region where the measured partial pressure is nearly constant at very low flow rates and a region with a clearly visible dependence between measured vapor pressure and flow rate. In Table 5.5 the average values for the low flow rate regimes from Figure 4.26. are summarized. To some extent the dependence between flow rate and measured partial pressure can be described by a linear dependence between inverse partial pressure and flow rate according to Equation (2.7). For C_{20} the data points in Figure 4.26 show a clear change of slope for flow rates exceeding 150 mL min^{-1}. Using these data to determine the equilibrium vapor pressure on the basis of Equation 2.7 gives a value which is extremely uncertain and not a useful estimate for the equilibrium vapor pressure (Table 5.6). The intercept is close to zero (-0.02 Pa^{-1}) with a huge error (-120%). Linear regression data for the low flow rate regimes gives intercepts which correspond to, as expected, the vapor pressures measured at the lowest flow rates with only small deviations (Table 5.6).

Table 5.5. Summary of the Data Independent of the Flow Rate for C_{20} at 373 K and C_{27}, C_{28} at 433 K.

	Range		P_m (Pa)		n	RSD
	F (ml/min)	P_m (Pa)	Average	STDEV		%
C_{20}	17–166	5.2–5.7	5.4	0.18	14	3.3
C_{27}	8–83	6.1–6.9	6.5	0.21	32	3.2
C_{28}	17–32	3.5–3.7	3.6	0.07	9	2

Table 5.6. Summary of the Linear Regression Parameters of P_m^{-1} as function of F for C_{20} at 373 K and C_{27}, C_{28} at 433 K.

			Linear Regression				RE (%)		P_s	Diff.
	ml/min	P_m (Pa)	a (cm^{-3} Pa^{-1} min)	b (Pa^{-1})	n	R^2	a	b	(1/b) Pa	%
C_{20}	17–166	5.2–5.7	0.321×10^{-4}	0.188	14	0.073	-103	2	5.3	-2
C_{20}	166–231	3.7–5.5	12.6×10^{-4}	-0.02	6	0.966	9	-120	----	----
C_{27}	8–83	6.1–6.9	1.74×10^{-4}	0.149	32	0.371	23	1	6.7	3
C_{27}	83–157	4.6–6.2	3.61×10^{-4}	0.135	20	0.493	24	8	7.4	14
C_{28}	17–32	3.5–3.7	2.59×10^{-4}	0.274	9	0.038	190	4	3.6	2
C_{28}	32–161	2.0–3.7	16.5×10^{-4}	0.227	11	0.995	2	2	4.4	23

Diff.(%): the relative difference between measured partial pressure for the low flow rate and the partial pressure derived from the intercept of linear regression data both for the low and high flow rate regimes. Diff.(%) = 100 ×($P_{\text{linear regression}} - P_{\text{low flow rate}}$)/ $P_{\text{low flow rate}}$.

For C_{27} and C_{28} the change in slope is not as clearly visible, but for all curves there seems to be a region with a low dependence between flow rate and measured partial pressure, although the upper limit for this region is at different flow rates. From Equation (2.7) the slope of the plot of inverse partial pressure versus flow rate is (x/D S Ps). The values for D, S and P_s are known. The surface area of the n-alkanes in the quartz boat is about 4 cm^2 and the vapor pressures are measured or can be taken from literature (5.3.3). The diffusion coefficients can be calculated from a combination of measured data and theoretical considerations (5.3.5). However, for a quartz boat filled with n-alkanes placed in a quartz tube x is difficult to estimate. Based on the dimensions of the quartz boat and the quartz tube x will be in the range of a fraction of mm to a few mm. The corresponding slopes calculated according tom Equation (2.7) are in the range of $3x10^{-4}$ to $2x10^{-3}$ cm^{-3} Pa^{-1} min for C_{20} and C_{27}, and $5x10^{-4}$ to $4x10^{-3}$ cm^{-3} Pa^{-1} min for C_{28}.

A comparison between the calculated values and the results of regression analysis of experimental data for different flow rate ranges shows that the experimental and calculated slopes are of similar order of magnitude. However, it is also clear that the difficulty of determining a consistent value for x limits the usefulness of Equation (2.7) for the experimental set-up used for vapor pressure measurements. Nevertheless, the experimental data and estimates based on Equation (2.7) demonstrate that measurements at low flow rates are adequate to derive equilibrium vapor pressure data. Although the values for the slopes have considerable uncertainty, due to the small value of the slopes, the uncertainty caused by extrapolating from small flow rates to a flow rate of zero are small. For flow rates in the range of some 10 cm^3 min^{-1}, the relative changes resulting from extrapolation to a flow rate of zero based on experimentally derived slopes for low flow rates are in the range of 1%. Using the upper end of values derived from Equation (2.7) would result in correction in the range of 10%. It therefore seems justified to conclude that uncertainties resulting from errors in extrapolating equilibrium vapor pressures to a flow rate of zero are negligible, as long as the measurements are made at low flow rates in the range of some 10 cm^3 min^{-1}.

It should be noted that many equilibrium vapor pressure techniques described in literature use large surface areas, for example by coating glass beads (Vasiltsova et al., 2005; Verevkin 2004; Carruth et al., 1973; Wania et al., 1994) or quartz sand (Addison 1981; Rothman 1980), and silver wire (Eggertsen et al., 1969) with the sample. The method used here is based on using low flow rates, which allows using a very simple method or sample preparation.

5.3.2. Comparison of Partial Pressure Measured Isothermally and by Temperature Programming

A plot of partial pressures measured by temperature programs with different heating rates versus partial pressures measured by isothermal conditions in the temperature range of 358 to 413 K for C_{20} is shown in Figure 5.7. The results obtained for a heating of 5 K/min clearly differ from the isothermal result. The relative difference between partial pressures obtained by isothermal conditions and temperature programs is shown in Figure 5.8. The relative differences for heating rates of ±0.1, ±0.5, ±1.0, ±2.0 and ±5.0 K/min are on average around 6% to 8%, 9% to 12%, 9% to 22%, 8% to 13% and 45% to 78%. This indicates that partial pressures measured by temperature programs with low heating rates, such as ±0.1 K/min are within the uncertainties of the measurements generally identical to results from isothermal measurements.

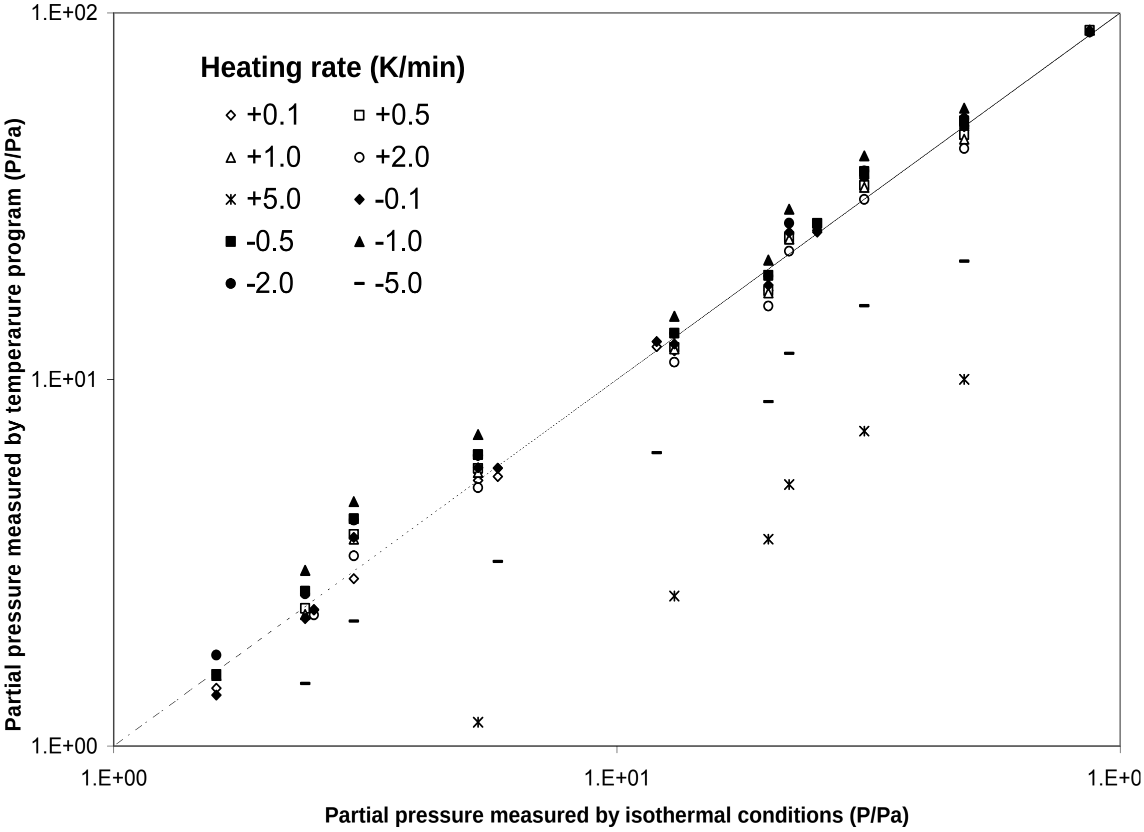

Figure 5.7. The partial pressures measured by temperature programs as function of the partial pressures measured by isothermal conditions for C_{20}.

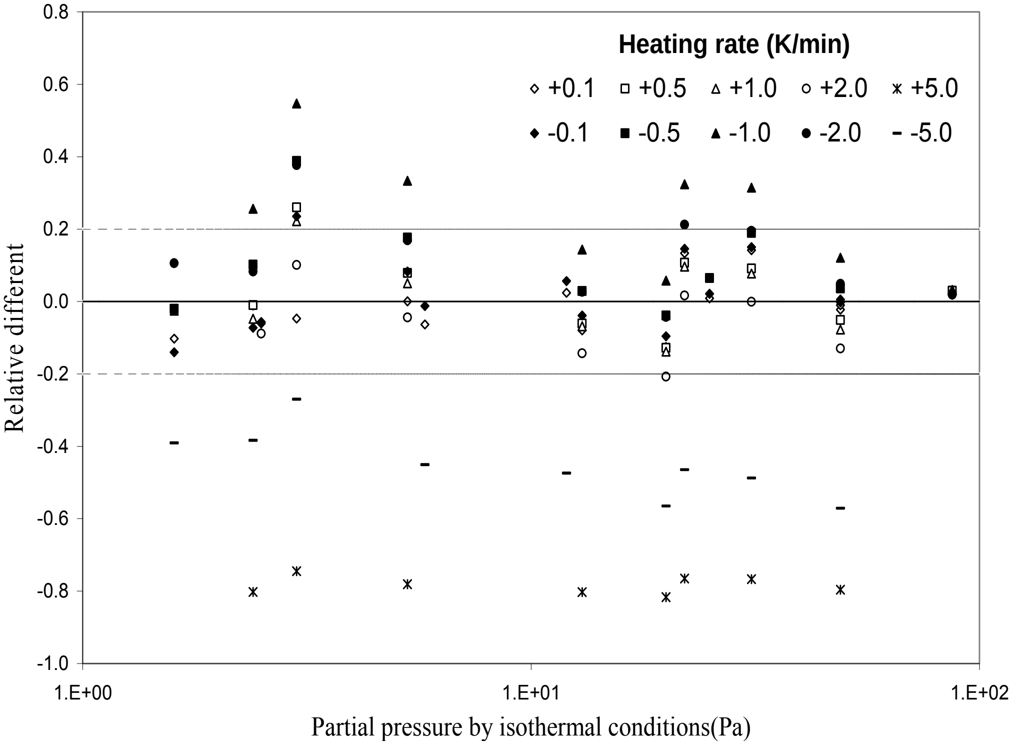

Figure 5.8 Relative difference between the partial pressures measured by isothermal conditions and temperature program as function of partial pressure. Relative difference = $(P_{\text{temp. program}} - P_{\text{isothermal}}) / P_{\text{isothermal}}$.

The partial pressures of C_{20} and C_{27} measured by temperature programs with +0.1 or -0.1 K/min heating rates for a wide range of temperatures are compared with that measured under isothermal conditions (Figure 5.9). The relative differences are shown in Figure 5.10. For both C_{20} and C_{27}, the agreement is good (generally within less than 20%

relative difference) for partial pressures exceeding 0.01 Pa. For lower partial pressures, there is more scatter and in some cases the relative differences exceeded 20%.

This comparison shows that the results of measurements of the equilibrium vapor pressures for n-alkanes using temperature programs with low heating rates agree for values exceeding 0.01 Pa with results from isothermal studies. For very low vapor pressures the differences are larger, but considering the overall difficulties in measuring very low equilibrium vapor pressures, such data are still useful. The advantage of temperature programmed vapor pressure studies is the possibility to cover a wide range of temperatures, and thus vapor pressures, in one experiment. In the following subchapters, the partial pressures measured by isothermal conditions and temperature programs with +0.1 or -0.1 K/min heating rates are combined. It has to be remembered that, duo to the similarity of the experimental set-up for isothermal and temperature programmed measurements, the consistency between the results only allows evaluation of the reproducibility of the measurements, but provides little information about possible systematic bias. Therefore a detailed comparison with literature data, which are based on a range of experimental methods, will be conducted in the next subchapters.

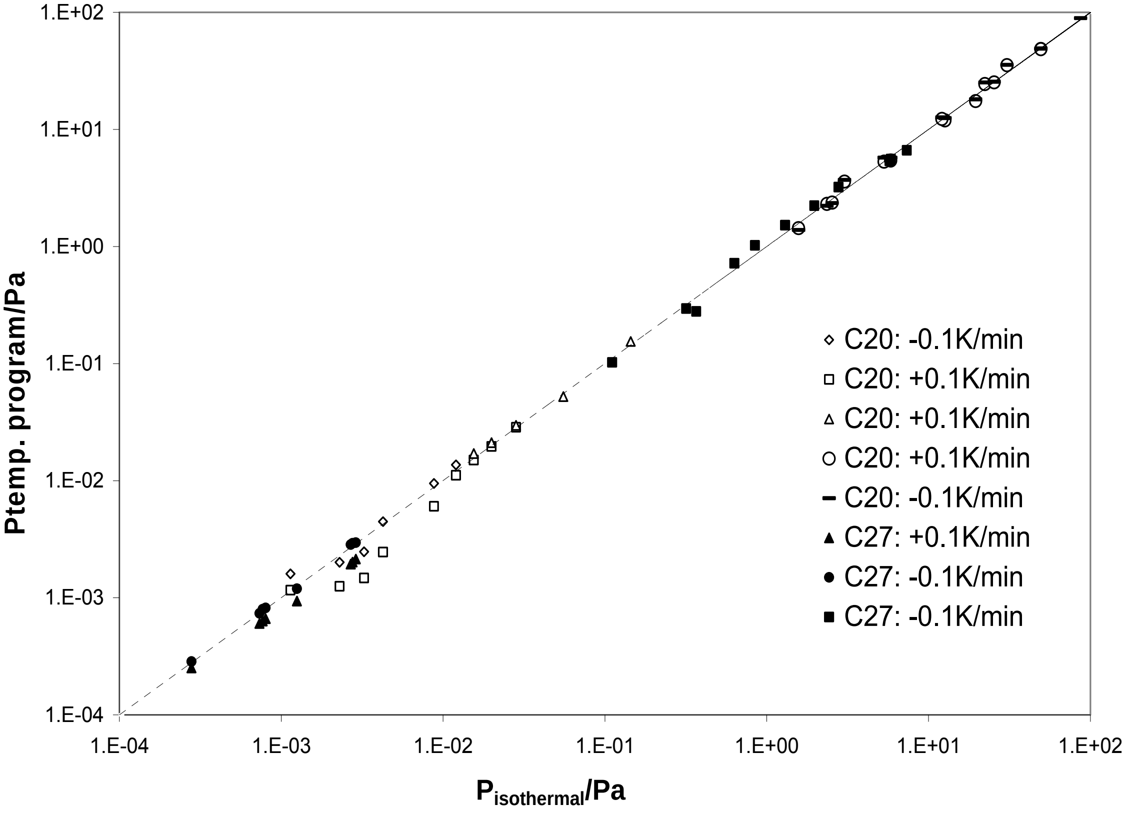

Figure 5.9. The partial pressures measured by temperature programs as function of the partial pressures measured by isothermal conditions for C_{20} and C_{27}.

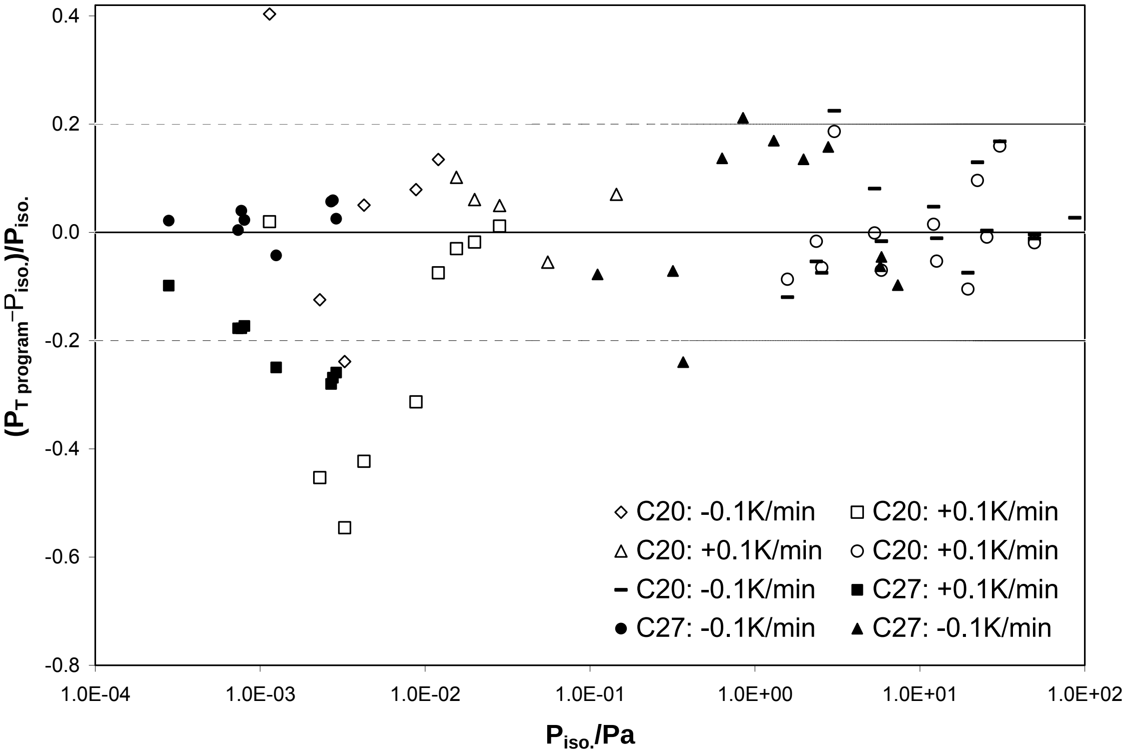

Figure 5.10. Relative difference between the partial pressures measured by isothermal conditions and temperature program with +0.1 and -0.1 K/min heating rates as function of partial pressure. Relative difference = ($P_{\text{temp. program}}$ - $P_{\text{isothermal}}$)/ $P_{\text{isothermal}}$.

5.3.3. Comparison of Partial Pressures from This Work with Literature Data

A compilation of measured partial pressures from literature and this work for C_{20}, C_{26}, C_{27} and C_{28} are shown in Figures 5.11 to 5.14. The data are presented in the form of Arrhenius type plots, which allows for easy interpolation of the data for comparison. There are no partial pressures in literature available for C_{20} below the temperature of 312

K and for C_{27} below the temperature of 351 K. Therefore partial pressures below above temperatures for C_{20} and C_{27} from this work are not included in the comparison.

Overall the different data sets agree reasonably well, but it has to be considered that, duo to the logarithmic pressure scale small relative differences in pressure will be difficult to see. For C_{20} the literature values from Piacente et al; 1991 in the temperature range of 315 to 366 K are constantly higher than the measurements from this work (Figure 5.11). Between 340 K and 420 K, the partial pressures from this work and Chirico et al., 1989; Grenier et al., 1981; Macknick et al., 1979; Mokbel et al., 2007; Myers et al., 1955 and Sasse et al; 1988 are in agreement, although there is some scatter between the data from different groups. For temperatures higher than 420 K, the vapor pressures measured in this work are at the high end of the published data. Nevertheless, with the exception of the data sets by Piacente et al. (1991) the data agree within the uncertainties of the measurements.

The partial pressures for C_{26} from this work and Grenier et al; 1981 are in good agreement (Figure 5.12). The data of Piacente et al; (1991 and 1994) exhibit some scatter, but on average they are close to those from this work. From Figure 5.13, it is noted that for C_{27} the result of this work, Morecroft 1964, Piacente et al; 1994(1), Piacente et al; 1991 and Sayawa et al; 2006 are close, but the result of Piacente et al; 1994(2), and Pompili et al; 1990 differ substantially and systematically from above data. As shown in Figure 5.14, the partial pressures for C_{28} from this work are slightly higher than literature values except the data in the temperature range of 424-459 K from Piacente et al; 1994 and in the temperature range of 469-492 K from Piacente et al; 1991, which are in agreement with this work. Although the available data for C_{28} exhibit significant and to some extent systematic variability, the data from this work agree within this – variability with the published measurements.

Overall the vapor pressure measurements from this work agree very well with published data. The comparison with literature data shows no indication for systematic bias of the measurements conducted in this work.

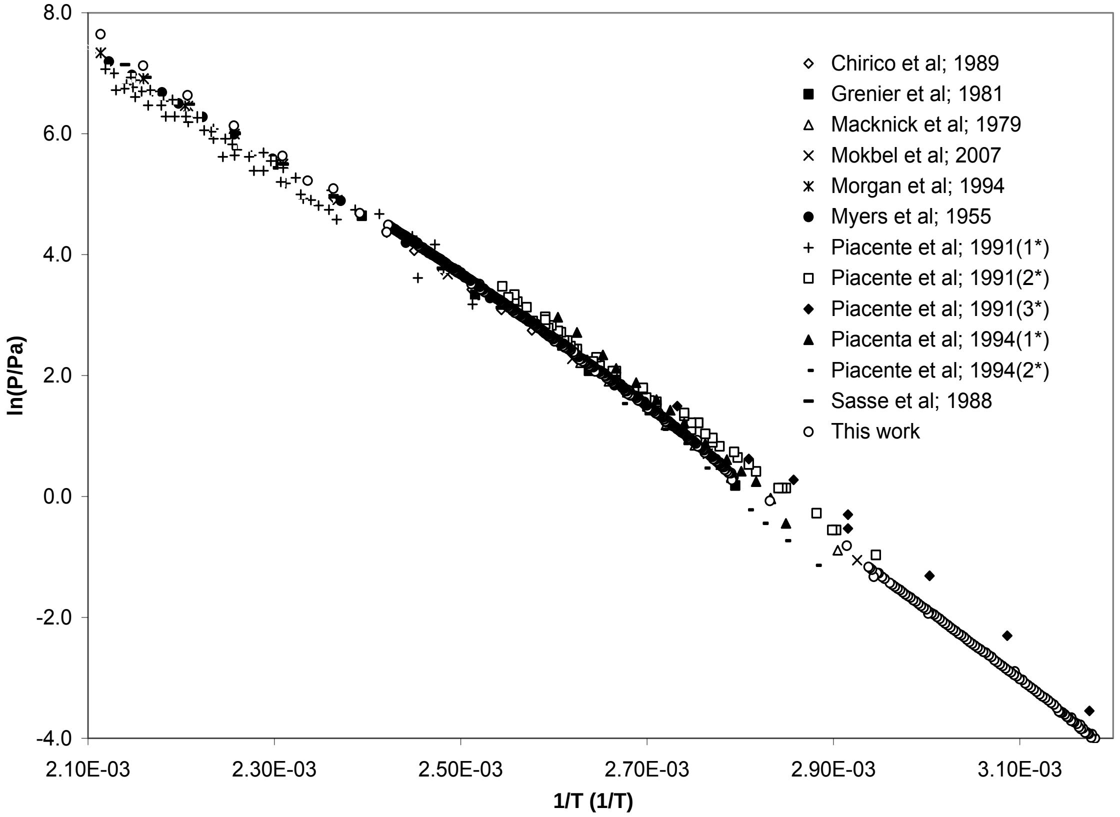

Figure 5.11. Partial pressures from literature and this work for C_{20}, *Multiple data sets are given in the literature.

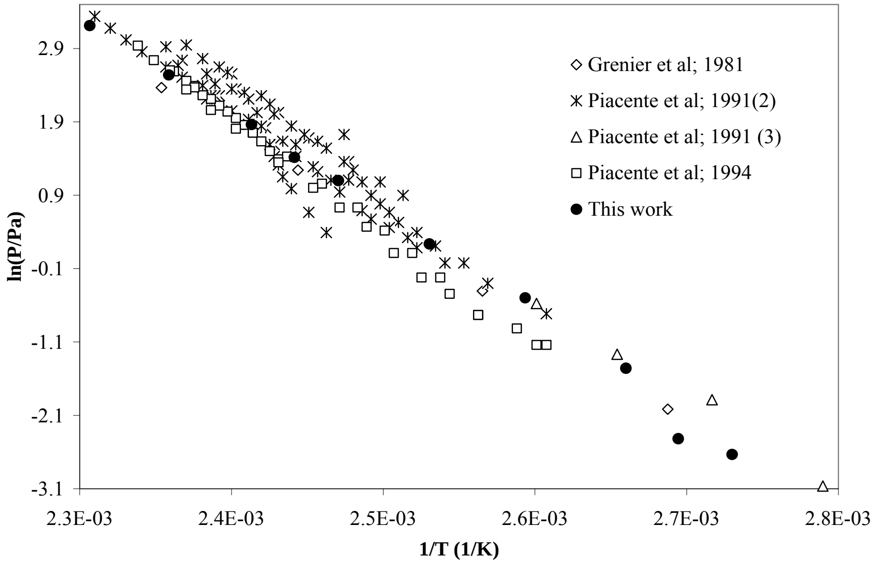

Figure 5.12. Partial pressures from literature and this work for C_{26}.

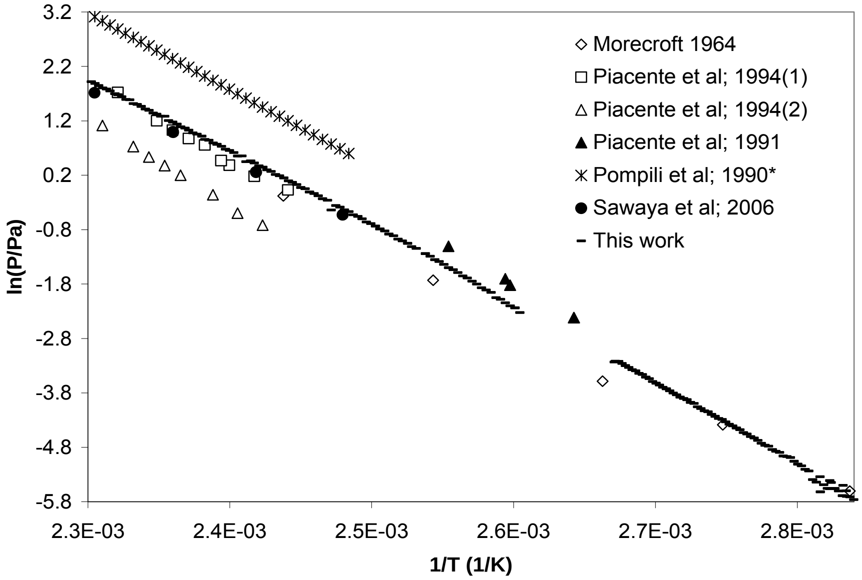

Figure 5.13. Partial pressures from literature and this work for C_{27}. *The partial pressures are calculated from given linear regression parameters in the literature.

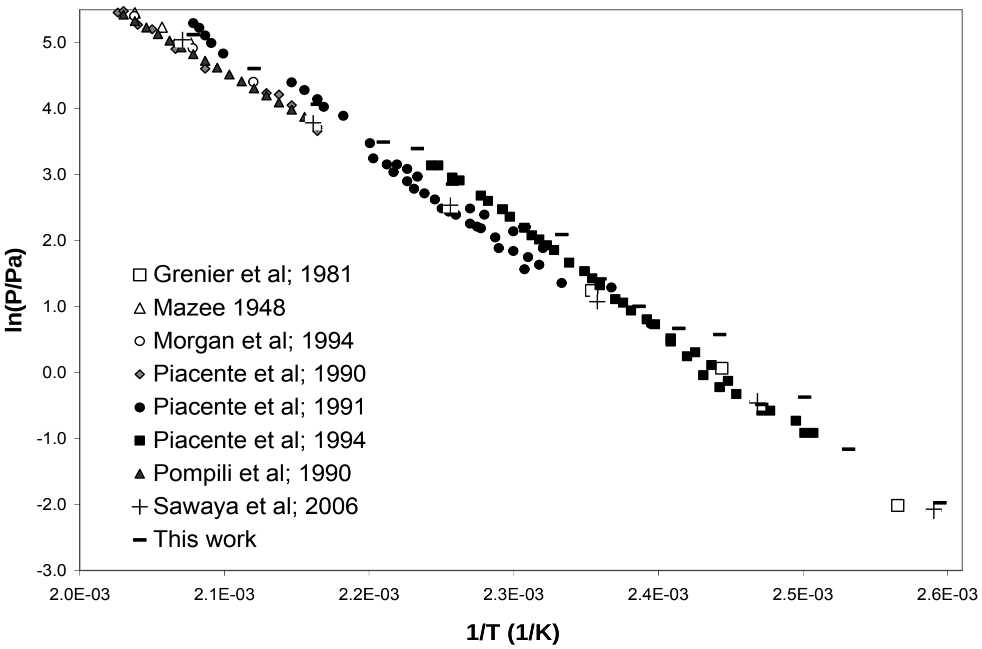

Figure 5.14. Partial pressures from literature and this work for C_{28}.

5.3.4. Evaporation Enthalpies

Evaporation enthalpies for n-alkanes measured by various techniques were summarized in Chickos et al., 2003. Results of evaporation enthalpies measured by correlation gas chromatography (CGC) were reported in Chickos et al., 1981, 1995, 1997, 2002 and 2004, respectively. Vaporization enthalpies of n-alkanes were also calculated according to the Clausius-Clapeyron equation, from the partial pressure data from this work, Piacente et al., 1991, 1994 and Pompili et al., 1990. For comparison purpose, the vaporization enthalpies are converted to ΔH_{vap} (298 K) by Equation (5.1) and averaged if multiple values are available. Since the C_{Pg} values in Equation (5.1) are not available for most of the n-alkanes, Equation (5.2) is used to estimate (C_{Pl} - C_{Pg}), and C_{Pl} is estimated from the group-contribution method (Chickos et al., 2003; Tu et al., 1996).

$$\Delta H_{vap}\left(298\,\mathrm{K}\right) \approx \Delta H_{vap}\left(T_m\right) + \left(C_{P_l} - C_{P_g}\right)\left(T_m - 298\right) \qquad (5.1)$$

$$\left(C_{P_l} - C_{P_g}\right) = \left[10.58 + 0.26 C_{P_l}(298\,\mathrm{K})\right] \qquad (5.2)$$

where: T_m is the mean temperature of the range at which the measurements were conducted; C_{pl} and C_{pg} are the heat capacities of the liquid and gas phase of n-alkanes.

The vaporization enthalpy at 298 K as function of n-alkane carbon number is shown in Figure 5.15 The vaporization enthalpies of n-alkane C_{20}, C_{26}, C_{27} and C_{28} derived from the partial pressures of this work measured under isothermal conditions and temperature programming agree with those reported by of Chickos et al., 2003. The vaporization enthalpies at 298 K derived from the partial pressure data measured by the Torsion/Knudsen effusion method by the Piacente group are systematically higher. The data derived from correlation gas chromatography by the Chickos group constantly gives lower result.

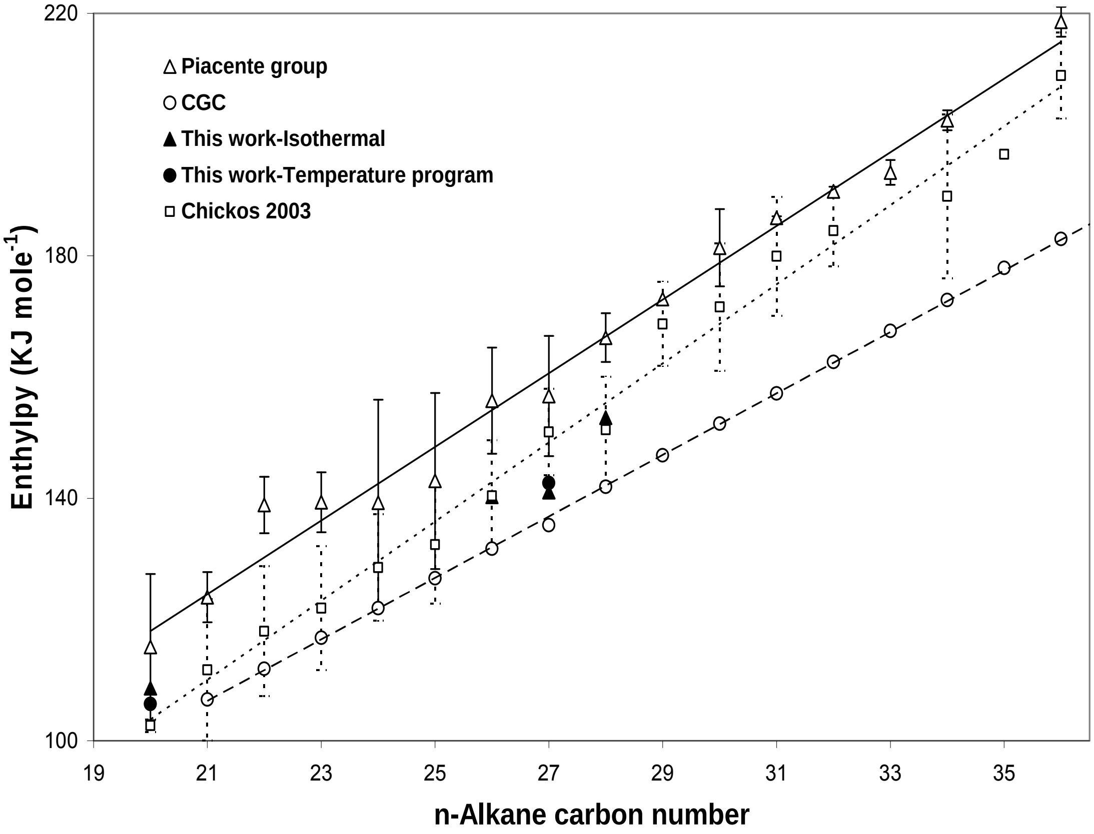

Figure 5.15. Vaporization enthalpy at 298 K as function of n-alkane carbon number. The error bars are standard deviations of average values.

5.3.5. Partial Pressures above Mixtures of n-Alkanes

For ideal mixtures the activity coefficients of the components of the mixture are unity and the total partial pressure as well as partial pressures can be calculated by Raoult's law. Figure 5.16 shows the measured and calculated total partial pressure against the composition of the mixture for C_{27} and C_{28}. Activity coefficients can be determined from the ratio of measured partial pressures over the partial pressure calculated for an ideal mixture. As an example, the measured activity coefficients for C_{27} in binary and ternary mixtures for different temperatures are summarized in Table 5.7. Compared to the calculated total partial pressure, the relative pressure difference between the experimental and calculated values is generally less than 5%.

The partial pressures of mixtures can be measured using temperature programming, which allows determining activity coefficients for a range of temperatures in one experiment. The average experimental activity coefficient for C_{27} is close to one (0.96-1.08) and most relative standard deviations are better than 5%. Similar results were obtained for C_{26} and C_{28} as well (see for example Figure 4.34 and Table 5.7).

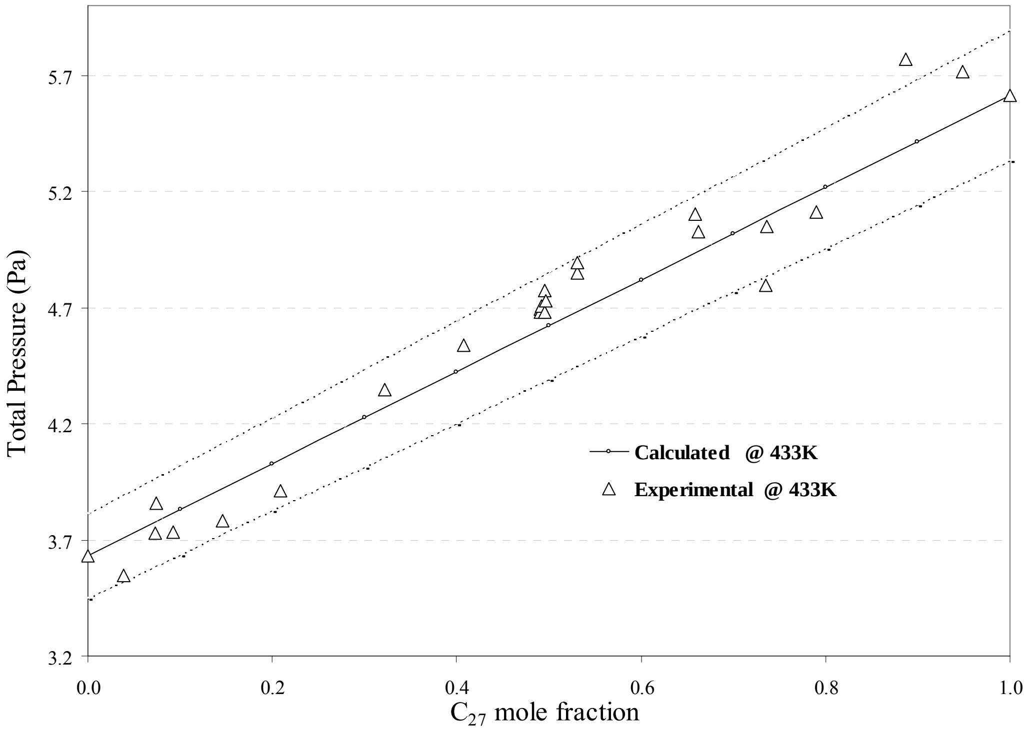

Figure 5.16. Calculated and measured total partial pressures of a binary mixture of n-alkanes (C_{27} and C_{28}) as function of composition. The dotted lines show the range of 105% and 95% of the calculated total partial pressure for ideal mixtures.

Table 5.7. Summary of the Activity Coefficients for C_{27}.

	Temp.	Mol fraction	Activity coefficient for C_{27}				
Mixture	K	of C_{27}	Range	Average	STDEV	RSD%	n
C_{27} & C_{28}	433	0.039 - 0.949	0.93 -1.09	1.03	0.05	4.5	23
C_{27} & C_{28}	443	0.489 - 0.490	0.99 - 1.01	1.00	0.02	2.0	2
C_{27} & C_{28}	453	0.489	0.97	0.97			1
C_{27} & C_{28}	398-448#	0.095 - 0.084	0.84 - 1.01	0.96	0.04	4.0	230
C_{27} & C_{28}	398-423#	0.065 - 0.064	0.96 - 1.06	1.02	0.03	3.0	117
C_{26},C_{27},C_{28}	433	0.462 - 0.199	0.99 - 1.14	1.08	0.04	3.7	9
C_{26},C_{27},C_{28}	443	0.463 - 0.199	0.93 - 1.05	1.00	0.04	4.0	5
C_{26},C_{27},C_{28}	453	0.199 - 0.462	0.93 - 1.17	1.02	0.10	9.8	5

#: partial pressure measured by temperature program with 0.2 K/min heating rate.

Strictly speaking perfect ideal mixtures do not exist simply because there are no two compounds having the exactly the same molecule size and van der Waals interactions. However, for compounds with similar chemical structures mixtures will be close to ideal. The experimental results are in full agreement with the expectation that n-alkane mixtures are nearly ideal.

5.3.6. Measurement of Diffusion Coefficients

For small values of x, the diffusion coefficient (D) derived from vapor pressure measurements using Equation (2.8) depends on F*. For larger values of x (8.50 and 9.50 cm), D values do not show a clear dependence on F* for a wide F* range. Nevertheless, this suggests the existence of some bias duo to an unidentified factor, which is not considered in Equation (2.8).

A plot of inverse P_m as function of F* for the same x shows a high degree of correlation. However, (x/a) (a is the slope of $P_m^{-1} \sim F^*$ curve), which should be equal to ($D \times S \times P_s$) according to Equation (2.7), changes notably especially for small x. This does not agree with the expectation that (x/a) is constant, since D, S and P_s have fixed values at constant temperature. It implies that the measured value of x completely adequate to describe the diffusion process. This may create bias for the determination of D from x/a and the known values for x, S, and P_s The magnitude and possible correction of this bias will be looked at in some more detail in the next paragraphs.

According to Equation (2.8), x/(D×S×P_s) is the slope of the P_m^{-1} versus F* curve, which should be proportional to x since D, S, and P_s are independent of x as well as F*. Therefore a plot of x/(D×S×P_s) as function of x should be a straight line passing through the origin. As an example, Figure 5.20 shows such a plot for C_{20}. The curve does not pass through the origin and x/(D×S×P_s) is zero for x equal to 0.55 cm (calculated from the linear regression equation in Figure 5.17). This suggests that the value of x, the measured diffusion distance in Equation (2.8) should be replaced by a corrected diffusion distance (x - x^t), which results in a modified Equation:

$$\frac{S\left(P_S/P_m-1\right)}{F^*}=\frac{x}{D}-\frac{x^t}{D} \qquad (5.3)$$

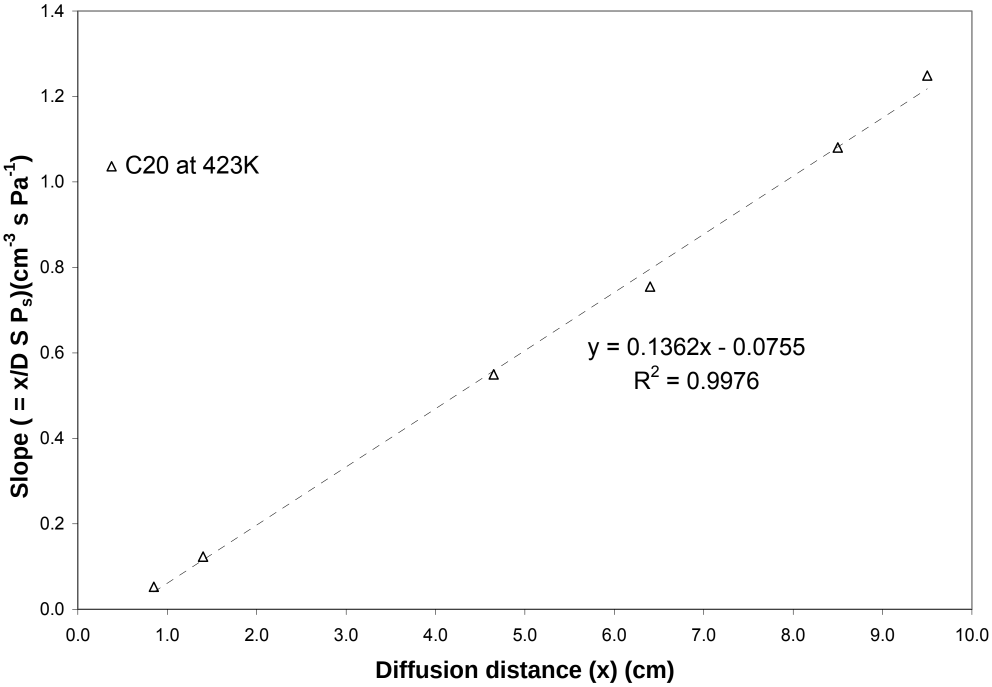

Figure 5.17. The dependence of slope of the P_m^{-1} versus F* linear regressions on x for C_{20}.

Possible source for this correction is turbulence at the transition of the diffusion tube into the tube which is continuously flushed with a carrier gas at flow rate F*. Based on Equation 5.3, $S(P_s/P_m-1)/F^*$ as function of x is linear with a slope of 1/D and an y-axis intercept of $-x^t/D$. For experimental reasons partial pressures were determined under fixed x and varying flow rates and therefore a data set with exactly identical flow rates and varying x is not available. However, the linear regression parameters of $P_m^{-1} \sim F^*$ curves for constant x allow calculation of P_m values at any chosen flow rates for those values of x, which were used to study the dependence between flow rate and P_m (Tables 4.15 and 4.16). The chosen flow rates, derived linear regression parameters of $S(P_s/P_m-1)/F^*$ as function of x under the chosen flow rates F*, D (1/a) and x^t ($-D\times b$) are listed in Table 5.8. Consistent with the concept that a non-zero value for x^t is the result of turbulence, x^t increases systematically with increasing F*. There is an indication that the slope 1/a (and therefore D) slightly changes as function of flow rate, possibly a result of the complex transition from diffusion limited transport to laminar flow at the junction of the t-piece. However, these changes are only small. The average D is 0.076 $cm^2\ s^{-1}$ (RSD: 2.1%) for C_{20} at 423 K and 0.048 $cm^2\ s^{-1}$ (RSD: 1.5%) for C_{28} at 463 K under 2.3 atmospheres, which is the pressure inside the saturator.

Table 5.8. Linear Regression Parameters of $S(P_s/P_m-1)/F^*$ as Function of x and Derived D, x^t.

Result for C_{20} at 423 K							
F^*(ml/s)	a (cm^{-2} s)	b (cm^{-1} s)	R^2	RE a, %	RE b, %	D (cm^2 s^{-1})	x^t (cm)
0.32	12.59	-2.63	0.997	2.2	67.3	0.079	0.21
0.43	12.99	-4.00	0.998	1.9	40.0	0.077	0.31
0.55	13.23	-4.80	0.998	1.8	31.5	0.076	0.36
0.66	13.38	-5.32	0.998	1.7	3.0	0.075	0.40
0.77	13.49	-5.69	0.998	1.7	25.1	0.074	0.42
0.89	13.58	-5.96	0.998	1.6	23.5	0.074	0.44
1.00	13.64	-6.17	0.998	1.6	22.5	0.073	0.45
1.35	13.76	-6.58	0.998	1.6	20.7	0.073	0.48
1.69	13.84	-6.83	0.998	1.5	19.6	0.072	0.49
Result for C_{28} at 463 K							
F^*(ml/s)	a (cm^{-2} s)	b (cm^{-1} s)	R^2	RE a, %	RE b, %	D (cm^2 s^{-1})	x^t (cm)
0.23	19.99	-11.38	0.977	10.7	73.5	0.050	0.57
0.34	20.43	-13.54	0.997	11.7	69.4	0.049	0.66
0.45	20.65	-14.62	0.999	12.4	68.3	0.048	0.71
0.51	20.72	-14.98	0.998	12.6	68.1	0.048	0.72
0.56	20.78	-15.30	0.997	12.8	68.0	0.048	0.74
0.68	20.87	-15.70	0.995	13.1	68.2	0.048	0.75
0.73	20.90	-15.87	0.994	13.2	68.1	0.048	0.76
0.79	20.93	-16.01	0.993	13.3	68.1	0.048	0.76
0.90	20.98	-16.24	0.991	13.5	67.7	0.048	0.77
1.01	21.02	-16.42	0.990	13.6	66.4	0.048	0.78

F^*: flow rate at saturator temperature and pressure. RE: relative error. a, b: slope and intercept of the curve of $S(P_s/P_m-1)/F^*$ as function of x.

The dependence of x^t as function of $1/F^*$ and F^* for C_{20}, C_{28} is shown in Figure 5.18. The values for x^t are larger for C_{28} than for C_{20} at the same flow rate. This possibly is the result of the different temperaturse at which the measurements were made and the resulting differences in viscosity and density of the carrier gas. The values of x^t change notably for relatively small flow rates. However, at high flow rate, x^t approaches a constant level of 0.56 cm and 0.84 cm for C_{20} and C_{28}, respectively. For the flow rate range studied here, the relation between F* and x^t can be described by an inverse linear dependence between F* and x^t (Figure 5.18)

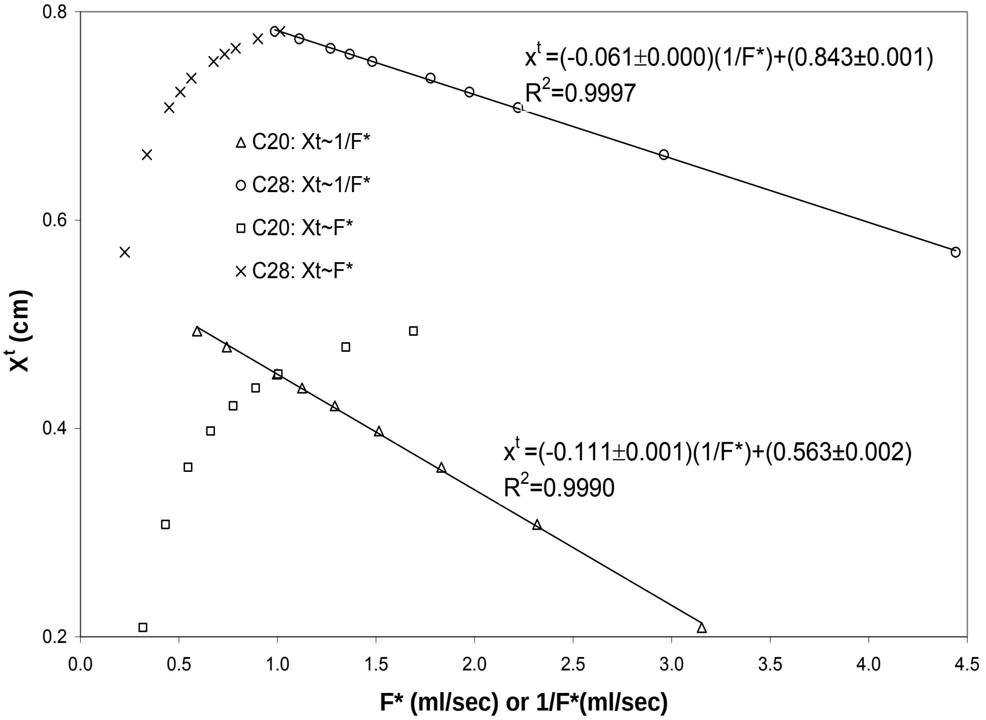

Figure 5.18. Dependence of x^t on 1/F* and F*.

Neglecting the possible temperature dependence of x^t, the flow rate dependence of x^t can be used to determine a corrected value for D by using a corrected value for x. A comparison of corrected and uncorrected D values for C_{20} is shown in Figure 5.19. These measurements were with under a gas flow rate (F=21.4 ml/min) and a diffusion distance of 9.40 cm. The x^t is estimated to be in the range of 0.08 to 0.10 cm which results in a correction of a 1.2% or less for these experimental conditions. Due to the simplifications and approximations made, this correction has substantial uncertainty. However, since the correction is extremely small, this uncertainty will have little influence on the accuracy of the measured diffusion coefficients.

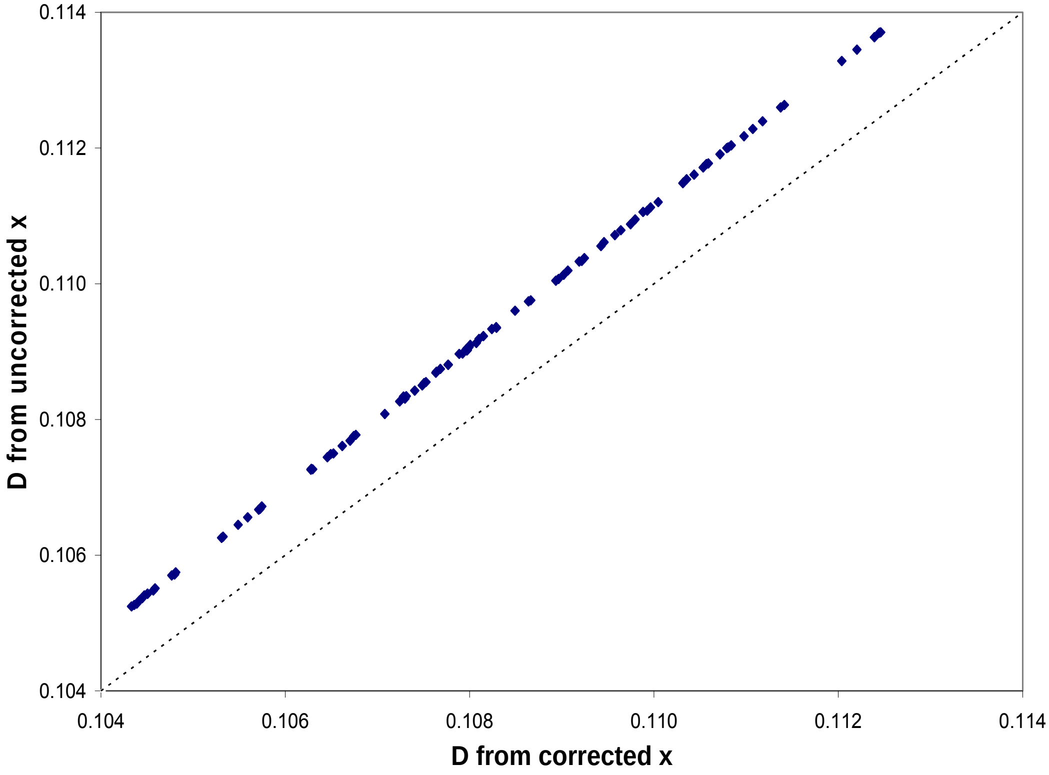

Figure 5.19. Plot of D derived from corrected x versus D derived from uncorrected x for n-alkane C_{20} in the temperature range of 440 K to 464 K. The dotted line shows the 1:1 correspondence.

The linear regression equation for the curve of lnD(T) as function of lnT for C_{20} data set in the temperature range of 440 K to 464 K is lnD(T) = (1.46±0.02)×lnT + (-11.1 ± 0.1), or, when comparing two diffusion coefficient for different temperatures, $(D_1/D_2) = (T_1/T_2)^{1.46}$. The diffusion coefficient is proportional to $T^{1.5}$ according to kinetic theory. The reported experimental dependence of D on temperature in literature ($D_1/D_2 = (T_1/T_2)^n$) is n = 1.61 to 2 (Bradley et al., 1948, n = 2; Katsanos et al., 1983, n = 1.61; Fuller et al., 1966, n= 1.75; Seager et al., 1963, n=1.70).

Reported D values for heavy n-alkanes are rare and no experimental values for the diffusion coefficients of n-alkanes heavier than C_{18} are available in literature. D values for other n-alkanes are reported by Altshuller *et al.*, 1960 (C_{10}, in H_e); Bradley *et al.*, 1948 (C_{16} to C_{18} in air); Cummings *et al.*, 1953 (C_{10}, C_{12} in He); Fuller *et al.*, 1965 (C_1, C_6 to C_8 in He, C_1, C_2 in H_2, C_2, C_4 and C_6 to C_8, C_{10}, C_{12} in N_2); Gavril *et al.*, 2004 (C_2 in N_2); Huang *et al.*, 1972 (C_1, C_2, C_4, C_6 to C_8 and C_{10} in H_2, C_7 and C_{10} in He); Karaiskakis *et al.*, 2004 (C_1 to C_6 in H_2, C_1, C_7 in H_e, C_6 in Air), 1984 (C_5 to C_8 in H_e); Nagasaka, 1973 (C_5 in He, Air, N_2 and H_2). In order to allow direct comparison, D values are converted to n-alkane/helium binary diffusion coefficient at 298 K and 1 atmosphere if necessary by Equation (5.4) (Byron 1960; Geankoplis 1972) assuming the collision diameters of H_2, He, Ar or N_2 can be ignored compared to that of n-alkanes:

$$D_{A-C_n} = \left(\frac{8}{3}\right)\left(\frac{k^3}{2\pi^3}\right)^{1/2} T^{1.5} \frac{\left(\frac{1}{m_A}+\frac{1}{m_{C_n}}\right)^{1/2}}{P\left(d_{C_n}\right)^2} \qquad (5.4)$$

where: k = Boltzmann constant; m_A, m_B = molecular weight of A, B; d_{Cn} = collision diameters of n-alkane; P = pressure.

An empirical equation named Fuller-Schettler-Giddings equation (Fuller *et al.*, 1969, 1966, 1965) is often used to estimate D for organic compounds. The D from literature, the Fuller-Schettler-Giddings equation and this work as function of n-alkane carbon number are shown in Figure 5.20. The error bars are the standard deviations of D values from different publications. When the carbon number (Nc) is less than 10, the result from the Fuller-Schettler-Giddings equation and experimental data are in reasonable agreement. For Nc is between 10 and 18, the D values calculated from the Fuller-Schettler-Giddings equation are systematically higher than the published measurements. The new data for C_{20} and C_{28} from this work support this finding and demonstrates that this trwnd continues to higher carbon numbers.

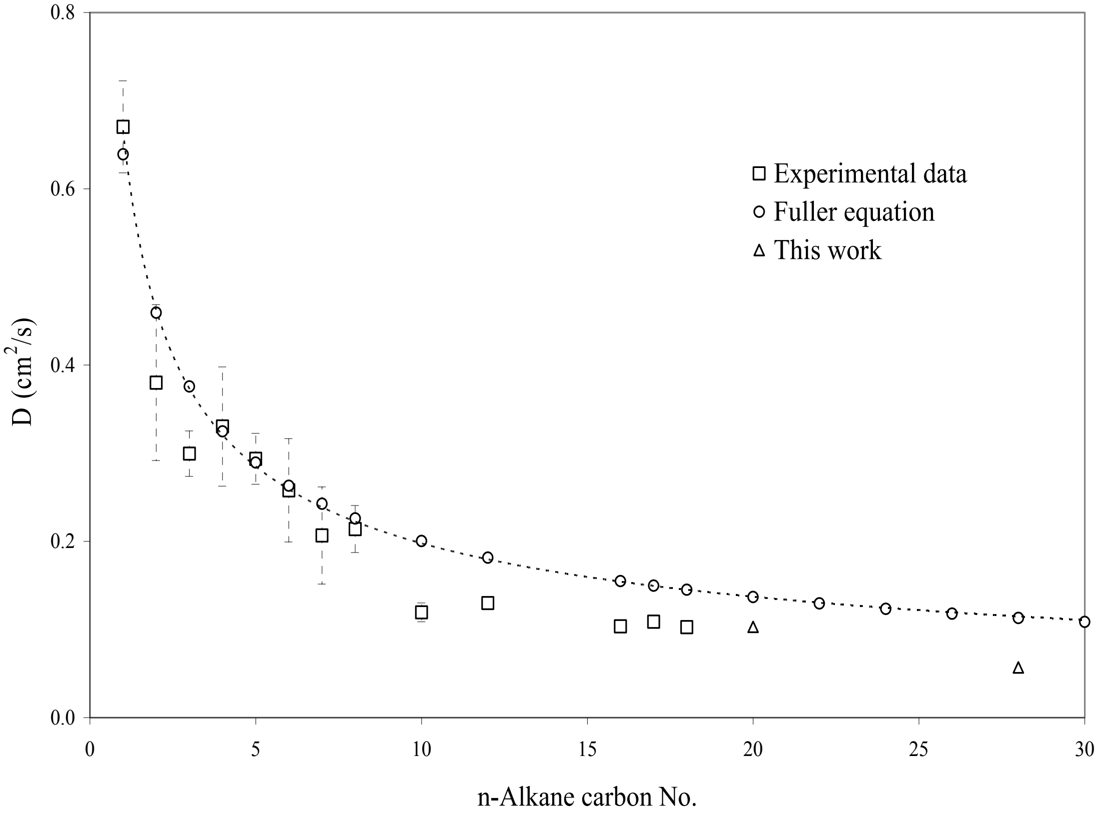

Figure 5.20. Comparison of n-alkane diffusion coefficient.

5.4. Studies of Thermal Behavior of n-Alkanes by TDI/GC

In contrast to the time integrated signals, which have been used for TDI calibration (5.1) the temperature and time dependence of the TDI signal depends in a rather complex way on the type of sample and the experimental conditions. A simple example is the time or temperature dependence of vapor pressure on sample size (Figure

4.27). This dependence can be explained by the dependence between sample size and surface area. The n-alkane is dispersed on the sample boat bottom as a liquid layer once the reactor temperature is above the melting point of C_{27} (332 K). The surface area of C_{27} will increase with increasing sample mass until it is sufficient to cover the bottom of the boat. Therefore, up to a certain limit, increasing the sample size increases the surface area, which reduces the mass transfer resistance up to the point where the measured vapor pressure is effectively identical to the equilibrium vapor pressure. Indeed, the vapor pressure measured for a sample size of 100 mg is very close to the equilibrium vapor pressure (Figure 4.27 and Table 4.12). It should be noted that the measurements were conducted using a temperature programmed with a heating rate of 2 K/min. This may cause small differences between measured and equilibrium vapor pressure, but for a heating rate of 2 K/min this difference is, as shown in Subchapter 5.2.2, usually not very large.

For mg amounts of n-alkanes on a smooth quartz surface, surface effects are unlikely to have any impact on the equilibrium vapor pressure and differences between measured and equilibrium vapor pressure for small samples are therefore most likely the consequence of mass transfer limitations. When spiking μg amounts of n-alkanes on a smooth quartz surface or quartz fiber filters we can see some similarities to the experiments using mg amounts, but also several differences (Figure 4.15 and 5.21).

First of all, with increasing temperature at some point the measured vapor pressure abruptly drops to effectively zero. This can be readily explained by the depletion of the small reservoir of n-alkanes, which is consistent with the finding that the temperature at which the drop in vapor pressure occurs systematically decreases with decreasing sample size.

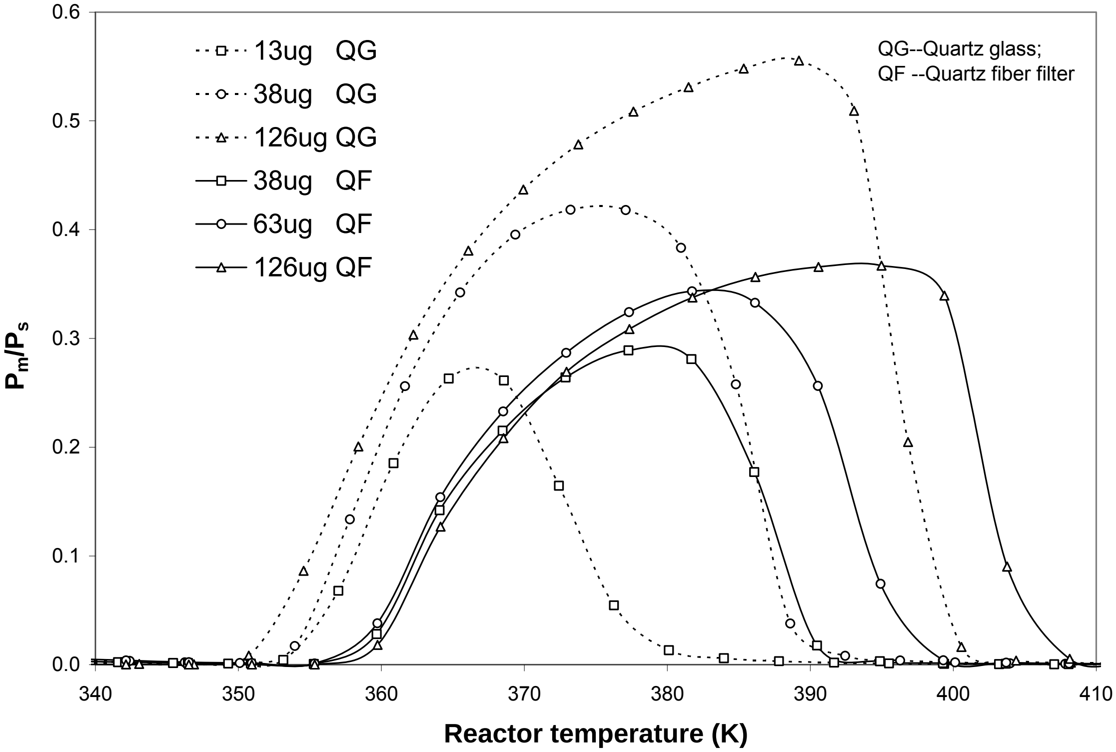

Figure 5.21. The ratio of measured (P_m) over equilibrium vapor pressure (P_s) against reactor temperature for different masses of C_{20} spiked on quartz glass and a quartz fiber filter.

The significant difference between measured and equilibrium vapor pressures (Figure 5.21) may be due to mass transfer limitation as well as possible surface effects.

The experiments using a smooth quartz surface were conducted by spiking a solution containing the n-alkane into a quartz boat with a surface area of about 4 cm^2. Due to the spreading of the solution and the complexity of the solvent evaporation it is difficult to accurately determine the surface area of the n-alkane. Assuming that the n-alkane is uniformly spread out over the surface of the quartz boat, the thickness of the layer can be estimated from the mass of n-alkane, the density of C_{20}, and the surface area of the quartz boat. For the experiments discussed here the surface layer thickness is in the range of 100 nm to 400 nm. It is therefore unlikely that for these experiments surface effects have a substantial impact on equilibrium vapor pressure. Therefore, similar to the experiments with mg amounts of n-alkanes, the reduced measured vapor pressure is most likely the consequence of mass transfer limitations.

Similar to the determination of diffusion coefficients (subchapters 4.4 and 5.3.6) the mass transfer limitations can be estimated using Equation 2.8. However, in contrast to the diffusion coefficient studies, here several of the experimental parameters, especially the surface area (S) and the diffusion distance (x) are poorly defined. Nevertheless, the experimental observations allow a first order estimate of the ratio S/x from a rearranged version of Equation 2.8 ($S/x=F/D*P_m/P_s/(1- P_m/P_s)$). It should be noted that this approach is for the description of steady state conditions. Due to the dynamic character of the experiments (temperature programming, depletion of sample during the experiment) such an approach cannot completely describe the observation. Nevertheless, based on the flow rate of 22 mL/min (Table 3.5), a carrier gas pressure of 2300 hPa in the reactor and a temperature of 370 K and using a diffusion coefficient of 0.1 cm^2/s for C_{20} (see subchapters 4.4 and 5.3.6) the ratio of S/x is in the range of 1 cm to 3 cm for values of P_m/P_s of 0.3-0.6 (Figure 4.21). These ratios are compatible with surface areas of about 1 cm^2 and an effective diffusion distance in the range of several mm.

Thermodesorption of C_{20} from quartz fiber filters is significantly less efficient than evaporation from a smooth quartz surface as can be seen from the shift in the thermodesorption peaks towards higher temperatures (Figure 4.15) and the decrease in the ratio of measured vapor pressure over bulk-phase equilibrium vapor pressure (Figure 5.21). The internal surface area of quartz fiber filters is substantial. It can be calculated from the internal surface area per unit mass, the weight per unit filter area and thickness of the quartz fiber filters, which are 1.65 $m^2\ g^{-1}$ (Mader *et al.*, 2001), 8.5×10^{-3}g cm^{-2} and 0.05 cm, respectively. The thickness of the n-alkane layer, which is calculated from the internal surface area, the mass of spiked C_{20}, and its density, is in the range of a 4-11 nm (Table 5.9). The internal surface area on average available for each n-alkane molecule is in the range of 10^{-15} cm^2. This compares with a total surface areas of $4x10^{-14}$ cm^2 for C_{20}, which can be estimated from n-alkane surface areas reported by Lekomtsev *et al*. (2002). This shows that on average the area of the n-alkane molecules which is in direct contact with the quartz fiber filter surface is only a small percentage of the total surface area. It cannot be excluded that a surface adsorption effect contributes to a decreases in vapor pressure. For the part of the thermograms which is not determined by the depletion of n-alkane, there is a small dependence in the thermodesorption behavior for samples of different sizes (Figure 5.21 and Table 5.9). This indicates that for these samples the partial pressure of C_{20} may be impacted by adsorption effects, but that for these examples the influence is small.

Table 5.9. Estimated Quartz Fiber Filter Coverage for Filters Spiked with C_{20}.

Spiked C_{20} (1.258µg C/µl)				Filter		Thickness of layer
Volume µl	Mass µg	Volume µL	Number of molecules	Area^a cm^2	Internal area available cm^2	nm
30	37.7	0.048	8.1×10^{16}	0.80	112	4.3
50	62.9	0.080	13×10^{17}	1.07	150	5.3
100	126.0	0.16	2.7×10^{17}	1.07	150	11

Area^a: External surface area covered by the spiked solution

The mass transfer processes of molecules from the thin layer on the quartz fibers include two steps: 1) Diffusion from inside of the filter to the filter surface; 2) Transport from the filter surface into the carrier gas stream. Reduced mass transfer can be due to different effects: 1) Reduction of available cross section for diffusion due to the filter material; 2) Increase of the diffusion distance due to a labyrinth effect similar to that in packed column chromatography; 3) The reduction of turbulent mass transfer due to the suppression of turbulence by the filter material; 4) Reduction of the area over which the n-alkane is spread due to the filter's ability to better absorb the solvent (prior to evaporation) than a smooth quartz surface. The influence of all these factors is difficult to estimate, but with the exception of 4) the influence is most likely small. The filter is only 0.05 cm thick and about 94% of the filter is void space.

When spiking a C_{20}/C_{27} binary mixture on quartz glass, C_{20}'s thermodesorption peak shifts to higher temperature whereas C_{27}'s does not change significantly compared to that of pure C_{27} (Figure 4.16). According to Equation (2.10), the partial pressure is proportional to mol fraction. Therefore C_{20} in a mixture will have lower partial pressure than pure C_{20} and the thermodesorption peak will be shifted to higher temperatures. This is consistent with the measurements of equilibrium vapor pressure measurements for mixtures of n-alkanes (Figure 4.34 and Table 4.14). During the volatilization of C_{20}, the mol fractions both for C_{20} and C_{27} change. When C_{27} begins to evaporate notably, C_{20} is almost totally depleted. Therefore in these experiments C_{27} shows the same thermal behavior as pure C_{27}. The systematic shift of the peak maxima towards lower temperatures with decreasing sample size is, similar to the experiments with pure substances, due to the earlier onset of the depletion of the n-alkane in the sample.

Compared to pure C_{27} and C_{27} in C_{20}/C_{27} binary mixture, the peaks for n-alkanes in a 17 n-alkane mixture shift to substantially higher temperatures (Figure 4.18). This is due to the presence of heavier n-alkanes, which reduce the mol fraction of the lighter n-alkanes and thus reduce the equilibrium vapor pressure. The change of the n-alkane mol fraction with time and temperature is complex due to the evaporation of different n-alkanes at different rates. Figures 5.22 shows an example for the total n-alkane loss rate and Figures 5.23, 5.24 show two examples for the change of the mol fractions of several n-alkanes in the mixture as function of temperature. As result of the changing mol fractions therefore the pressures of individual n-alkanes change differently for different mixtures and for different total masses of n-alkane.

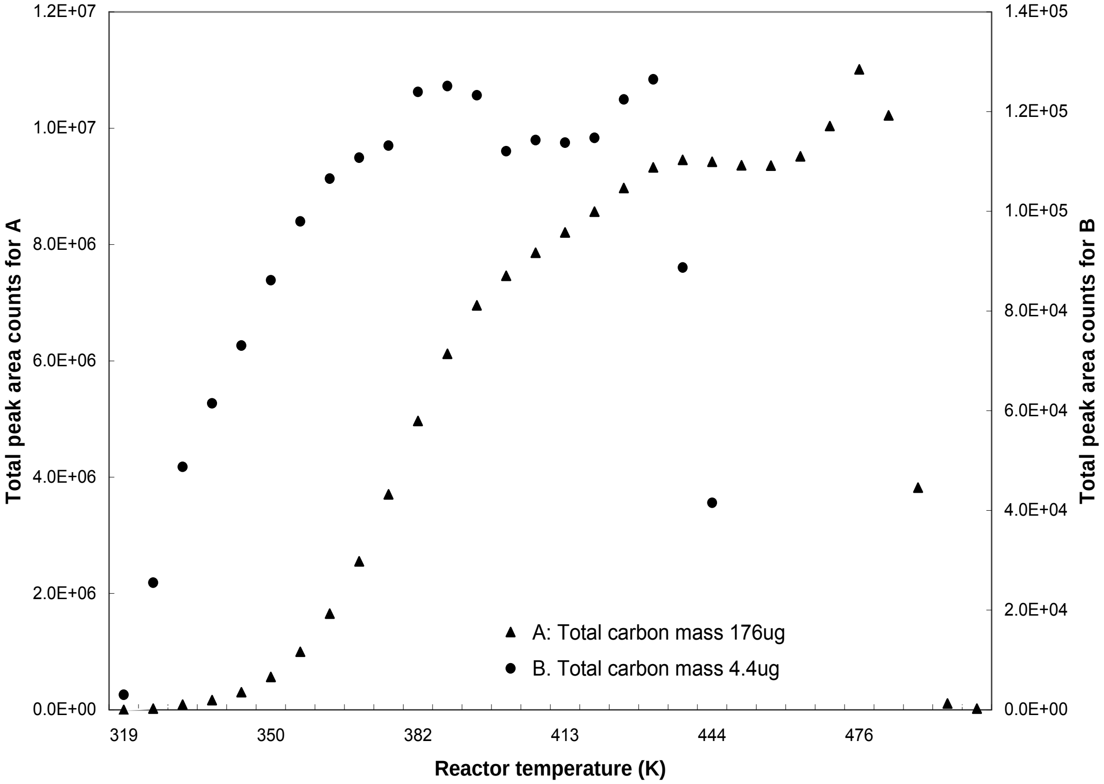

Figure 5.22. Total n-alkane loss rate as function of temperature. Different volumes of 17 n-alkane mixture were spiked on clean quartz fiber filters and the total carbon masses were 176 μg and 4.4 μg, respectively. The total peak area counts were the sum of individual n-alkane peak area counts during the sampling period. The samples were run using a temperature program with a heating rate of 2 K/min.

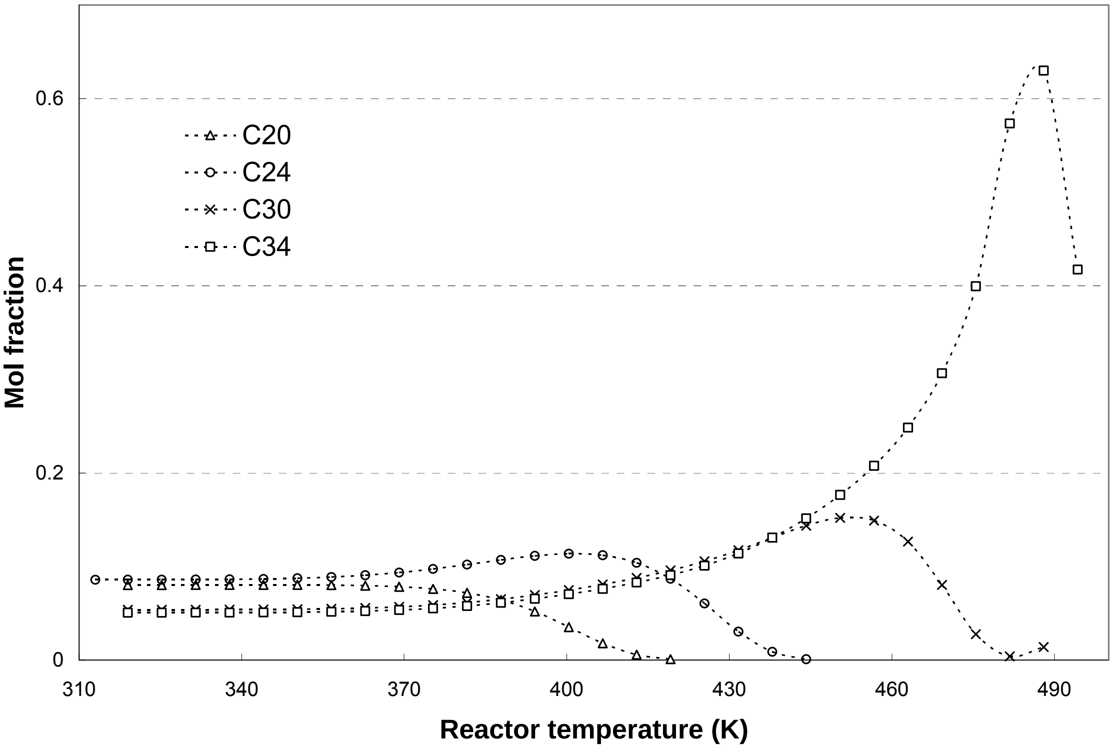

Figure 5.23. The mol fractions of several n-alkanes in the mixture as function of temperature. 17 n-alkane mixture was spiked on a clean quartz fiber filter and the total carbon mass was 176 μg. The samples were run by temperature program of 2 K/min.

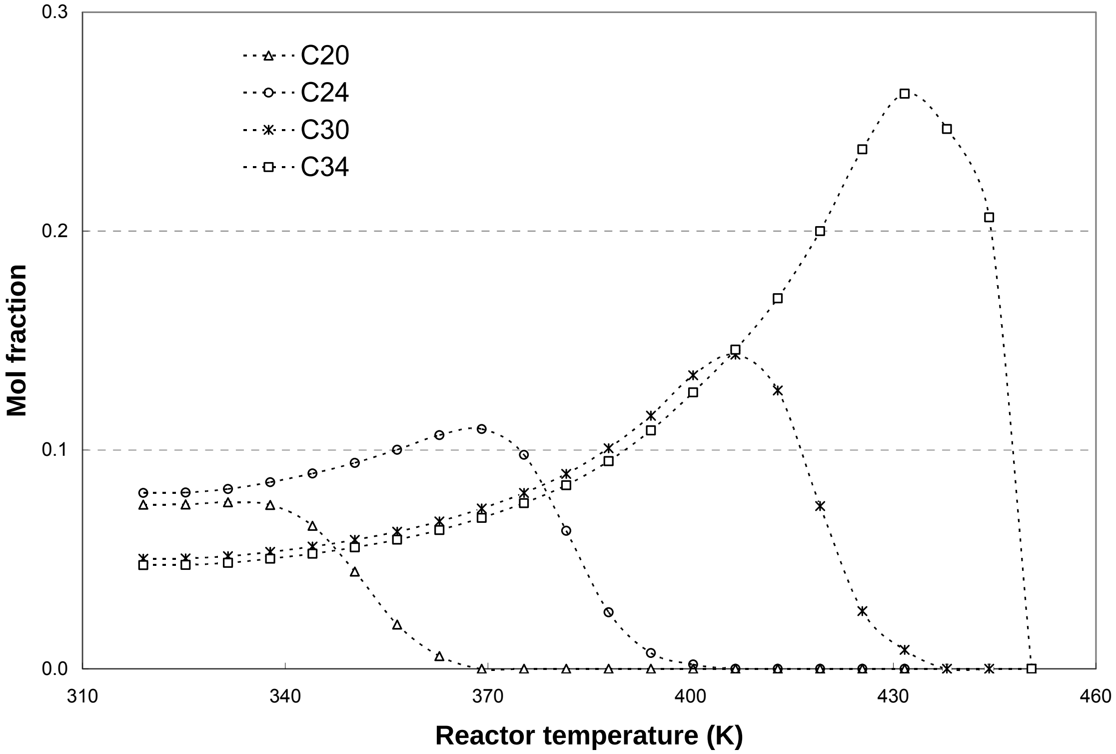

Figure 5.24. The mol fractions of several n-alkanes in the mixture as function of temperature. 17 n-alkane mixture was spiked on a clean quartz fiber filter and the total carbon mass was 4.4 μg. The samples were run with temperature program with a heating rate of 2 K/min.

The thermal behavior of light n-alkanes in the 17 n-alkane mixture spiked on quartz fiber filter and quartz glass is in many aspects similar but there are also some differences (Figure 4.18). For the lightest n-alkane in Figure 4.18 (C_{18}) there is no difference in thermal behavior. Heavier n-alkanes on quartz glass evaporate at slightly lower temperatures than from a quartz fiber filter. The differences are small, but they increase systematically with increasing carbon number and the largest temperature difference is about 6 K (Figure 4.18). This behavior may be due to surface effects. For n-alkanes spiked on quartz glass the high surface coverage (see above) makes it unlikely that adsorption will significantly influence equilibrium vapor pressures. However, due to the large internal surface area of quartz fiber filters surface effects are more likely to have a significant impact. The total surface coverage for quartz fiber filters change with time and temperature due to the evaporative loss of material. This is shown in Figure 5.25. The initial relatively high thickness of the surface layer of about 20 nm is consistent with the finding that for the light n-alkanes there is no or very little evidence for an impact from surface adsorption effects. However, during the experiment the thickness of the n-alkane layer decreases due to the ongoing release of n-alkanes. The consequence is that for the heavier alkanes, evaporation occurs when the surface coverage is substantially reduced due to loss of the lighter alkanes (Figure 5.25). Neverthelessr, the overall impact is only small and the largest shift in peak maxima is 6 C towards higher temperature in the experiments using quartz fiber filters.

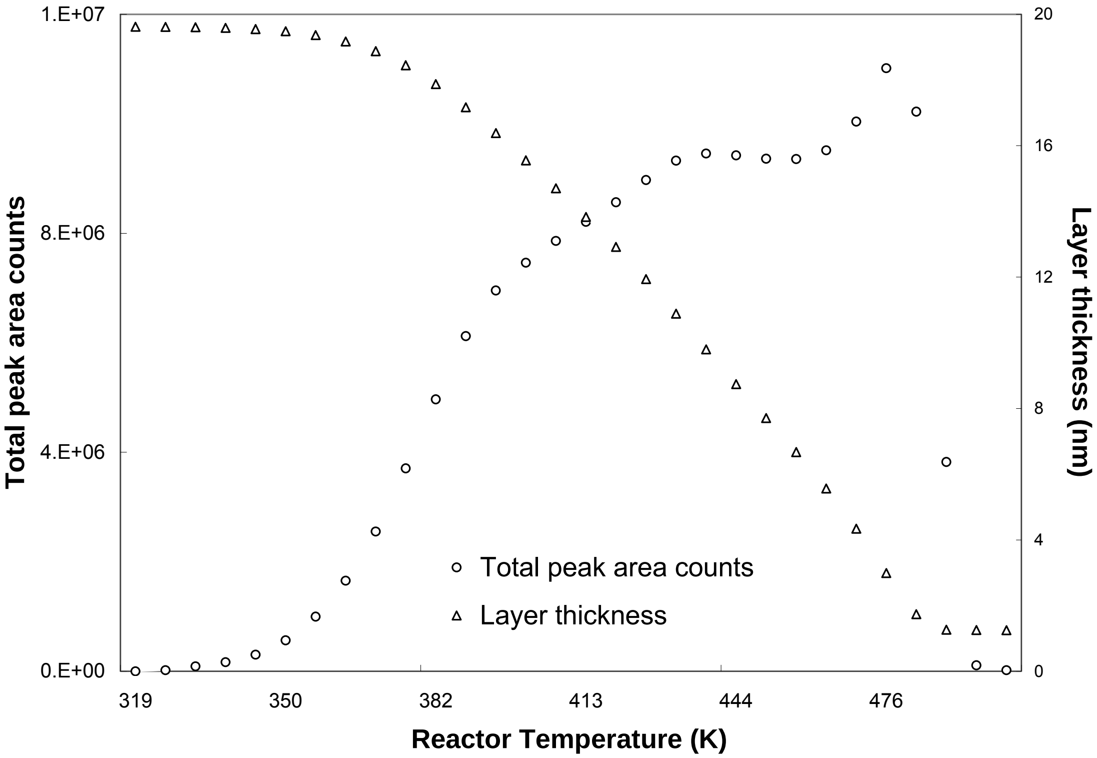

Figure 5.25. The total peak area counts for evolving n-alkanes and thickness of the surface layer as function of temperature. A 17 n-alkane mixture was spiked on a clean quartz fiber filter and the total carbon mass was 176 µg. The samples were run using a temperature program with a heating rate of 2 K/min.

A comparison of the vapor pressures measured when spiking different amounts of the 17 component n-alkane mixture on quartz fiber filters is shown in Figure 5.26 The peak maxima clearly shift towards lower temperatures for the smaller sample, which is expected due to the earlier onset of the depletion of the n-alkanes in the smaller sample. For temperatures below the peak maximum the vapor pressures of the individual n-alkanes are in many cases higher for the smaller sample. This seems to be counterintuitive, but can be explained by the complex time and temperature dependence of the n-alkane mol fraction for samples of different sizes (Figures 5.23 and 5.24). If the main cause for the changes in vapor pressure between the two samples containing different masses of n-alkane is the different development of mol fraction with time, for a given n-alkane and temperature the ratio of the vapor pressures and the ratio of mol fractions for the different samples will be identical and the ratio of these ratios should be unity. Many of the vapor pressure data in Figure 5.26 are very low and therefore a significant experimental scatter can be expected. Nevertheless, the average ratio of the ratios derived from the vapor pressure measurements shown in Figure 5.26 and the mol fractions shown in Figures 5.24 and 5.25 is 1.28 with an error of the mean of 0.25. If data based on vapor pressure measurements of less than 1 mPa are excluded, the average is 0.90 with an error of the mean of 0.10. There is considerable scatter and uncertainty, however the on average good agreement of the average with the value predicted is consistent with the concept that the differences in vapor pressure between the two experiments is primarily due to the different change of the mol fraction of the individual n-alkanes in the n-alkane mixture with time.

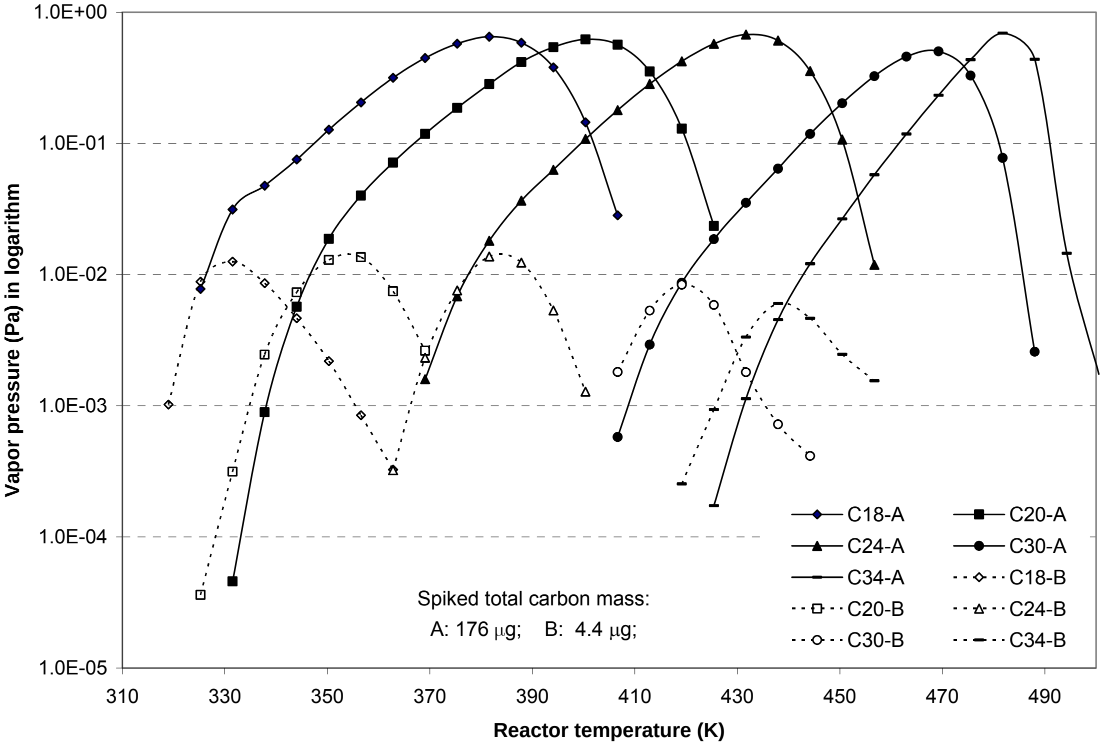

Figure 5.26. Partial pressures as function of temperature for selected n-alkanes evolving from mixtures of n-alkanes with different carbon mass spiked on quartz fiber filters.

The sample masses and therefore the average coverage of the internal surface of the quartz fiber filters differ by approximately a factor of 40 and for the smaller sample the average thickness of the n-alkane layer is very low, in the range of a nm to a fraction of a nm (Figure 5.27). Due to the uncertainty of measurements of very low vapor pressures the data in Figure 5.26 do not completely rule out that the interaction between quartz fiber surface and n-alkanes influence the n-alkane vapor pressure. However, it would be very difficult to reconcile a major influence of surface effects with the findings

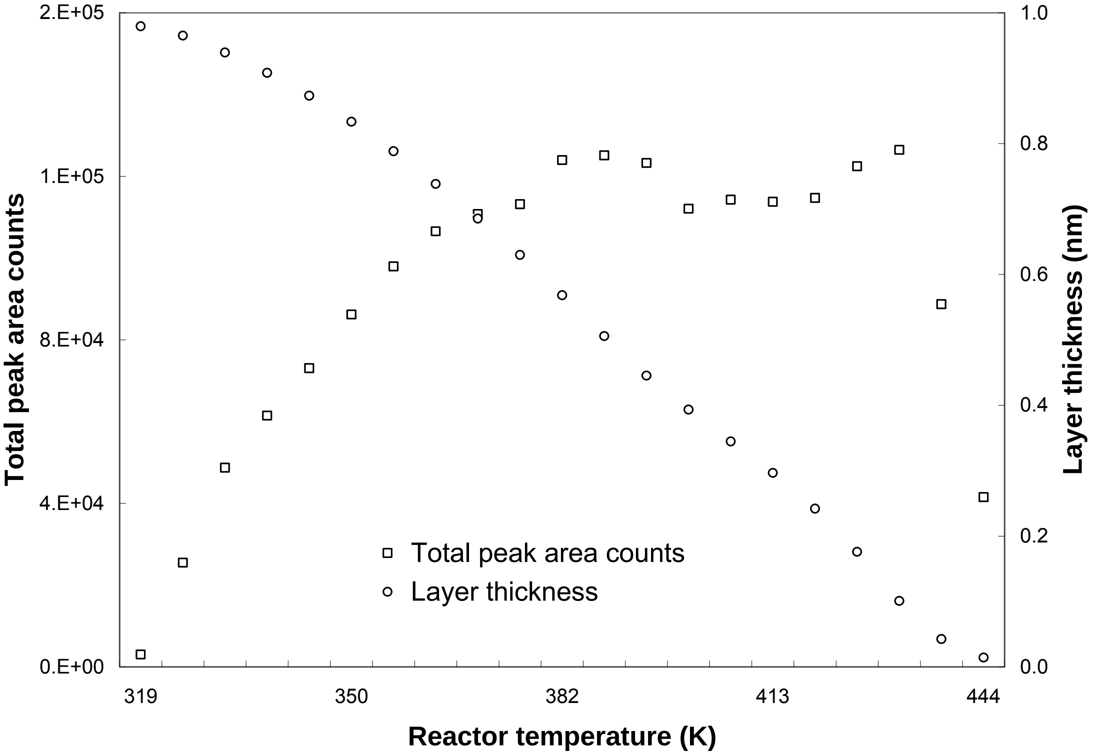

presented in Figure 5.26.

Figure 5.27. The total peak area counts and thickness of the surface layer as function of temperature. A 17 n-alkane mixture was spiked on a clean quartz fiber filter and the total carbon mass was 4.4 µg. The samples were run using a temperature program with a heating rate of 2 K/min.

Spiking n-alkanes on a quartz fiber filter which as been loaded with atmospheric PM results in a drastic change of the thermodesorption behavior compared to a sample spiked on a clean filter. The peak maximum temperatures change by about 10 to 30 K (Figure 4.19). The previously presented results show that changes in the mol fraction of n-alkanes substantially influence the measured vapor pressure. When n-alkanes are spiked on a quartz fiber filter with PM, the organic carbon content of the sample has to be considered since the spiked n-alkanes can form mixtures with the OC of the sampled PM. The measured average OC concentration is 4.5 μg C m^{-3}, equivalent to 18.2 μg C/cm^2 on the aliquot of the high volume filter the sampling rate of 1.13m^3/min and sampling duration of 24 hours is used for the estimate (see 4.1.4). A factor of 1.5 is used to convert OC to total organic mass. The average molecular weigh of the OC is not known, as simplified approximation an average molecular weight for OC of 367g/mol (average MW of n-alkane C_{18} to C_{34}) is used to calculate the moles of total organic compounds. Assuming that OC in the PM sample and the spiked n-alkanes are uniformly distributed on the filters a first order estimate of the mol fraction of the n-alkanes can be derived. It was found that in the temperature range of n-alkanes evolving, generally less than 10% of the total OC is released from the PM samples Therefore the content of PM OC can be treated as unchanged during the thermal analysis and the change in composition of the sample will mainly be due to the thermodesorption of n-alkanes.

Table 5.10 presents a comparison of equilibrium vapor pressures of pure n-alkanes, the equilibrium vapor pressures of the n-alkanes in the mixture, the measured vapor pressure and the vapor pressure estimate from a simplified mass transfer model (Equation 2.10) for the temperatures of the maxima of the thermodesorption peaks. The equilibrium partial pressure calculation uses an activity coefficient of 1. For comparison the same data are given for the measurements of samples spiked on clean quartz fiber filters.

Table 5.10. Result of Spiked n-Alkane on Quartz Fiber Filter and on/in PM Sample Filter.

	Vs	m	S_s	θ	M_f	D	T_m	Ps	Pmax	Pc	P_m/P_c
	μl	ng	cm^2			cm^2/s	K		Pa		
Case 1— Spiking M17 mixture on clean quartz fiber filter (F=15.0 ml/min)											
C_{20}	40	10628	0.8	24	0.04	0.12	407	40	6.20E-01	7.51E-01	0.8
C_{24}	40	13634	0.8	16	0.06	0.10	438	23	6.80E-01	6.54E-01	1.0
C_{30}	40	10652	0.8	5	0.13	0.10	457	20	5.00E-01	1.15E+00	0.4
C_{34}	40	11371	0.8	1	0.57	0.10	482	10	6.90E-01	2.52E+00	0.3
Case 2— Spiking M17 mixture on clean quartz fiber filter (F=25.2 ml/min)											
C_{20}	20	266	0.5	1	0.02	0.10	355	1.0	1.94E-03	4.84E-03	0.4
C_{24}	20	341	0.5	1	0.06	0.08	379	0.6	2.16E-03	6.92E-03	0.3
C_{30}	20	266	0.5	0	0.13	0.09	415	0.7	1.33E-03	1.69E-02	0.1
C_{34}	20	284	0.5	0	0.25	0.09	433	0.5	9.38E-04	2.04E-02	0.0
Case 3— Spiking M17 mixture on quartz fiber filter with PM (F=12.8 ml/min)											
C_{20}	10	133	0.2	7	0.008	0.10	361	3.1	6.70E-03	5.74E-03	1.2
C_{24}	10	170	0.2	6	0.011	0.09	391	1.8	5.14E-03	3.79E-03	1.4
C_{30}	10	133	0.2	5	0.005	0.10	445	4.7	2.23E-03	4.95E-03	0.5
C_{34}	10	142	0.2	4	0.007	0.10	469	4.6	1.33E-03	5.76E-03	0.2

Vs – Spiked solution volume; m – Mass of individual n-alkane; S_s – Solution occupied filter area; θ – Sum of the filter coverage of every n-alkane and OC; M_f – Mol fraction; D – Diffusion coefficient (D for C_{20} is from this work and others are estimated by the Fuller-Schettler-Giddings equation); T_m – Peak maximum temperature; Ps – C_{20} from this work, C_{24} from Grenier at al; 1981 and C_{30}, C_{34} from Mazee, 1948, Mazee, 1948. Pmax. –

Measured maximum partial pressure at T_m; Pc – Calculated partial pressure from Equation (2.10).

In most cases the calculated vapor pressures and the measured vapor pressures agree within a factor of 2-3, which can be expected from the simplified treatment of the complex mass transfer problem from the filter into the carrier gas and the poor characterization of some of the key parameters determining mass transfer, specifically the diffusion distance and cross section. However, the data also indicate that the discrepancy between measured and calculated vapor pressure is more pronounced for the heaviest n-alkanes. This may be due to increasing interaction between n-alkanes and surfaces with increasing carbon number. However, it should be noted that the measured vapor pressures of the n-alkanes listed in Table 5.10 are in most cases very low, and, as discussed previously, for heavy n-alkanes measurements of very low vapor pressures maybe biased due to interaction with the walls of the reactor or transfer lines.

5.5. n-Alkanes in PM Samples Characterized by TDI/GC

For the TDI/GC measurement, the unresolved complex mixture (UCM) peak can be seen in every sampling interval (Figure 4.21) and the target n-alkane peaks are located on the shoulder of the UCM peak. Nevertheless the peaks of the most abundant n-alkanes can be identified and integrated. Using the response factors for small carbon masses (Table 5.9) the n-alkane concentrations in the PM samples can be calculated. The average concentrations of individual n-alkanes for the analysed 9 SONTAS PM samples are in the range of 0.27 to 3.59 ng C/m^3 and the highest concentration is 9.47 ng C/m^3. Sample No. 26 was measured twice with different filter sizes and the measured concentrations are in agreement (see Table 4.9). For most samples, C_{29} has the highest concentration and n-alkanes C_{26} to C_{31} are dominant (the sum of concentrations of C_{26} to C_{31} is more than half of the total n-alkane concentrations). The n-alkanes contribute a very small fraction to PM OC concentration and the mass ratio of measured n-alkane to total PM OC is ~1%. The n-alkanes in above samples were also measured by organic solvent extraction/GC/MS (Irei 2002). Similar to this work, C_{34} and C_{29} have the lowest and highest average concentrations in the range of 0.43 to 5.06 ng C/m^3 (Irei 2002). The average concentrations for these 9 samples determined in this work by TDI/GC and by Irei (2002) are shown in Figure 5.28. While the overall pattern of n-alkane concentrations is similar, most of the concentrations from this work are lower. This may be due to the problems of measuring very low vapor pressures due to sample wall losses in the transfer line and reactor. However, it should also be noted that the PM samples were stored in the refrigerator for more than 4 years after being analyzed by Irei in 2002 and therefore degradation of the samples cannot be rule out.

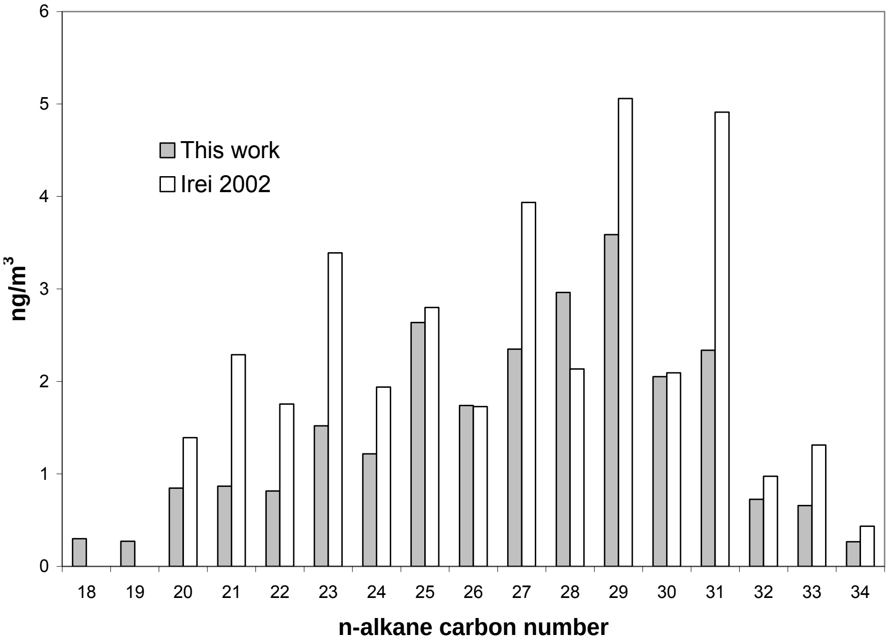

Figure 5.28. Average n-alkane concentrations by TDI/GC and GC/MS.

Compared to n-alkanes spiked on quartz fibers filter with PM, the peak maximum temperatures for n-alkanes of PM samples are about 60 K higher. The native n-alkane mass is small compared to total OC collected on PM filters. The mol fraction of the native n-alkanes in the PM samples therefore is very small, which qualitatively can explain a substantial decrease in equilibrium vapor pressure and therefore the shift of the peaks towards higher temperatures. Similar to the experiments with n-alkanes spiked on filters containing PM the loss of total OC below the temperatures at which the n-alkanes evolve is small and therefore the total OC content of the sample can be treated as constant. This allows to estimate n-alkane vapor pressures based on the same assumptions made for the calculations presented in Table 5.10 and to compare these estimates with measured n-alkane partial pressures (Table 5.11). Overall this comparison shows results; similar to the findings for samples spiked with n-alkanes, which suggests that n-alkanes in PM and n-alkanes spiked on the quartz fiber filters show similar thermo desorption behavior.

Table 5.11. Result of n-Alkanes in PM Sample Filter.

PM sample filter (F=13.3 ml/min)											
	Vs μl	m ng	S_s cm^2	θ	Mf	D cm^2/s	T_m K	Ps	Pmax Pa	Pc	P_m/P_c
C_{24}	N/A	N/A	3	4	1.4E-04	0.11	457	97	6.30E-03	1.08E-02	0.6
C_{30}	N/A	N/A	3	4	2.8E-04	0.12	499	92	6.20E-03	2.02E-02	0.3
C_{34}	N/A	N/A	3	4	1.8E-05	0.12	535	145	1.40E-03	2.04E-03	0.7

Vs – Spiked solution volume; m – Mass of individual n-alkane; S_s – Solution occupied filter area; θ – Sum of the filter coverage of every n-alkane and OC; M_f – Mol fraction; D – Diffusion coefficient (estimated by Fuller-Schettler-Giddings equation); T_m – Peak maximum temperature; Ps –C_{24} from Grenier at al; 1981 and C_{30}, C_{34} from Mazee, 1948, Mazee, 1948. $P_{max.}$ – Measured maximum partial pressure at T_m; Pc – Calculated partial pressure from Equation (2.10).

6. Conclusion

The combination of a Thermal Desorption Instrument (TDI) with medium fast on-line GC-FID instrumentation significantly extends the possibilities to use TDI for compound specific analysis of atmospheric PM. The instrument also allows studies of the thermodesorption behavior of individual compounds or groups of compounds from mixtures and complex samples. Using minor modifications, the instrument can de used to determine physico-chemical properties such as equilibrium vapor pressures, diffusion coefficients and activity coefficients for mixtures. The instrument was tested using a wide range of heavy n-alkanes (C_{18}-C_{34}) .

Due to the high linearity and excellent detection limits of GC-FID the instrument is suitable for studies covering a wide range of concentrations and vapor pressures. Combining the GC-FID with an on-line enrichment (trapping) step further reduced the lower limit of detection. A theoretical lower limit of less than 10^{-6} Pa (corresponding to a gas phase mixing ratio of less than 10 ppt) for n-alkane vapor pressures can be derived from the detection limit of the GC-FID measurements. However, the tests showed that for practical reasons, most likely wall effects, the lower limit for good quality vapor pressure measurements is more than an order of magnitude higher. Moreover, for extremely low vapor pressures the time to obtain stable signals is considerable, in extreme cases this may take several hours. Using several modifications of transfer lines it was possible to reduce the limitations resulting from wall effects, but not to entirely eliminate them. It seems likely that a redesign of the system could further reduce the impact of the limitations.

Overall calibrations and tests of the TDI as well as the TDI/GC showed that the instrument has very good reproducibility, and a linearity and detection limit fully adequate for the analysis of ambient PM samples. However, similar to effectively all existing methods for analysis of organic carbon (OC) and elemental (or black) carbon (EC) the problem of charring results in a poorly defined distinction between these two PM components.

Due to the thermal stability of n-alkanes the thermodesorption behavior of n-alkanes is not influenced by thermal decomposition or charring. Consequently their thermodesorption behavior can be described by their equilibrium vapor pressure, their activity in the sample mixture, and the mass transfer resistance for transfer from the sample to the carrier gas of the TDI system. For the interpretation of the studies of the thermodesorption behavior of n-alkanes a simplified theoretical description of the partial pressure of evolved n-alkanes was derived and compared with experimental observations.

For PM on filter samples or n-alkanes spiked on quartz fiber filters the processes determining the partial pressure of n-alkanes interact in a very complex way and the theoretical estimates often differ by a factor of two or more from the measurements. However, this is not too surprising since these experiments, similar to typical measurements of PM samples by thermodesorption analysis, were not designed for having well defined conditions for mass transfer.

Several series of experiments were conducted using modified experimental set-ups, which create better defined conditions for mass transfer. For these conditions it was found that the theoretical description provides a good approximation for experimental observations and allows identifying conditions, which can be used for measurements of equilibrium vapor pressures, activity coefficients for mixtures, and binary diffusion coefficients.

In principle the measurements of equilibrium vapor pressures are using the gas saturation (flow or transpiration) method, which was proposed about 150 years ago for measuring equilibrium vapor pressures. The results obtained for n-alkanes in this work demonstrate that the modified TDI/GC is a rapid and reliable method to measure very low equilibrium vapor pressures. The obtained vapor pressure data as well as evaporation enthalpies derived from the temperature dependence of vapor pressures are fully consistent with available literature data. There are several advantages of the developed TDI/GC method for measurements of vapor pressures. It allows measurements of very low vapor pressure. This is due to the high sensitivity of GC-FID as detection method and its selectivity, which avoids interference from impurities of the samples tested. Sample preparation is very easy and the required sample mass is low and temperature programmed measurements allow determining equilibrium vapor pressures for a wide range of temperatures in a relatively short time. Furthermore, equilibrium vapor pressures of individual compounds in a complex mixture can be determined. In this context the very simple sample preparation method, which effectively places no restrictions on the type of mixture which can be studied, is very advantageous. Finally it should be mentioned that GC-FID is an inexpensive, reliable measurement technique, which makes the described technique a promising tool to provide more experimental data for vapor pressure data of low volatility organic compounds.

Today, the measurement of diffusion coefficient of heavy organic compound is still a challenge and no published measured diffusion coefficients are available for direct comparison with the diffusion coefficients of the heavy n-alkanes studied here. The comparison with predictions from published empirical equations shows that the predictions slightly overestimate the observations for heavier n-alkanes. This is consistent with a trend, which is been suggested by the published diffusion coefficients for lighter n-alkanes. The temperature dependence of the diffusion coefficients, which was determined over a substantial temperature range using a reactor oven temperature program is in good agreement with theory. The method for measurements of diffusion coefficients developed here allows studies of substances with low vapor pressures, which for most other methods of diffusion coefficient measurements is a significant experimental challenge.

One of the limitations of the method is the limited selectivity resulting from the limited selectivity of the GC-FID detection. This is sufficient for analysis of samples of limited complexity, such as mixtures of n-alkanes, or the analysis of major components in complex samples, such as n-alkanes in atmospheric PM. However, it will not be sufficient for measurements of minor components in complex samples, for example PAHs in atmospheric PM. Using mass spectrometry for detection in combination with the medium fast GC separation would result in a highly selective and very sensitive analytical method. Developing such a method is very challenging, due to the complexity of an instrument combing three components on-line (TDI, GC, and MS). Furthermore, the large amount of complex data (in essence a three dimensional matrix), which such an instrument would create, would provide a challenge for data analysis. Nevertheless, such a method would provide extremely valuable information for the characterization of atmospheric PM or other samples, which are suitable for TDI analysis.

In summary the combination of thermodesorption and on-line gas chromatography is a powerful technique to investigate the thermal behavior of pure substances as well as complex samples, to determine basic physical chemistry parameters, such as equilibrium vapor pressures, diffusion coefficient and activity coefficients or to analyze the concentration of thermally stable organic compounds in complex samples such as atmospheric PM. The main focus of this dissertation was on the use of TDI for studies of atmospheric PM relevance; however the results indicate that there is a wide range of applications for which the developed methodology could be used directly or with minor modifications.

References

Adams, K. M., Davis L. I., Japar, S. M., Finley D. R, and Cary, R.A., Measurement of atmospheric EC: real-time data for Los Angeles during summer 1987, Atmospheric Environment, 24A, 597-604, 1990a.

Adams, K. M., Davis, Jr., L. I., Japar, S. M., Finley, D. R., Real-time, in situ measurements of atmospheric optical absorption in the visible via photoacoustic spectroscopy--IV. Visibility degradation and aerosol optical properties in Los Angeles. Atmospheric Environment, 24A, 605- 610, 1990b.

Addison, J. B., Measurement of vapor pressure of fenitrothion and matacil, Chemosphere, 10, 355-364. 1981.

Allen, J. O.; Durant, J. L.; Dookeran, N. M.; Taghizadeh, K.; Plummer, E. F.; Lafleur, A. L.; Sarofim, A. F.; Smith, K. A., Measurement of $C_{24}H_{14}$ Polycyclic Aromatic Hydrocarbons Associated with a Size-segregated Urban Aerosol. Environ. Sci. Technol. 32, 1928-1932, 1998.

Altshuller, A. P. and Cohen, I. R., Application of diffusion cells to the production of known concentrations of gaseous hydrocarbons, Anal. Chem., Vol. 32, No. 7, 802-810, 1960.

Andreae, M.O., Gelencser, A., Black carbon or brown carbon? The nature of light-absorbing carbonaceous aerosols, Atmos. Chem. Phys. Discuss., 6, 3419-3463, 2006.

Arhami, M., Kuhn, T., Fine, P. M., Delfino, R. J., Sioutas, C., Effects of sampling artifacts and operating parameters on the performance of a semicontinuous particulate EC/OC monitor, Environ. Sci. Technol, 40, 945-954, 2006.

Banar, M., Ozkan, A., Vardar, C., Characterization of an urban landfill soil by using physicochemical analysis and solid phase microextraction (SPME)-GC/MS, Environ. Monit. Asses, 127, 337-351, 2007.

Baranski, J., Bich, E., Vogel, E., Lehmann, J. K., Determination of binary diffusion coefficients of gases using holographic interfermetry in a Loschmidt cell, International Journal of thermophysics, 24, 1207-1220, 2003.

Beatty, J. W., Gaseous diffusion coefficients of pentane isomers, J. Chem. Phys., 51, 4673-4674, 1969.

Belcher, R., Erdey, L., Paulik, F., Liptay, G., A derivatographic study of potassium hydrogen phthalate, Talanta, 5, 53-57, 1960.

Birch, M.E., Analysis of carbonaceous aerosols: interlaboratory comparison, Analyst, 123, 851-857, 1998.

Birch, M.E., Dahmann, D., Fricke, H-H., Comparison of two carbon analysis methods for monitoring diesel particulate levels in mines, J. Environ. Monit., 1, 541-544, 1999.

Bradley, R.S. and Shellard, A. D., The rate of evaporation of droplets: 3. Vapor pressures and rates of evaporation of straight-chain paraffin hydrocarbons, Mathematical & physical sciences, 198, 1053, 239-251, 1948.

Byron, B. R., Transport phenomena, New York: Wiley, p510, 1960.

Cammenga, H. K., Current topics in materials science, edited by E. Kaldis (Amsterdam; New York: North-Holland, ISBN: 0444853898), 1980.

Cadle, S. H., Groblicki, P. J., and Stroup, D. P., Automated carbon analyzer for particle samples, Anal. *Chem.*, 52, 2201-2206, 1980.

Cadle, S. H., Groblichi, P. J., An evaluation of methods for the determination of organic and elemental carbon in particulate samples, Particulate Carbon: Atmospheric life cycle, George, T. W., Richard L. K., eds., Plenum Press: New York- London, 88-109, 1982.

Cadle, S. H., Groblichi, P. J., Mulawa, P. A., Problems in the sampling and analysis of carbon particulate, Atmospheric Environment, 17, 593-600, 1983.

Cadle, S. H., Mulawa, P. A., Atmospheric carbonaceous species measurement method comparison study: General Motors results, Aerosol Sci. Technol., 12,128-141, 1990.

Cao, J. J., Lee. S. C., Ho, K. F., Zou, S. C., Fung, K., Li. Y., Watson, J. G., Chow, J. C., Spatial and seasonal variations of atmospheric OC and EC in Pearl River Delta Region, China, Atmosphere Environment, 38, 4447-4456, 2004

Carruth, G. F. and Kobayashi. R., Vapor pressure of normal paraffins ethane through n-decane from their triple points to about 10 mm Hg, J. chem. Eng. Data. 18. 115-126, 1973.

Chang, S. G., Novakov, T., Formation of pollution particulate nitrogen compounds by NO - soot and NH_3 - soot gas-particle surface reactions, Atmospheric Environment, 9, 495-504, 1975.

Chen, L. W. A., Chow, J. C., Watson, J. G., Moosmuller, H., Arnott, W. P., Modeling reflectance and transmittance of quartz fiber filter samples containing elemental carbon particles: Implications for Thermal/Optical Analysis. J. Aerosol Sci. 35, 765-780, 2004.

Chickos, J. S.; Hyman,A. S.;Liina, H.;Liebman,J .F.; Measurement and estimation of the heats of vaporization of hydrocarbons, J. Org. Chem. 46, 4294-4296, 1981.

Chickos, J.S.; Hosseini,S. and Hesse D. G., Determination of vaporization enthalpies of simple organic molecules by correlations of changes in gas chromatographic net retention times, Thermochimica Acta, 249, 41-62, 1995.

Chickos, J. S. and Wilson, J. A., Vaporization enthalpies at 198.15K of the n-alkanes from C_{21} to C_{28}, J. Chem. Eng. Data, 42, 190-197, 1997.

Chickos, J. S., Webb, P., Nichols, T., Kiyobayashi, T., Cheng,P.-C., and Scott, L., The enthalpy of vaporization and sublimation of corannulene, coronene, and perylene at T = 298.15K, J. Chem. Thermodyn., 34, 1195-1206, 2002**.**

Chickos, J. S. and William E. Acree, Jr., Enthalpies of vaporization of organic and organometallic compounds, 1880 – 2002, J. Phys. Chem. Ref. Data,Vol.32, No.2, 1-360, 2003.

Chickos, J. S. and William, H., Vapor pressures and vaporization enthalpies of the n-alkanes from C_{11} to C_{31} at T = 298.15K by correlation gas chromatography, J. Chem. Eng. Data. 49. 77-85, 2004.

Chirico, R. D., Nguyen, A., Steele, W. V., and Strube, M. M., Vapor pressure of n-alkanes revisited. New high-precision vapor pressure data on n-Decane, n-Eicosane, and n-Octacosane, J. Chem. Eng. Data 34, 149-156, 1989.

Chow, J. C., Watson, J. G., Pritchett, L. C., Pierson, W. R., Frazier, C. A., Purcell, R. G., The DRI thermal/optical reflectance carbon analysis system: description, evaluation and applications in U.S. air quality studies. Atmospheric Environment, 27A, 1185-1201, 1993.

Chow, J. C., Watson, J. G., Crow. D., Lowenthal, D.H., Merrifield, T., Comparison of IMPROVE and NIOSH carbon measurements. Aerosol Sci. Technol., 34, 23-34, 2001.

Chow, J. C., Watson, J. G., $PM_{2.5}$ carbonate concentrations at regionally representative interagency monitoring of protected visual environment sites. J. Geo. Res., 107(D21), 8344, doi:10.1029/2001JD000574, 2002

Chow, J. C., Watson, J. G., Chen, L.-W. A., Arnott, W. P., Moosmuller, H., Fung , K., Equivalence of EC by Thermal/Optical Reflectance and Transmittance with Different Temperature Protocols. Environ. Sci. Technol, 38, 4414-4422, 2004.

Countess, R. J., Interlaboratory analyses of carbonaceous aerosol samples. Aerosol Science and technology, 12, 114-121, 1990.

Cummings, G. A., Ubbelohde, A. R., Collision of diameters of flexible hydrocarbons molecules in the vapor phase: the “Hydrogen effect.”, J. Chem. Soc., 3751-3755, 1953.

Currie, L. A., Benner, Jr. B. A., Kessler, J, D., Klinedinst, D. B., Klouda, G. A., Marolf, J. V., Slater, J. F., Wise, S. A., Cachier, H., Cary, R., Chow, J. C., Watson, J., Druffel, E. R. M., Masiello, C. A., Eglinton, T. I., Pearson, A., Reddy, C. M., Gustafsson, O., Quinn, J. G., Hartmann, P. C., Hedges, J. I., Prentice, K. M., Kirchstetter, T. W., Novakow, T., Puxbaum, H., Schmid, H., A critical evaluation of interlaboratory data on total, elemental, and isotopic carbon in the carbonaceous particle reference material, NIST SRM 1649a. J. Res. Inst. Stand. Technol. 107, 279-298, 2002.

Dan, M., Zhang, G., Li, X., Tao, H., Zhang, Y., The characteristics of carbonaceous species and their sources in PM2.5 in Beijing, Atmospheric Environment, 38, 3443-3452, 2004/

Demirbas, A., Effect of temperature on pyrolysis products from biomass, Energy Sources, Part A, 29, 329-336, 2007.

Eatough, D. J., Eatough, D. A., Lewis, L. and Lewis, E. A., Fine particulate particle chemical composition and light extinction at Canyonland National Park using organic particulate material concentrations obtained with a multisystem, multichannel diffusion denuder sampler J. Geo. Res., 101, 19,515-19,531, 1996.

Eggertsen, T. T., Seibert, E. E. and Stross, F. H., Volatility of high boiling organic materials by a flame ionization detection method, Anal. Chem. 41, 1175-1179, 1969.

Erbil, H. Y., Avci, Y., Simultaneous determination of toluene diffusion coefficient in air from thin tube evaporation and Sessile drop evaporation on a solid surface, Langmuir, 18, 5113-5119, 2002.

Flynn, J. H., Thermal analysis kinetics – past, present and future, Thermochimica Acta, 203, 519-526, 1992.

Fung, K., Particulate carbon speciation by MnO_2 oxidation, Aerosol Sci. Technol., 12, 122-127, 1990.

Fuller, E. N., Ensley, K. and Giddings, J. C., Diffusion of halogenated hydrocarbons in helium. The effect of structure on collision cross sections, J. Phys. Chem., 73, 11, 3679-3695, 1969.

Fuller, E. N., Schettler, P. D. and Giddings, J. C., A new method for prediction of binary gas-phase diffusion coefficient, Ind. Eng. Eng., 58(5), 19-27, 1966.

Fuller, E. N. and Giddings, J. C., A comparison of methods for predicting gaseous diffusion coefficients, J. Gas Chromatogr. July, 222-227, 1965.

Gavril, D., Atta, K. R. and Karaiskakis, G., Determination of collision cross-section parameters from experimental measured gas diffusion coefficients, Fluid Phase Equilibria, 218, 177-188, 2004.

Geankoplis, C. J., Mass transfer phenomena, Holt, Rinehart and Winston, Inc. p25, 1972.

Gelinas, Y, Prentice, K. M., Baldock, J. A., Hedges, J. I., An improved method for the quantification of graphitic and soot BC in complex soil and sediment matrices. Environ. Sci. Technol., 35, 3519-3525, 2001.

Gregorowicz, J., Kiciak, K. and Malanowski, S., Vapor pressure data for 1-butane, cumene, n-octane and n-decane and their statiscally consistent reduction with the Antoine equation, Fluid Phase Equilib. 38, 97-107, 1985.

Grenier-Loustalot, M. F., M. Potin-Gautier, and P. Grenier, Applications analytiaues de la mesure des tensions de vapeur par saturation d'un gaz inerte gas des alcanes normaux et des polyethylenglycols, Anal. Lett. 14, 1335-1349. 1981

Gundel, L. A., Guyot-Sionnest, N. S., Novakov, T., A study of the interaction of NO_2 with carbon particles, Aerosol Science and Technology, 10, 343-351, 1989.

Guo, W-J., Chuang, T-H., Huang, S-T., Leu, W-T., Hsiao, S-H., Thermal degradation behavior of aromatic poly(ester-imide) investigated by pyrolysis-GC/MS, J. Polym. Res, 14, 401-409, 2007.

Gustafsson, O., Haghseta, F., Chan, C., MacFarlane, J., Gschwend, P. M., Quantification of the dilute sedimentary soot phase: Implications for PAH speciation and bioavailability. Environmental Science & Technology, 31, 203-209, 1997.

Gustafsson, O., Bucheli, T., Kukulska, Z., Andersson, M., Largeau, C., Rouzaud, J-N., Reddy, C., Eglinton, T., Evaluation of a protocol for the quantification of black carbon in sediments. Global Biogeochem. Cycles, 15, 881-890, 2001.

Hansen, A. D. A., Kapustin, V. N., Kopeikin, V. M., Gillette, D. A., Bodhaine, B. A., Optical absorption by aerosol BC and dust in a desert region of central Asia, Atmospheric Environment, 27, 2527-2531, 1993.

Haykiri-Acma, H., Yaman, S., Slow-pyrolysis and –oxidation of different biomass fuel samples, J. Environ. Sci. & Health, Part A, 41, 1909-1920, 2006.

Hitzenberger, R., Petzold, A., Bauer, H., Ctyroky, P., Pouresmaeil, P., Laskus, L., Puxbaum, H., Intercomparison of thermal and optical measurement methods for EC and BC at an urban location, Environ. Sci. Technol., 40, 6377-6383, 2006.

Holler, R., Tohno, S., Kasahara, M., Hitzenberger, R., Long-term characterization of carbonaceous aerosol in Uji, Japan. Atmospheric Environment, 36, 1267-1275, 2002.

Huang, T-C; Yang, F. J. F; Huang, C-J; Kuo, C-H; Measurement of diffusion coefficients by the method of gas chromatography, J. Chromatography, 70, 13-24, 1972.

Irei, S., Source identification of primary organic airborne particulate matter using molecular markers, Dissertation, 2002.

Iwatsuki, M., Kyotani, T., Matsubara, K., Fractional determination of elemental carbon and total soluble and insoluble organics compounds in airborne particulate matter by thermal analysis combined with extraction and heavy liquid separation, Anal. Sci., 14, 321-326, 1998.

Jacobson, M. C., Hansson, H-C., Noone, K. J., Charlson, R. J., Organic atmospheric aerosols: review and state of the science, Rev. Geophys., 28, 267-294, 2000.

Japar, S. M., Szkarlat, A. C., Gorse, Jr, R. A., Heyerdahl, E. K., Johnson, R. L., Rau J. A., and Huntzicker, J. J., Comparison of the solvent extraction and thermal-optical carbon analysis methods: Application to diesel vehicle exhaust aerosol Environ. Sci. Technol, 18, 231-234, 1984.

Kadowaki, S., Characterization of carbonaceous aerosols in the Nagoya urban area. 1. Elemental and OC concentrations and the origin of organic aerosols. Environ. Sci. Technol., 24, 741-744, 1990.

Karaiskakis, G., Gavril, D.,Determination of diffusion coefficient by gas chromatography, J. Chromatogr. A., 1037, 147-189, 2004.

Karaiskakis, G. Katsanos, N. A., Rate coefficients for evaporation of pure liquids and diffusion coefficients of vapors, J. Phys. Chem. 88, 3674-3678, 1984.

Katsanos, N. A; Karaiskakis, G; Temperature variation of gas diffusion coefficients measured by the reversed-flow sampling technique, J. Chromatography, 254, 15-25, 1983.

Kamruddin, M., Ajikumar, P. K., Dash, S., Tyagi, A. K., Raj. B., Thermogravimetry-evolved gas analysis-mass spectrometry system for materials research, Bull. Mater. Sci., 26, 449-460, 2003.

Kim, Y. P., Moon, K., Lee, J. H., Baik, N. J., Concentrations of carbonaceous species in particles at Seoul and Cheju in Korea. Atmospheric Environment, 33, 2751-2758, 1999.

Kleefeld, S., Hoffer, A., Krivacsy, Z., Jennings, S. G., Importance of organic and BC in atmospheric aerosols at Mace Head, on the West Coast of Ireland, Atmospheric Environment, 36, 4479-4490, 2002.

Knudsen, M., Ann. Physik, 28, 75, 999; 29, 179, 1909.

Kopinke, F-D., Remmler, M., Reactions of hydrocarbons during thermodesorption from sediments, Thermochimica Acta, 263, 123-139, 1995.

Kos, G., Ariya, P. A., Determination of a wide range of volatile and semivolatile organic compounds in snow by use of solid-phase micro-extraction (SPME), Anal. Bioanal. Chem., 385, 57-66, 2006.

Krivacsy, Z., Hoffer, A., Sarvari, Zs., Temesi, D., Baltensperger, U., Nyeki, S., Weingartner, E., Kleefeld, S., Jennings, S. G., Role of organic and black carbon in the chemical composition of atmospheric aerosol at European background sites, Atmos. Environ., 35, 6231-6244, 2001.

Kuhlbusch, T. A. J., Method for determining black carbon in residues of vegetation fires. Environ. Sci. Technol., 9, 2695-2702, 1995.

Kuhlbusch, T. A. J., Hertlein, A-M., Schutz, L. W., Sources, determination, monitoring, and transport of carbonaceous aerosols in Mainz, Germany, Atmospheric environment, 1097-1110, 1998.

Kwon, K. C., Ibrahim, T. H., Park, Y. and Simmons, C. M., Pseudobinary molecular diffusion of vapors into air, Adv. In Environ. Resear., 8, 667-678, 2004.

Kwon, K. C., Park, Y., Simmons, C. M., Tibere, G. L., Molecular diffusion of volatile-liquid capors into air, Chem. Eng. Comm., 190, 1449-1467, 2003.

Langmuir, I., The vapor pressure of metallic tungsten, Phys. Rev., 2. 329-342, 1913(a).

Langmuir, I., The evaporation, condensation and reflection of molecules and the mechanism of adsorption, Phys. Rev., 8. 149-176, 1913 (b).

Langmuir, I., The constitution and fundamental properties of solid and liquids, J. Am. Chem. Soc., 38, 2221- 2295, 1916.

Lavanchy, V. M. H., Gaggeler, H.W., Nyeki, S., Baltensperger, U., Elemental carbon (EC) and black carbon (BC) measurements with a thermal method and an aethalometer at the high-alpine research station Jungfraujoch. Atmospheric Environment, 33, 2759-2769, 1999.

Leifeld, J., Thermal stability of black carbon characterized by oxidative differential scanning calorimetry, Organic Geochemistry, 38, 112-127, 2007.

Lekomtsev, A. S., Chernyshev, I. V., Volume and Surface Area of Alkane Molecules and Their Solvation Enthalpies, Russian Journal of General Chemistry, Vol. 72, No. 5, 2002, pp. 696--700. Translated from Zhurnal Obshchei Khimii, Vol. 72, No. 5, pp. 747--751, 2002.

Lin, C., Friedlander, S. K., A note on the use of glass fiber filters in the thermal analysis of carbon containing aerosols, Atmospheric Environment, 22, 605-607, 1988a.

Lin, C., Friedlander, S. K., Soot oxidation in fibrous filters. 1. deposit structure and reaction mechanisms, Langmuir, 4, 891-898, 1988b.

Lin, J. J., Tai, H-S., Concentrations and distributions of carbonaceous species in ambient particles in Kaohsiung City, Taiwan. Atmospheric Environment, 35, 2627-2636, 2001.

Li, S., Lyons-Hart, J., banyasz, J., Shafer, K., Real-time evolved gas analysis by FTIRmethod: an experimental study of cellulose pyrolysis, Fuel, 80, 1809-1817, 2001.

Liousse, C., Cachier, H., Jennings, S. G., Optical and thermal measurements of black carbon aerosol content in different environments: variation of the specific attenuation cross-section, sigma. Atmospheric Environment, 27, 1203-1211, 1993.

Mackenzie, R. C. Thermal analysis and some analytical applications**.** Anal. Proc.,19(4), 202-4. 1982

Macknick, A. B. and Prausnitz, J. M., Vapor pressures of high-molecular-weigh hydrocarbons, , J. Chem. Eng. Data. 24, 175-178, 1979.

Mader, B. T., Pankow, J. F., Gas/solid partitioning of semivolatile organic compounds (SOCs) to air filters. 2. Partitioning of polychlorinated dibenzodioxins, polychlorinated dibenzofurans, and polycyclic aromatic hydrocarbons to quartz fiber filters, Atmospheric Environment 35, 1217-1223, 2001.

Malinauskas, A. P., Gaseous diffusion. The systems He-Kr, Ar-Kr, and Kr-Xe, J. Chem.Phys., Vol. 45, No. 12, 4704-4709, 1966.

Malinauskas, A. P., Gaseous diffusion. The systems He-Ar, Ar-Xe, and He-Xe, J. Chem. Phys., Vol. 42, No. 1, 156-159, 1965.

Materazzi, S., Gentili, A., Curini, R., Applications of evolved gas analysis Part 1: EGA by infrared spectrometry, Talanta 68, 489-496, 2006.

Mazee, W. M., Some properties of hydrocarbons having more than twenty carbon atoms, Recl. Trav. Chim. 67, 197-213, 1948.

Meszaros, E., Jakab, E., Varhegyi, G., TG/MS, Py-GC/MS and THM-GC/MS study of the composition and thermal behavior of extracted components of Robinia pseudoacacia, J. Anal. Appl. Pyrolysis, 79, 61-70, 2007.

Minoura, H., Takahashi, K., Chow, J. C., Watson, J. G., Multi-year trend in fine and coarse particle mass, carbon, and ions in downtown Tokyo, Japan. Atmospheric Environment, 40, 2478-2487, 2006.

Mokbel, I., Razzouk, A., Hajjaji, A., Msakni, N., Jose, J., A gas saturation apparatus for very low vapor or sublimation pressure measurements (10^{-3}Pa): vapor-liquid equilibria of n-alkanes (n-C_{10}, n-C_{24}, n-C_{28}), J. Chem. Eng. Data, 52, 1720-1725, 2007.

Morecroft, D. W., Vapor pressure of some high molecular weight hydrocarbons, J. Chem. Eng. Data 9, 488-490, 1964.

Morgan, D. L. and Kobayashi, R., Direct vapor pressure measurements of ten n-alkanes in the $C_{10} – C_{28}$ range, Fluid Phase Equilib. 97, 211-242, 1994.

Myers, H. S. and Fenske, M. R., Measurement and correlation of vapor pressure data for high boiling hydrocarbons, Ind. Eng. Chem. 47, 1652-1658, 1955.

Nagasaka, M., Binary diffusion coefficients of n-pentane in gases, J. Chem. Eng. Data, 18, 388-390, 1973.

Newkirk, A. E., Thermogravimetric measurements, Anal. Chem., 32, 1558-1563, 1960.

Newkirk, A. E., Laware, R., Thermogravimetric analysis of potassium hydrogen phthalate, Talanta, 9, 169-173, 1962.

Nguyen, T. H., Brown, R. A., Ball, W. P., An evaluation of thermal resistance as a measure of BC content in diesel soot, wood char, and sediments, Organic Geochemistry, 35, 217-234, 2004.

Novakov, T., Chang, S. G., Harker, A. B., Sulfates as pollution particles: catalytic formation on carbon (soot) particles, Science, 186, 259-261, 1974.

Novakov, T., BC in atmosphere, Particulate Carbon: Atmospheric life cycle, George, T. W., Richard L. K., eds., Plenum Press: New York- London 19-37, 1982.

Ohta, S., Hori, M., Murao, N., Yamagata, S., Gast, K., Chemical and optical properties of lower troposperic aerosols measured at Mt. Lemmon in Arizona. J. Global Environment Engineering, 2, 67-68, 1996.

Ohta, S. and Okita T., Measurements of particulate carbon in urban and marine air in Japanese areas, Atmos.Environ. 18, 2439-2445, 1984.

Ozawa, T., Kinetics analysis of derivative curves in thermal analysis, J. Thermal Anal., 2, 301-324, 1970.

Park, S. S., Bae, M.S., Schauer, J. J., Ryu, S. Y., Kim, Y. J., Cho, S. Y., Kim, S.J., Evaluation of the TMO and TOT methods for OC and EC measurements and their characteritics in PM2.5 at an urban site of Korea during ACE-Asia, Atmospheric Environment, 39, 5101-5112, 2005.

Parungo, F., Kopcewicz, B., Natgamoto, C., Schnell, R., Sheridan, P., Zhu, C., Harris, J., Aerosol Particles in the Kuwait Oil Fire Plumes: Their Morphology, Size Distribution, Chemical Composition, Transport, and Potential Effect on Climate. J. Geophys. Res. 97, 15,867-15,882, 1992.

Paserba, K. R., Gellman, A. J., Effects of conformational isomerism on the desorption kinetics of n-alkanes from graphite, J. Chem. Phys., 115, 6737-6751, 2001.

Penner, J. E., Novakov, T., Carbonaceous particles in the atmosphere: a historical perspective to the Fifth International Conference on Carbonaceous particles in the atmosphere. J. Geo. Res., 101, 19,373-19,378, 1996.

Piacente, V., Fontana, D. and Scardala, P., Enthalpies of vaporization of a homologous series of n-alkanes determined from vapor pressure measurements, J. Chem. Eng. Data, 39, 231-237, 1994.

Piacente, V., Ferro, D., Gatta G. D., Vaporization enthalpies of a series of α, ϖ - alkane-diols from vapor pressure measurement, Thermochimica Acta, 223, 65-73, 1993.

Piacente, V., Pompili, T., Scardala, P. and Ferro, D., Temperature dependence of the vaporization enthalpies of n-alkanes from vapor-pressure measurements, J. Chem. Thermodyn. 23, 379-396, 1991.

Pompili,T. and Piacente,V., Enthalpy of vaporization of n-heptacosane and n-nonacosane from their vapor pressure determinations, Thermochimica Acta, 170, 289, 1990.

Pouwels, A. D., Eijkel, G. B., Boon, J. J., Curie-point pyrolysis-capillary gas chromatography-high-resolution mass spectrometry of microcrystalline cellulose, J. Anal. Appl. Pyrolysis, 14, 237-280, 1989.

Regnault, v., Ann. Chim. Phys., 15, Ser. 3, 129, 1845.

Reisinger, P., Wonaschutz, A., Hitzenberger, R., Petzold, H., Bauer, H., Jankowski, N., Puxbaum, H., Chi, X., Maenhaut, W., Intercomparison of measurement techniques for black or elemental carbon under background conditions in wintertime: influence of biomass combustion. Environ. Sci. Technol., 42, 884-889, 2008.

Reisen, F., Arey, J., Atmospheric reactions influence seasonal PAH and nitro-PAH concentrations in the Los Angeles Basin. Environ. Sci. Technol. 39, 64-73, 2005.

Rothmam, A. M., Low vapor pressure determination by the radiotracer Transpiration method, J. Agric. Food. Chem. 28, 1225-1228, 1980.

Rouholahnejad, F., Tabrizchi, M., A new method for measuring the diffusion coefficient in a gas phase, J. Phys. Chem. A 110, 11208-11213, 2006.

Rubli, S., Medilanski, E., Belevi, H., Characterization of total organic carbon in solid residues provides insight into sludge incineration processes, Environ. Sci. Technol., 34, 1772 – 1777, 2000.

Rupprecht, E. G., Patashnick, H., Beeson, D. E., Green, R. E., Meyer, M. B., A new automated monitor for the measurement of particulate carbon in the atmosphere, In Proceedings, PM: Health and Regulatory Issues, Cooper, J. A., and Grant, L. D., Eds. Air and waste management association, Pittsburgh, PA, 262-267, 1995.

Sasse, K., Jose, J., and Merlin, J.-C., A static apparatus for measurement of low vapor pressure. Eperimental results on high molecular-weight hydrocarbons. Fluid Phase Equilib. 42, 287-304, 1988.

Sawaya, T., Mokbel, I., Ainous, N., Rauzy, E., Berro, C., Jose, J., Experimental vapor pressures for six n-alkanes (C21, C23, C25, C27, C29, C30) in the temperature range between 350K and 460K, J. Chem. Eng. Data, 51, 854-858, 2006.

Schnelle-Kreis, J., Welthagen, W., Sklorz, M., Zimmermann, R., Application of direct thermal desorption gas chromatography and comprehensive two-dimensional gas chromatography coupled to time of flight mass spectrometry for analysis of organic compounds in ambient aerosol particles J. Sep. Sci., 28, 1648-1657, 2005.

Seager, S. L., Geertson, L. R. and Giddings, J. C., Temperature dependence of gas and vapor diffusion coefficients, J. Chem. Eng. Data, Vol. 8, No. 2, 168-169, 1963.

Smalley, I. J., Lill, G. O., Bentley, S. P., Wood, D. R., Thermogravimetry of potassium hydrogen phthalate, and its use as a thermal standard, Canadian Mineralogist, 15, 30-35, 1977.

Statheropoulos, M., Kyriakou, S. A.,Quantitative thermogravimetric - mass spectrometric analysis for monitoring the effects of fire retardants on cellulose pyrolysis. .Analytica Chimica Acta, 409, 203-214, 2000.

Stefan, J., Sitzber. Akad. Wiss. Wien 68, 385, 1873.

Stevens, R. K., McClenny, W. A., Dzubay, T. G., Analytical methods to measure the carbonaceous content of aerosols, Particulate Carbon: Atmospheric life cycle, George, T. W., Richard L. K., eds., Plenum Press: New York- London. 111-129, 1982.

Strehlow, R. A. The temperature dependence of the mutual diffusion diffusion coefficient for four gaseous systems, J. Chem. Phys., 21, 2101-2106, 1953.

Tolgyessy, P., Vrana, B., Hrivnak, J., Large volume headspace analysis using solid-phase microcolumn extraction, Chromatographia, 66, 815-817, 2007.

Tu, Chein-Hsiun and Liu, Cp. P., Group-contribution estimation of the enthalpy of vaporization of organic compounds, Fluid Phase Equilib. 121, 45-65, 1996.

Turpin, B. J., Huntzicker, J. J., Adams K. M., Intercomparison of photoacoustic and thermal-optical methods for the measurement of atmospheric elemental carbon. Atmospheric Environment, 24A, 7, 1831-1835, 1990.

Turpin, B. J.; Saxena, P., Andrews, E., Measuring and simulating particulate organics in the atmosphere: problems and prospects, Atmos. Environ., 34, 2983-3013, 2000.

Vasiltsova, T. V., Verevkin, S. P., Bich, E., Heintz, A., Bogel-Lukasik, R. and Domanska, U., Thermodynamic properties of mixtures containing ionic liquids. Activity coefficients of ethers and alcohols in 1-methyl-3-ethyl-imidazolium bis(trifluoromethyl- sulfonyl) imide using the transpiration method, J. Chem. Eng. Data. 50, 142-148, 2005.

Verevkin, S. P., Determination of vapor pressures and enthalpies of vaporization of 1,2-alkanediols, Fluid Phase Equilib. 224, 23-29, 2004.

Vege, C.; Rodriguez, A, L.; Second virial coefficients, critical temperatures, and the Molecular shapes of long n-alkanes, J. Chem. Phys., 105, 4223-4233, 1996.

Vyazovkin, S., Kinetic concepts of thermally stimulated reactions in solids: a view from a historical perspective, Int. Reviews in physical chemistry, 19, 45-60, 2000.

Wall, L. A., Flynn, J. H., Straus, S., Rates of molecular vaporization of alkanes, J. Phys. Chem. 74, 3237-3242, 1970.

Walker, R. E. Dehaas, N. and A. A. Westenberg., Measurement of milticomponent diffusion coefficients for the CO2-He-N2 system using the point source technique, J. Chem. Phys., 32, 1314-1316, 1960.

Wania, F. Shiu, W. Y. and Mackay D., Measurement of vapor pressure of several low-volatility organochlorine chemicals at low temperatures with a gas saturation method, J. Chem. Eng. Data. 39, 572-577, 1994.

Waterman, D., Hordield, B., Leistner, F., Hall, K., Smith, S., Quantification of polycyclic aromatic hydrocarbons in the NIST standard reference material (SRM1649A) urban dust using thermal desorption GC/MS, Anal. Chem. 72, 3563-3567, 2000.

Widmann, J F., Duchez, J., Yang, J. C., Conny, J. M., Mulholland, G. W., Measurement of the optical extinction coefficient of combustion-generated aerosol, Aerosol Science, 36, 283-289, 2005.

Williams, B. J., Goldstein, A. H., Kreisberg, N. M., An in-site instrument for speciated composition of atmospheric aerosols: thermal desorption aerosol GC/MS-FID (TAG), Aerosol Sci. and Techl., 40, 627-638, 2006.

Wolff, G. T., Groblicki, P. J., Cadle, S. H., Countess, R. J., Particulate carbon at various locations in the United States, Particulate Carbon: Atmospheric life cycle, George, T. W., Richard L. K., eds., Plenum Press: New York- London, 297-315, 1982.

Xia, T. K. and Landman, U., Molecular evaporation and condensation of liquid n-alkane films, J. Chem. Phys. 101, 2498-2507, 1994.

Yang, H., Yu, J. Z., Uncertainties in charring correction in the analysis of elemental and organic carbon in atmospheric particles by thermal/optical methods, Environ. Sci. Technol., 36, 5199-5204, 2002.

Yu, J. Z., Xu, J. H., Yang, H., Charring characteristics of atmospheric organic particulate matter in thermal analysis, Environ. Sci. Technol. 26, 754-761, 2002.

Yu, J. Z., Yang, H., Hongyi, Zhamg., Lau, A. K. H., Size distributions of water-soluble organic carbon aerosols and its resolved thermal characteristics, Atmos. Environ. 38, 1061-1071, 2004.

Zeng, C., Li, J., Wang, D., Chen, T., Zhao, C., Chen, C., Infinite dilute activity and diffusion coefficients in polymers by inverse gas chromatography, J. Chem. Eng. Data, 51, 93-98, 2006.

Zhao. C., Li. J., Jiang, Z., Chen, C., Measurement of the infinite dilution diffusion coefficients of small molecule solvents in silicone rubber by inverse gas chromatography, European Polymer Journal, 42, 615-624, 2006.